THESIS FOR THE DEGREE OF DOCTOR OF PHILOSOPHY

Optimal Energy and Flexibility Dispatch of Grid-Connected Microgrids

KYRIAKI ANTONIADOU-PLYTARIA

Department of Electrical Engineering
Division of Electric Power Engineering
Chalmers University of Technology
Gothenburg, Sweden 2022

Optimal Energy and Flexibility Dispatch of Grid-Connected Microgrids
KYRIAKI ANTONIADOU-PLYTARIA
ISBN 978-91-7905-700-8

Doktorsavhandlingar vid Chalmers Tekniska Högskola
Ny serie nr. 5166
ISSN 0346-718X

Power Grids and Components
Division of Electric Power Engineering
Department of Electrical Engineering
Chalmers University of Technology
SE-412 96 Gothenburg
Telephone +46 (0)31 772 1000

Chalmers Bibliotek, Reproservice
Gothenburg, Sweden 2022

To my family

Optimal Energy and Flexibility Dispatch of Grid-Connected Microgrids

KYRIAKI ANTONIADOU-PLYTARIA
Division of Electric Power Engineering
Department of Electrical Engineering
Chalmers University of Technology

Abstract

This thesis proposes an optimization model to efficiently schedule energy and flexibilities of a grid-connected microgrid (MG) with non-dispatchable renewable energy sources and battery energy storages (BESs). The model can also be used to coordinate the MG operation with the connected upstream distribution grid and to assess the MG flexibility considering economic viability, technical feasibility, and BES degradation. The performance of the model was tested for both deterministic and stochastic formulations using two solution approaches i.e., day-ahead and rolling horizon, in different simulation and demonstration test cases. In these test cases, the model optimizes the schedule of the MG resources and the energy exchange with the connected main grid, while satisfying the constraints and operational objectives of the MG. The flexibilities from the MG would also be optimized when the MG provided flexibility services (FSs) to the distribution systems. The coordination with the distribution system operator (DSO) was proposed to ensure that the microgrid operation would not violate the technical constraints of the distribution grid.

Two types of test systems were used for the simulations studies: 1) distribution grids with grid-connected MGs and 2) building MGs (BMGs). The distribution test systems included the 12-kV electrical distribution grid of the Chalmers campus and a 12.6-kV 33-bus standard test system, while the BMGs were based on real residential buildings i.e., the HSB LL building and the Brf Viva buildings. Results of the Chalmers' test case showed that the MGs' economic optimization could reduce the annual cost for the DSO by up to 2%. Centralized coordination, where the MG resources were scheduled by the DSO, led to an even higher reduction, although it also led to sub-optimal solutions for the MGs. Decentralized coordination was applied on the 33-bus network with a bilevel optimization framework for energy and flexibility dispatch. Two types of FSs were integrated in the bilevel model i.e., the baseline (FS-B) and the capacity limitation (FS-C). The latter has found to be more promising, as it could offer economic incentives for both the DSO and the MGs. In the studies of the BMGs, the BESs were modeled considering both degradation and real-life operation characteristics derived from measurements conducted at the buildings. Results showed that the annual building energy and BES degradation cost could be reduced by up to 3% compared to when the impact of BES degradation was neglected in the energy scheduling. With the participation of the BMG in FS-C provision, the building's operation cost could be further reduced depending on the flexibility price. A 24-h simulation of the BMG's operation yielded an economic value of flexibility of at least 7% of its daily energy and peak power cost, while the DSO could benefit from the FS assuming that the dispatched flexibility could be used to reduce the subscription fee that guarantees a certain power level. For

frequent flexibility provision i.e., multiple times within a year, the value of flexibility for the MG operator could be reduced due to the BES degradation.

To demonstrate the practical use of the proposed model, an energy management system was designed to integrate the model and employ it to optimize the energy schedule of the BMGs' BESs and energy exchange with the main grid. The energy dispatch was performed in real-time based on the model's decisions in real demonstration cases. The demonstration results showed the benefits of the model in that it helped reduce the energy cost of the BMG both in short term and in long term. The model can also be used by the MG operators to quantify the potential and assess the value of microgrid flexibility. Moreover, with the help of this model, the MG can be employed as a flexible resource and reduce the operation cost of the connected distribution grid.

Keywords: Battery energy storage, energy management, energy scheduling, distribution network, flexibility, microgrids, optimization.

Acknowledgements

First of all, I would like to thank my supervisors Prof. Anh Tuan Le and Dr. David Steen as well as my examiner Prof. Ola Carlson for their consistent support and guidance throughout this period. I would also like to thank Dr. Ali Fotouhi and Dr. Ioannis Bouloumpasis for dedicating so much of their time to help me and for always being there, whenever I wanted to think aloud.

The work of this thesis has been carried out within the 2017-2020 m2M-GRID project "From micro to Mega-GRID: Interactions of micro-grids in active distribution networks" and the 2019-2023 FlexiGrid project "Enabling flexibility for future distribution grid". The m2M-GRID project has received funding from the Swedish Energy Agency in the framework of the joint programming initiative ERA-Net Smart Energy Systems' focus initiative Smart Grids Plus, with support from the European Union's Horizon 2020 research and innovation programme under grant agreements No 646039 and No 775970. The FlexiGrid project has received funding from the European Union's Horizon 2020 research and innovation programme under grant agreement No 864048. The financial support is gratefully acknowledged. I would also like to thank my project partners for their help and the interesting discussions that contributed to my work.

Over the years, I had the pleasure to share the office with many fantastic colleagues: Selam, Ehsan, Christos, Anant, Ioannis, Rahmat and Hannes. It has been a privilege to get to know all of you! My warmest gratitude also goes to all colleagues at the division of Electric Power Engineering who have been there to answer my questions, teach me, and share their knowledge and experience. Many thanks to Georgios Mademlis for being such an amazing friend and very special thanks to my dearest friend Ankur Srivastava, who has stood by me through thick and thin.

Besides my friends at Chalmers, I would also like to thank my other friends who have been there for me during this journey. Eleni and Apostolis, even from afar, I have always felt you by my side. Erik, thank you for being so extremely generous with your time whenever I needed help or moral support. My ballet dance friends in Gothenburg, thank you for being the nicest company, whenever I needed to get out of my head. Last but not least, my family, where life began and love will never end. Thank you for supporting me in any possible way.

Κέλλυ Αντωνιάδου/Kelly Antoniadou
Gothenburg, September 2022

List of Acronyms

Below is the list of acronyms that have been used throughout this thesis listed in alphabetical order:

ANN	Artificial Neural Network
BES	Battery Energy Storage
BFM	Branch Flow Model
BMG	Building Microgrid
BMG-EMS	Building Microgrid Energy Management System
BRP	Balance Responsible Party
CHP	Combined Heat and Power
CS	Case Study
DA	Day-ahead
DER	Distributed Energy Resource
DMS	Distribution Management System
DO	Deterministic Optimization
DoD	Depth-of-discharge
DR	Demand Response
DRR	Demand Response Resource
DSO	Distribution System Operator
EaaS	Energy-as-a-Service
ECIU	Expected Cost of Ignoring Uncertainty
EMS	Energy Management System
EV	Electric Vehicle
EVPI	Expected Value of Perfect Information
ES	Energy Service
FS	Flexibility Service
FSP	Flexibility Service Provider

OPF	Optimal Power Flow
LFM	Local Flexibility Market
LP	Linear Programming
LR	Linear Regression
LSTM	Long Short-term Memory
MILP	Mixed-Integer Linear Programming
MIP	Mixed-Integer Programming
MDP	Markov Decision Process
MG	Microgrid
MG-EMS	Microgrid Energy Management System
ML	Machine Learning
MODEFlex	Microgrid Optimal Dispatch of Energy & Flexibility
NN	Neural Network
OPF	Optimal Power Flow
QCP	Quadratically Constrained Programming
PCC	Point of Common Coupling
PV	Photovoltaic
RES	Renewable-based Energy Sources
RH	Rolling Horizon
SCADA	Supervisory Control and Data Acquisition
SO	Stochastic Optimization
SoC	State-of-charge
SoE	State-of-energy
TSO	Transmission System Operator

Nomenclature

Below is the nomenclature of indices, sets, parameters, and variables that have been used throughout this thesis. The symbols are listed in alphabetical order in each category. The sets, parameters, and variables are also defined in the text, where they first appear.

Indices

i,j	Indices for distribution network buses
m	Index for MG buses that are PCC with the main distribution grid
k,n	Index for charging/discharging sample data
c	Index for iteration loop
p	Index for lifecycle loss function sample point
t	Index for time step
w	Index for scenarios.

Sets

$\mathcal{D}$	Set of distribution network buses
$\mathcal{S}$	Set of substation buses i.e., buses with TSO-DSO interface
$\mathcal{H}$	Set of time discretization steps of the look-ahead time horizon)
$\mathcal{H}_f/\mathcal{H}_{f'}$	Set of time steps belonging to the flexibility activation period.
$\mathcal{K}$	Set of charging data
$\mathcal{M}$	Set of MG buses
$\mathcal{M}_i$	Set of PCC buses i.e., buses with distribution grid and MG interfaces
$\mathcal{N}$	Set of discharging data
$\mathcal{P}$	Set of sample points of the BES lifecycle loss function
$\mathcal{W}$	Set of scenarios.

Parameters

B_1	Pre-exponential factor used in empirical cycle aging model
B_2	Exponential factor used in empirical cycle aging model
Δt	Time interval
H	Percentage of end-of-life retained capacity of a BES [%]
η_m^{ch}	Charging efficiency of BES
η_m^{dis}	Discharging efficiency of BES
K_m^{BES}	Power to energy ratio related to the technology of BES
K_m^{DR}	Power to energy ratio related to the technology of DRR
$\widehat{\rho}_{mp}$	Sample point of lifecycle loss percentage
A^c	Calendar aging coefficient
B_i	Shunt susceptance from bus i to ground
$C_m^{B,0}$	Replacement cost of the BES
C_m^{CHP}	Operation cost of the CHP plant (related to the scheduling period)
C_m^f	Fuel cost of the CHP plant
$C^{im,SS}$	Energy transmission charge paid by the DSO
C^{im}	Grid charge for energy transmission paid by the MG customers
C^{ex}	Reimbursement fee paid to producers of small-scale generation
C_m^{pen}	Penalty [$/kW] for not providing the flexibility.
DoD_{mp}	Sample point of DoD
$E_m^{DR,init}$	The part of energy available from DRRs that has already been curtailed at the beginning of the time horizon
E_m^{max}	Installed capacity of BES
G_i	Shunt conductance from bus i to ground
$\boldsymbol{H}$	Adjacency matrix
I_c	Average C-rate of a BES over the scheduling period
Λ^{peak}	Power-based grid tariff paid by the MG customers
$\Lambda^{SS,peak}$	Power-based grid tariff paid by the DSO
M	A very large number (used with the linearization technique called big-M approach)
N^{it}	Number of iterations
Π_w	Probability of occurrence of scenario w.
P_{mp}^-	Sample measurement of output power from the battery cells

P_{mk}^{+}	Sample measurement of input power to the battery cells
P_{m}^{Cap}	Capacity limit
P_{mk}^{ch}	Sample measurement of charging power absorbed from the grid
P_{mp}^{dis}	Sample measurement of discharging power injected to the grid
P_{tm}^{H}	Heating output from the CHP plant
$P_{m}^{G,min}$	Minimum electrical power output from the CHP plant
P_{tm}^{L}	Active power of load demand
$P_{tm}^{L,r}$	Available responsive load
P_{max}^{-}	Maximum discharging power of BES
P_{max}^{+}	Maximum charging power of BES
P_{tm}^{PV}	Active power from solar generation
Λ_t	Spot price [$/kWh]
Q_{tm}^{L}	Reactive power of load demand
R_{ij}	Resistance of line $i-j$
R_{m}^{CHP}	Ratio of electrical power to heating power output
S_{ij}^{max}	Rated apparent capacity of line $i-j$
SoE_{m}^{min}	Lower state-of-energy limit
SoE_{m}^{max}	Upper state-of-energy limit
SoE_{mk}^{ch}	Sample measurement of BES state-of-energy during charging
SoE_{mn}^{dis}	Sample measurement of BES state-of-energy during discharging
T	Temperature
V_{max}	Upper voltage limit
V_{min}	Lower voltage limit
X_{ij}	Reactance of line $i-j$

Variables

ξ_{tmp}	Positive variable indicating choice of lifecycle loss function sample point p
ρ_{tm}	Percentage of lifecycle loss for one cycle at a specific DoD
$\phi(DoD)$	Lifecycle as a function of DoD
b_{tmp}	Binary variable used with adjacency constraints
c_{m}^{B}	Cycle aging cost (calculated over the scheduling period)
c_{m}^{DER}	Operation cost (calculated over the scheduling period) associated with the DER owned by the MG

c_{tm}^{DoD}	Cycle aging cost per time step t
c_{m}^{im}	Cost of MG's imported energy (calculated over the scheduling period)
c_{m}^{peak}	Cost of the MG's peak imported power drawn from the main grid (calculated over the scheduling period)
δ_{tm}^{Pim}	Procured flexibility amount (deviation from the imported power baseline profile)
δ_{tm}^{Pex}	Procured flexibility amount (deviation from the exported power baseline profile)
dod_{tm}	Depth-of-discharge (DoD)
e_{tm}^{DR}	The part of energy available from DRRs that has already been curtailed at time t
$e_{tm}^{DR,end}$	The part of energy available from DRRs that has already been curtailed by the end of the time horizon
f_m	Value of the objective function of MG m (MG's total cost)
f_{wm}^{DO}	Total MG's deterministic cost for scenario w naively treating forecast as perfect information
$f_{wm}^{DO,PI}$	Total MG's deterministic cost for scenario w assuming perfect forecast
f_{m}^{SO}	Total MG's expected cost
$\pi_{tm}^{fl,Cap}$	Flexibility price
$\pi_{tm}^{fl,im}$	Flexibility price
$\pi_{tm}^{fl,ex}$	Flexibility price
p_j	Active power injection at bus j
p_{ji}	Active power flow from bus j to bus i
p_{tm}^{-}	Power output from the battery cells (before battery losses have been taken into account)
p_{tm}^{+}	Power input to the battery cells (after battery losses have been taken into account)
$p_{tm}^{MG,ex}$	Exported power to the main grid
$p_{tm}^{MG,im}$	Imported power from the main grid
p_{tm}^{ch}	Charging power of BES (power absorbed from the grid)
p_{tm}^{dis}	Discharging power from BES (power injected to the grid)
p_{tm}^{DR}	Curtailed (or increased) power from DRRs
p_{tm}^{flex}	Procured amount of flexibility
$p_{tm}^{fl,p}$	Expected net power per time step of the flexibility activation period
p_{tm}^{G}	Electrical power output from the CHP plant
p_{c}^{PCC}	Average active power exchange at PCC

p_{ti}^{SS}	Active power at the substation
q_j	Reactive power injection at bus j
q_{ji}	Reactive power flow from bus j to bus i
q_{tm}^{DR}	Reactive power of DRRs
q^{idx}	Percentage of the difference between the estimated SoE and the measured SoC at one time step
q_{tm}^{G}	Reactive power from the CHP plant
Q_m^l	Percentage of cycle-based capacity loss a BES
Q^r	Percentage of retained BES capacity after a rest period
$Q^{r,0}$	BES capacity percentage at the beginning of a rest period
r_m^{ex}	Revenue of MG m due to exporting energy to the main grid
r_m^{flex}	Revenue of MG m from selling flexibility
$c_i^{SS,peak}$	Cost of the distribution network's peak power measured at the substation
c_m^p	Cost of the MG's peak power drawn from the main grid
q_{ti}^{SS}	Reactive power at the substation
soc	State-of-charge (SoC)
soe_{tm}	State-of-energy (SoE)
ν_i	Voltage at bus i
v_i	Square of voltage magnitude at bus i
x_{tmn}	Positive variable indicating choice of discharging sample measurement n
y_{tmk}	Positive variable indicating choice of charging sample measurement k
z_{tm}^{BES}	Binary variable that indicates if the BES is charging or discharging

Contents

Chapter 1

Introduction

This chapter presents the problem overview and the main research questions that are being addressed in this thesis. It describes the objectives and the main contributions of the thesis and it also includes the publications that resulted from the thesis work.

1.1 Background

Under the Paris agreement, which has been in effect since 2016, the European Union (EU) countries have committed to significant reductions of CO_2 emissions to achieve the EU goal of carbon neutrality by 2050 and contribute to the global goal of limiting the Earth's temperature rise to 1.5°C above pre-industrial levels by the end of the 21^{st} century. Despite all encouraging actions to address the problem of climate change, it seems that humanity is falling behind. The highest ever level of global emissions was recorded in 2021 completely eliminating the positive effect of CO_2 reductions caused by the lockdown measures imposed during the previous year due to the COVID-19 pandemic [1]. The alarming findings from the latest United Nations' Intergovernmental Panel on Climate Change (IPCC) report [2] indicate that unless global CO_2 emissions are cut by 43% by 2030, in comparison to the 2019 levels, it will be statistically impossible to limit the temperature rise to 1.5°C.

To fight climate change and balance in time the amounts of carbon emitted to the atmosphere and absorbed by the atmosphere, sweeping actions are required to reduce the global emissions, as the technological readiness level of direct air carbon capture and storage technologies is low and their potential is predicted to be limited by 2030 [2]. To this end, the generation of electrical energy is undergoing a transition from fossil-based energy sources to renewable-based energy sources (RESs) such as solar energy, wind power, and others. Sweden, in particular, has set ambitious energy goals of 100 % renewable energy production by 2040 and zero net emissions of greenhouse gases by 2045 [3, 4]. Apart from the necessity to replace the fossil-based electric energy sources with RESs, the integration of more RESs is also driven by the need to support growing electricity demand and electrification requirements.

Despite the fact that the EU has so far focused on large-scale deployment of RESs,

small-scale integration of renewables has also been achieved with residential photovoltaics (PVs) thanks to the feed-in tariffs and the solar panel subsidies which make own production from PVs worthwhile and appealing to the consumers. This marks the transition of the former passive consumers to active prosumers i.e., electrical energy consumers that also have the capability of producing their own electrical energy, which can be used either for self-consumption or exported to the main grid.

Following a decrease in the battery cost [5], the installation of residential, stationary battery energy storages (BESs) has increased, signifying their value in reducing the prosumers' electricity cost. Behind-the-meter BESs can be combined with residential PVs to increase the self-supply level of end-users during the day and help small-scale RESs owners increase their revenue by maximizing self-consumption of PV generation [6] and by engaging in energy arbitrage (load-shifting). These BESs are also a promising application for recycling retired electric vehicle (EV) BESs, which can be re-used as second-life BESs load-shifting and peak-shaving.

The coupling of small-scale generation with residential BESs promotes the integration of microgrids (MGs) i.e., clusters of local energy sources, energy storages, and customers represented as a single controllable entity [7]. The term "microgrid" has been subjected to many definitions. According to the U.S. Department of Energy MG is [8]: "a group of interconnected loads and distributed energy resources (DERs) within clearly defined electrical boundaries that acts as a single controllable entity with respect to the grid. An MG can connect and disconnect from the grid to enable it to operate in both grid-connected or island mode." The Conseil International des Grandes Réseaux Électriques (CIGRÉ) Working Group C6.22 Microgrid Evolution Roadmap (WG6.22) provided the following definition: "MGs are electricity distribution systems containing loads and DERs, (such as distributed generators, storage devices, or controllable loads) that can be operated in a controlled, coordinated way either while connected to the main power network or while islanded."

MGs can be employed at various locations including both rural and urban areas. Off-grid solutions are usually ideal for remote rural areas. In cities, on the other hand, grid-connected MGs can be formed by clusters of DERs that are integrated in commercial or residential buildings. These MGs can also be defined as building MGs (BMGs) [9, 10], when the management of the DERs is in tight relation with the electricity load consumption of a building or clusters of buildings.

1.2 Motivations and scope of the thesis

Up until now, the driving force for the deployment of MGs [7] around the globe has been the need to have uninterrupted and reliable power supply in remote locations or areas. These MG projects are still vital for the ongoing access to electricity especially for areas severely affected by extreme weather phenomena e.g. wildfires, hurricanes etc. Therefore, the main focus of their application has been islanding capability, black-start capability, and grid-forming control. In the case of grid-connected MGs, the focus in the literature has shifted from the grid-forming control to the optimal

energy management, which is the main focus of the thesis. The thesis studies the operation of grid-connected MGs without making any distinction between clusters that possess and clusters that do not possess islanding capability. The studied clusters are always connected to the grid and therefore their operation is similar to the operation of grid-connected MGs.

Energy management, which is also known as scheduling or dispatch (these three terms are used interchangeably in the thesis), refers to the control of the energy consumed or produced by the MG resources and the control of the energy exchanges between the MG and other connected grids. This operation is performed by the MG energy management system (MG-EMS). A comprehensive literature review on optimal energy scheduling of MGs can be found in Section 2.2.

Many studies on optimal MG energy scheduling e.g., [11–16], assume MG-EMSs that operate in uncoordinated schemes i.e., without coordinating with the distribution system operator (DSO) to solve the MG energy scheduling problem. Others have applied coordinated energy management of grid-connected MGs considering interaction with the DSO e.g., [17–20]. It is unspecified, however, in these studies, how the MG integration can affect the cost of the DSO, if the unbundling of network operation is considered, which is why the coordinated energy scheduling studied in this thesis assumes utility restructuring (also known as deregulation). Restructuring separated the generation, transmission, and distribution thus breaking the monopoly that bundled these services together. The unbundling framework of power system operation is the existing regulatory framework in EU countries [21] and many states in the United States of America (U.S.A.) [8].

The thesis also focuses on the realistic representation of the BES operation and associated cost. Energy storage emerges as a critical resource in MG energy management [11] offering energy services (ESs) that benefit MG owners such as increased self-consumption of RES-based generation and energy arbitrage [22]. In fact, the main focus of this thesis is the MG system that consists of PV and energy storage systems, which has been characterized as the basic MG [23]. The basic MG can serve smaller loads such as a number of buildings and, therefore, it can easily be deployed by residential electricity customers. Thus, the models developed for this thesis and the proposed solutions are relevant to the end-users and have high chances of practical applications in MG projects likely to be implemented by residential customers in the near future. Many recent studies [11–13, 15–20, 24–37] have published results on optimal MG energy dispatch considering stationary energy storage. The proposed scheduling solutions can be applied by the MG-EMSs and enable the end-users to fully utilize the BES potential in reducing their energy costs.

However, the studies that consider BES dispatch often oversimplify the BES scheduling model to reduce the complexity of the optimal MG energy scheduling problem, as is discussed in the literature review in Section 2.3. For the same reason, the impact of degradation is often ignored. However, the link between BES dispatch and BES degradation is essential, as it can be exploited to further reduce the operation cost of the MG [9]. The challenge to introduce a linear mathematical model

that can realistically represent the non-linear BES behavior and the induced BES degradation motivated the focus of the thesis on BESs.

Another aspect of the grid-connected MG operation is the dispatch of the MG flexibility. MGs at distribution system level can be introduced as new flexibility sources that can offer demand-side flexibility services (FSs). Such sources are urgently needed because the increasing share of both large-scale and small-scale RESs in the energy mix increases the flexibility needs of system operators [38]. Using alternative flexibility sources to avoid the operation of expensive and fossil-fuel based generators for the sole purpose of containing infrequent high-peak periods will offer significant cost savings [39]. Local FSs can also offer economic and sustainable solutions for the future challenges concerning the distribution grid operation. The DSO can act as the intermediate responsible party for technical validation of demand-side FSs traded in day-ahead (DA) and intra-day markets or s/he can act as the flexibility procurer [40]. These FSs can mitigate the impact of the high-peak conditions incurring lower capital expenditures compared to the upgrade of distribution grid infrastructure, which can take up to 10-12 years, or other FSs such as grid reconfiguration [41]. Even if the network reinforcement costs cannot altogether be avoided, deferring these costs with the support of FSs can be economically beneficial.

The ideas of flexibility quantification and demand-side FSs provided from DERs or DERs aggregators such as MG operators, which have recently gained attention as is evident by a number of recent studies e.g., [38, 41–48], is also investigated in the thesis. As shown by the extensive literature review in Section 2.4, these studies estimate the technically available flexibility without examining whether this amount of flexibility is also economically viable or optimal.

Finally, the thesis work did not focus on every aspect related to MG energy management. Although communication and control interfaces have been successfully used in real-life demonstrations of some of the developed models, the thesis did not study interoperability aspects regarding the integration of the MG components to the MG's or DSO's control centers i.e., the MG controller or the DSO's supervisory control and data acquisition (SCADA) system, respectively. To guarantee the successful practical applications of the proposed models and solutions, irrespective of the vendors that provide each deployed software and technology, the existing interoperability standards and ontologies must be considered. In the thesis, it is assumed that all the equipment employed by the control center that implements the solution is fully interoperable. Furthermore, the MG-EMSs typically dispatch the resources within a look-ahead time horizon and some input data, such as electricity load demand and RES-based generation, have uncertain values over the time horizon. Therefore, forecast profiles of these values are used instead. The development of forecasting models was out of the scope of this thesis. For this reason, historical data or pseudo measurements were used in the majority of the case studies. Actual forecasts were used, however, in one case study which evaluated the effect of short-term and high-resolution forecast errors on the optimal MG energy scheduling.

1.3 Objectives

The overarching goal of the thesis was to develop and validate an optimization model that optimizes the use of flexible resources of a grid-connected MG. The model was developed to more accurately characterize the operational costs of MGs/BMGs considering the profit from load shifting, the revenue from the FSs, and the cost of BES degradation, which has often been neglected in the literature on optimal MG energy management. The model could dispatch the MG resources either in an uncoordinated manner or assuming interaction with the DSO to coordinate the dispatch of the resources with the operation of the DSO's grid. To achieve its primary goal, the thesis has the following objectives:

1. To compare and evaluate optimal solutions from different energy scheduling strategies satisfying operational targets of: 1) each MG operator or 2) the DSO, in a distribution network with grid-connected MGs considering the unbundled framework of network operation.

2. To incorporate an improved BES dispatch model, which can capture a more realistic BES operation performance, and BES degradation models in the optimization model for MG energy and flexibility dispatch.

3. To quantify the MG flexibility considering both its technical and its economic feasibility.

4. To apply stochastic assessment of flexibility with sufficient computational efficiency to respond to close to real-time flexibility requests.

5. To define a methodology for short-term flexibility assessment and dispatch.

6. To introduce an optimization framework of coordinated operation between the DSO and the MG operators for the optimal allocation and dispatch of MG flexibility in a distribution network with grid-connected MGs and use this framework to quantify the value of local flexibility for both the MGs and the main grid operator as well as analyze its impact on the dispatch of the MG resources.

7. To verify the effectiveness of the proposed model with simulation studies of real test systems and demonstrate its performance on physical MG testbeds.

1.4 Main research questions

Within the scope of this thesis the following research questions (RQs) have been identified in the effort towards the accomplishment of its goal:

- **RQ-1:** How can MG energy scheduling strategies affect the cost for the DSO in the unbundled framework of operation?

- **RQ-2:** How can the mathematical model of the BES be improved to capture

both real-life performance characteristics and the impact of degradation, while having a formulation that does not add complexity to the optimal energy and flexibility dispatch problem?

- **RQ-3:** How much does BES degradation impact the cost of the MG energy scheduling solution?
- **RQ-4:** How should uncertainties be handled when short-term and high-resolution load forecasts are used in optimal MG energy scheduling?
- **RQ-5:** How can the technically and economically feasible MG flexibility be assessed and how is its economic value affected by different factors?
- **RQ-6:** How can the interaction between the DSO and the MG operators be employed to determine the optimal allocation and dispatch of the MG flexibility in a distribution network with multiple grid-connected MGs?

The thesis examines these questions, which are related to the research gaps highlighted in Section 2.6 and presents findings that can provide answers or further knowledge and insight on the studied subject.

1.5 Contributions

To answer the research questions and achieve the objectives mentioned in the previous sections, a model for the **M**G **O**ptimal **D**ispatch of **E**nergy and **Flex**ibility, which will be called *MODEFlex* model in this thesis, was developed. The model can be integrated to an MG-EMS, which interacts with the MG resources and dispatches them according to the solution of the optimization problem that is formulated from the MODEFlex model. The optimal solution is related to either the economic operation or the level of interaction with the main grid. It can be employed by an MG operator or a DSO, depending on the implemented coordination scheme, to implement the multi-period optimal dispatch of the MG resources. The MG energy management follows a market-based approach to offer ESs such as energy arbitrage and peak power cost minimization to the MG customers in order to minimize the energy cost paid them. In correspondence to its objectives, the main contributions of the thesis are the following:

1. A long-term evaluation study of MG energy scheduling strategies:
   Unlike existing studies, the operation cost and performance of the DSO's grid and its grid-connected MGs were assessed considering the unbundling of network operation. The link between the expected BES lifetime, which is affected by BES degradation, and the applied energy scheduling strategy was also investigated.

2. BES dispatch considering a measurement-based model and degradation:
   A measurement-based BES model, which could capture real-life operation characteristics derived from BES measurements, and cycle aging models, which calculated the impact of degradation to the BES capacity and the degradation

cost, were incorporated in the MODEFlex model. Moreover, the effect of the BES's depth-of-discharge (DoD) on the BES capacity was assessed both in cycle and in calendar aging, in contrast to many optimal BES studies that have often ignored the dependency of aging to the DoD.

3. Integration of FS models in the optimization model for MG energy dispatch:
The integration of local FS models in the optimal energy scheduling model, which has rarely been considered in energy scheduling studies, introduced the comprehensive formulation of the MODEFlex model. In particular, two FSs were modeled: 1) the baseline FS (FS-B) and 2) the capacity limitation FS (FS-C). The MG customers could increase their revenues by providing these FSs to a flexibility procurer e.g., the DSO. Therefore, the MODEFlex model can be employed by the MG operators to reduce the MG's operation cost through both ESs and FSs and can be used to calculate the optimal amount of flexibility that the MG can offer upon a request. The integration of the FS models in the optimal energy scheduling model meant that both the technically and the economically feasible flexibility were considered in the calculation of the flexibility amount that could be offered.

4. A stochastic MODEFlex model with improved efficiency and quality:
The MODEFlex model was also formulated using scenario-based stochastic optimization (SO) to account for uncertainties of the model's input data i.e., forecasts of load consumption and PV generation values. The stochastic MODEFlex model was used to implement optimal energy and flexibility dispatch of a BMG in a rolling horizon (RH) scheme. Unlike other studies using RH approach, each update in the forecast values updates the whole control trajectory of the MG resources, while the dispatched active power of the resources is not discretized and thus the impact of the forecast errors is even further minimized. The model considered look-ahead uncertainty thanks to the stochastic formulation and, instead of considering real-time uncertainty realization, adjustments to the deterministic control decisions were dynamically being implemented with the RH approach to deal with close to real-time uncertainty. These adjustments, in addition to a scenario reduction technique that was implemented, improved the computational efficiency and the scalability of the formulated SO problem.

5. A methodology for stochastic assessment and dispatch of flexibility:
The stochastic MODEFlex model was used to introduce a versatile methodology for flexibility assessment. The methodology can be implemented with different flexibility activation periods and notification times for flexibility requests. It can be used to dispatch intra-day flexibility on a short notice (up to close to real-time) to alleviate unscheduled network congestions i.e., unrelated to network maintenance. It can also be used to define flexibility evaluation metrics and can easily be adjusted to fit the specific needs of the flexibility procurer.

6. Development of a bilevel optimization model for flexibility dispatch:

Assuming that flexibility was procured by the DSO and provided by the MGs, a leader and multi-follower approach was defined which formulated a bilevel optimization problem with the upper level (UL) i.e., the leader, being the DSO and the lower level (LL) i.e., the followers, being the MGs. The bilevel model assumed AC OPF for the distribution network modeling of the UL and the MODEFlex model for each MG at the LL. The solution of the bilevel optimization problem yielded the optimal allocation and amount of MG flexibility. The model can be used to determine the optimal amount and price of flexibility dispatch as well as the value of flexibility for both the procurer and the providers. It can also give valuable information regarding the flexibility potential of a network area and reveal network areas that could benefit from the implementation of local flexibility markets (LFMs).

7. Validation of the MODEFlex model with studies on real test systems:
The real distribution network of a university campus was employed in the long-term evaluation study where different MG energy scheduling strategies were implemented. Furthermore, a real energy-flexible residential building was used as a BMG in multiple studies of the thesis. Comprehensive evaluation of the BES dispatch under the proposed MODEFlex model was performed under different technical and degradation BES models revealing which modeling approach could yield the maximum reduction to the electricity cost of the building residents. A different case study on the same BMG demonstrated the effect of BES capacity and flexibility price on the dispatched flexibility and the daily economic value of flexibility for the MG customers. In addition, the BMG was used to study the effects of load forecasting errors on the BMG's operation cost. Finally, a BMG-EMS was designed to implement online and real-time control of the on-site DERs in two physical test sites. The MODEFlex model incorporating the measurement-based BES model was integrated in the BMG-EMS of each BMG testbed and its performance was validated through real-life demonstrations on the BMGs.

1.6 Structure of the thesis

The thesis is organized in nine chapters:

- **Chapter 1** presents the background and the scope of the thesis as well as its objectives, the main contributions, and the identified research questions.
- **Chapter 2** presents a state-of-the-art survey on MG energy management and demand-side flexibility. Emphasis is given on BES scheduling and degradation models as well as FSs models integrated in the MG energy management problem. Industrial perspectives of grid-connected MGs are also discussed.
- **Chapter 3** defines the operational framework of the studied MG systems and presents the basic structure of a MODEFlex problem as well as the methodology that was used in the thesis for its solution.

- **Chapter 4** presents the formulation of the optimization models that were developed to solve the MODEFlex problems studied in the thesis.
- **Chapter 5** deals with deterministic energy management of BMGs and analyzes the effect of load forecasting errors to BMG's cost.
- **Chapter 6** presents the solution of the stochastic MODEFlex problem for a BMG and a probabilistic approach to quantify the BMG's flexibility.
- **Chapter 7** compares the results of different energy scheduling strategies of grid-connected MGs and investigates their impact on the cost and operation of the MGs and the DSO grid.
- **Chapter 8** solves the deterministic MODEFlex problem in coordination with the DSO to present results of the optimal allocation, dispatch, and value of flexibility.
- **Chapter 9** concludes the thesis and provides suggestions for future work.

1.7 List of publications

The following publications are based on the work presented in the thesis:

(I) **Kyriaki Antoniadou–Plytaria**, Ludvig Eriksson, Jakob Johansson, Richard Johnsson, Lasse Kötz, Johan Lamm, Ellinor Lundblad, David Steen, Le Anh Tuan, and Ola Carlson, "Effect of short-term and high-resolution load forecasting errors on microgrid operation costs," to be presented in *Innovative Smart Grid Technologies Conference (ISGT-Europe)*, Novi Sad, Serbia, Oct. 10-12, 2022.

(II) **Kyriaki Antoniadou–Plytaria**, David Steen, Le Anh Tuan, Ola Carlson, Baraa Mohandes, and Mohammad Ali Fotouhi Ghazvini, "Scenario-based stochastic optimization for energy and flexibility dispatch of a microgrid," in *IEEE Trans. Smart Grid*, May 2022. DOI: 10.1109/TSG.2022.3175418

(III) Erik Francisco Alvarez, Luis Olmos, Andres Ramos, **Kyriaki Antoniadou–Plytaria**, David Steen, and Le Anh Tuan, "Values and impacts of incorporating local flexibility services in transmission expansion planning," in *Electric Power Systems Research*, vol. 212, p. 108480, Nov. 2022. DOI: 10.1016/j.epsr.2022.108480

(IV) **Kyriaki Antoniadou–Plytaria**, David Steen, Le Anh Tuan, Ola Carlson, and Mohammad Ali Fotouhi Ghazvini, "Market-based energy management model of a building microgrid considering battery degradation," in *IEEE Transactions on Smart Grid*, vol. 12, no. 2, pp. 1794-1804, Mar. 2021. DOI: 10.1109/TSG.2020.3037120

(V) **Kyriaki Antoniadou–Plytaria**, David Steen, Le Anh Tuan, and Ola Carlson, "Energy scheduling strategies for grid-connected microgrids: A case study

on Chalmers campus," in *Proc. Innovative Smart Grid Technologies Conference (ISGT-Europe)*, Bucharest, Romania, Sep. 29–Oct. 2, 2019. DOI: 10.1109/ISGTEurope.2019.8905472

(VI) **Kyriaki Antoniadou–Plytaria**, Ankur Srivastava, Mohammad Ali Fotouhi Ghazvini, David Steen, Le Anh Tuan, and Ola Carlson, "Chalmers campus as a testbed for intelligent grids and local energy systems," in *Proc. 2nd International Conference on Smart Grid Energy Syst. and Technologies (SEST) Europe*, Porto, Portugal, Sep. 9–11, 2019. DOI: 10.1109/SEST.2019.8849014

The numbering is used to refer to the papers throughout the thesis. The abstract of these papers can be found in Appendix A. Note that Paper III also appears in the proceedings of *Power System Computation Conference (PSCC)*, which was held in Porto, Portugal, June 27-July 1, 2022.

In addition, the author has contributed to the following publication, which is not covered in the thesis:

(I) Mohammad Ali Fotouhi Ghazvini, **Kyriaki Antoniadou-Plytaria**, David Steen, Le Anh Tuan, "Two-stage demand-side management in energy flexible residential buildings," submitted to *IET Smart Grid*, May 2022.

Chapter 2

State-of-the-art and Industrial Perspectives

The following section is an overview of the state-of-the-art on MG energy and flexibility dispatch. Special focus is given in the use of BES as a flexible resource. The models of FSs and the quantification of flexibility are also discussed and the most recent studies on demand-side flexibility offered from MGs are reviewed. Industrial perspectives of MGs and their integration into existing distribution grids are also discussed.

2.1 Energy management system

MGs are defined as clusters of distributed energy sources (generation, storage, flexible loads, etc.) and energy consumers (non-flexible load). The MGs can operate either in grid-connected or in island mode and many MGs can support seamless transition between the two modes to increase supply reliability for the customers. In grid-connected mode, the difference between the MG generation and consumption can be imported or exported to the main grid. In island mode, the MG is completely autonomous i.e., energy is supplied exclusively from the MG resources and any excess in generation must be stored or curtailed, if self-consumption is not an option.

Regardless of the mode of operation, an MG can be considered as a controllable entity, which is represented as a single entity to the distribution grid. This can be achieved with the help of the MG controller, which is the key component of the MG in control of the producing and consuming units (distributed generation, flexible loads, storage) that are clustered together to form the MG. The MG controller ensures that the operation of the MG is both secure and reliable as well as efficient and economical.

The MG-EMS is an intelligent automation system employed by the MG controller and its main task is to optimally balance load and supply both in the planning phase and in the delivery phase (either by MG resources or through interconnec-

tions). The MG-EMS belongs to the tertiary control level, which is the highest level of the three-level hierarchical MG control architecture [8], where the primary and secondary levels deal with controlling active and reactive power sharing among the MG resources in short timescales i.e., milliseconds to seconds, to achieve frequency and voltage regulation. The IEC 61970 standard [49] on EMS application program interface has defined EMS as "a computer system comprising a software platform providing basic support services and a set of applications providing the functionality needed for the effective operation of electrical generation and transmission facilities so as to assure adequate security of energy supply at minimum cost".

The use of the MG-EMS is essential in dispatching the MG resources in an intelligent, secure, and reliable manner and in achieving coordination both among the MG components as well as with other grids. The MG-EMS determines the power exchange between the MG and the other grids at the points of common coupling (PCCs), which are the physical interfaces of the MG and the other grids with the connection to the MG. Typically, the MG has one PCC with the upstream, main distribution grid. Clearly, through the PCCs the scheduling of the MG resources affects the operation of the interconnected system (e.g., voltage profile, utilization of feeders). The MG resources are managed by the MG-EMS, while the objectives and strategies that determine the scheduling decisions of the MG-EMS are defined by the MG operator. If the MG operator is different from the DSO and the MG operates in grid-connected mode, then these objectives might not be co-aligned with the operational objectives that optimize the operation of the main distribution network. Therefore, it can be beneficial to employ the distribution management system (DMS), which is a part of the utility control centre, to schedule either directly or indirectly the MG resources with the aim to ultimately control the active (and/or reactive) power exchange at the PCCs.

Through the control of the power exchange at the PCCs, the operation between multiple grid-connected MGs and the distribution network can be coordinated. This can ensure the satisfaction of grid technical constraints, contribute to an economical operation of the interconnected systems and assist in ancillary services. To achieve this level of coordination, a control and communication MG interface should be developed as an add-on DMS functionality to integrate the MG energy scheduling with the network optimal power flow (a functionality already available at the DMS). Such an interface would allow MGs and DSO to exchange information including desired MG schedule, the voltage at PCC and flexibility requests among others.

2.2 Optimal energy scheduling of MGs

The optimal energy management of MGs has been extensively studied in recent literature, mainly as a DA scheduling problem with the MG-EMS operating in uncoordinated schemes i.e., without considering interaction with the DSO, even when the MG is connected to the main grid (e.g., [11–16, 24, 27, 34, 50]). A part of the research on MG energy management specifically focuses on BMGs [51, 52] and investigates solutions that can be applied by a BMG energy management system (BMG-EMS),

which is also known as home energy management system (HEMS), especially when the energy management is applied for a single residence. Reducing the peak consumption is also considered in the energy management models through peak power tariffs or penalties e.g., [53–55]. Typically, when studies seek to reduce peak power costs, the peak demand is minimized in the short-term, with the assumption that the consumer will be charged with respect to the daily peak demand. Apart from the DA scheduling, there is also research that focuses on model predictive control (MPC) [52], also known as receding or rolling horizon (RH) control, which utilizes feedback in an iterative process that adjusts and improves the control output multiple times within the (typically daily) scheduling time horizon, which is typically 24 hours. Control of conventional generators, control of energy storage and demand response (DR) are usually employed to minimize the operation cost of the MG. An exhaustive review on solution approaches and uncertainty handling approaches that have been proposed for MG energy management can be found in [56].

The majority of the studies on building energy management use low time resolution of load and generation profiles, which also yields a low-time resolution control. The time resolution, also known as time granularity, refers to the length of the time interval between the dispatch of two consecutive operational set-points. The time resolution has most frequently been 1 hour, which is not sufficient to capture the peak power patterns, as studies on the impact of time resolution have shown [57]. In latest research, 15-minute time intervals have frequently been employed. Although this is an improvement, it does not necessarily bring the energy scheduling closer to real-time control. This can be achieved with the iterative process of the RH approach. The low time resolution of most recent studies [52] that employ RH control, which typically use hourly time discretization steps, makes them incompatible with close to real-time control. Moreover, these studies do not usually implement peak power reduction and RH optimization concurrently.

2.2.1 Forecasting

Most often the MG energy scheduling has been formulated either as deterministic optimization (DO) or stochastic optimization (SO) problem; the latter in order to address uncertainties without enforcing conservative costly solutions, as is the case with robust optimization. Typically, MG resources are dispatched hourly within a look-ahead time horizon of 24 hours. However, the need to mitigate the effects of intermittent RES generation has motivated researchers to study intra-hour dispatch schemes. Since the problem uses a look-ahead horizon and requires forecasts of the uncertain input values (e.g., load demand) at each dispatch time step, it is obvious that there is a need for both *short-term* and *high-resolution* forecasts.

Machine learning (ML) models such as neural networks (NNs) have successfully been employed to provide electric load forecasts in the last 30 years [58]. However, there has been a lack of studies that seek to satisfy the two-fold requirement, as only a few publications (e.g., [59–62]) have developed forecast models with a resolution of a few minutes.

2.2.2 Multiple grid-connected MGs

The future distribution grid of multiple, grid-connected MGs could create new challenges for the DSOs and requires proper control and coordination of different network entities. Therefore, a lot of studies (e.g., [17–20, 63–69]) have also been applying coordinated energy management of grid-connected MGs considering interaction between the MG-EMSs and the DSO. The MG energy scheduling is the result of a decision-making process, where the MGs and the DSO (or an MG aggregator) need to exchange information to determine the interactions between the MGs and the main grid (e.g., power exchange, energy prices). In this decision making process, there is often a hierarchical structure (see e.g., [69]), where a central controller operated by the DSO or the MG aggregator determines the power exchanges between the main grid and the MGs. This type of hierarchy can also be used to indirectly schedule the power exchanges e.g., through the use of price signals (energy/flexibility prices or penalties). In this case, the DSO is acting as the leader (upper level) that determines the price signals and the MG operators are the followers (lower level) that respond to these price signals and schedule their resources and power exchanges according to them. When the hierarchical structure consists of two levels of decision making, then the coordinated MG energy scheduling problem can be formulated as a bilevel optimization problem.

Applications of both stochastic [63–65] and deterministic [17, 18, 66, 67] bilevel optimization can be found in the recent literature on coordinated energy management of grid-connected MGs. The same concept has also been applied for other clusters of resources at the lower level, such as virtual power plants, and different main grid operators at the upper level e.g., energy communities [70] instead of utility companies. In most works, the DSO is at the upper level and is viewed as a supervisor for the energy exchange among all interconnected network entities. Therefore, these studies usually assume that the DSO has full knowledge of MG information, which extends beyond the PCC data such as the MGs' objectives, MG grid constraints, as well as DERs and customer data in order to solve the bilevel optimization problem (e.g., [19, 20, 63, 67]). Full knowledge helps to simplify the bilevel optimization problem, as it can then be transformed into an equivalent single-level mathematical problem with complementarity constraints (MPCC), as in [63, 66]. Full MG information, however, comes into conflict with the requirements for reduced MG data sharing.

According to the guidelines provided in [71], the DMS should not require any information of the MG network and capacity configuration (except perhaps of the status of some tie-line switches) in order to be functional. In this regard, some methods have been developed for coordinated MG energy scheduling with limited information exchange with the DSO. Authors in [64] propose a decentralized solution for the same problem, which was solved in a centralized manner in [63]. Specifically, the MGs share information only about the power exchange at the PCC and iteratively increasing penalties are introduced to incorporate the coupling of the different entities and ensure convergence of the solution. Multi-period energy scheduling with inter-temporal constraints for generators and energy storage is considered in [17],

where the MGs can also exchange energy with each other. In this case, the DSO first sends the energy exchange schedule to the MGs and then receives information from them to update it iteratively until the optimal decision is reached. The DMS does not require any MG values as input except from PCC measurements and the MG information related to the worst-case operating cost. In the multi-MG concept in [18], the aggregator only requires the scheduled energy exchange of each MG at PCC and the corresponding MG profits in order to generate a congestion price signal and avoid violation of PCC capacity.

Studies on coordinated MG energy management often ignore the distribution network modeling or simplify it using DC power flow equations. If the grid constraints are considered, then this applies to the main grid, while the MG grid constraints are neglected. The network power flow within the MGs was only considered in [67], where an equivalent single-level problem was solved. As it was mentioned, this approach requires that the DSO has data/measurements of the MG network and/or resources. In this case, full information of the MG configuration was shared with the DSO to ensure that the global grid constraints i.e., the technical constraints of the entire grid including the connected MGs, would be satisfied with the application of the individual optimal solution.

What is missing from recent publications is a study of the MG integration considering the unbundled framework of operation. All of the previously mentioned studies assume that both the DSO and the MGs can own and schedule DERs and they trade energy with each other. Thus, the proposed methodologies and the published results are not particularly relevant to the European DSOs, where unbundling rules usually apply to their operation.

2.3 BES scheduling

Energy storage enables smart grid integration, electromobility, and FSs that can be provided to the power system [72]. The focus on connecting stationary storage units to energy systems has particularly increased due to the need for dispatchable RESs. Stationay energy storages support the integration of RESs by reducing the grid power fluctuations the RESs cause and can offer many other services that benefit the grid operators (e.g., peak shaving, load leveling, frequency regulation [73]). BESs have mostly been used in frequency regulation, which accounts for about half of their applications, while energy arbitrage accounts for about 10% according to [22]. However, as recent research has been investigating the potential contribution of energy arbitrage in reducing the energy cost, the BES has started to emerge as a critical resource for energy management. This is evident by many research publications on MGs [11–13,17–20,25–37] and BMGs [9,10,74] that seek to optimize the MG energy management through the optimal scheduling of stationary BESs. Many of the above-mentioned studies (e.g., [13,17–20,33–35]), however, do not consider BES degradation.

Publications that do consider the effect of battery degradation on energy management usually neglect the impact of calendar aging [12,26–30,32], which reduces the

BES capacity during open-circuit periods. Instead, they focus on cycle aging, often disregarding the effect of the DoD as a stress factor [26, 27, 32]. In addition, most works use simplified BES scheduling models, which could reduce the reliability of the scheduling solution.

As was observed from the literature review, the mathematical models employed in energy scheduling of MGs with stationary BESs had at least one of the following shortcomings: 1) simplified BES scheduling model assuming constant BES charging/discharging efficiencies and/or maximum power rates and 2) no implementation of a degradation model to consider the impact of BES degradation. Below is a detailed review of the state-of-the-art on optimal BES dispatch focusing on BES degradation and BES scheduling models to present the modeling approaches that have been used in recent publications.

2.3.1 BES degradation

Some of the most recent studies that have published results on optimal BES dispatch (not necessarily using the MG concept) and consider BES degradation cost are [12,26–32,75–78]. A penalty is often used in the objective function in order to reduce BES stress, usually by avoiding deep cycle depths and/or high power rates [27,76,77]. Other works consider the impact of low state-of-charge (SoC) [28–30, 75], while the simplest approach is to limit the number of cycles [26].

In [27], a mixed-integer non-linear programming model links the degradation cost to the cycle depth and updates the BES capacity per time-step. The battery degradation in [76] is a function of the power rates, while authors in [77] link degradation cost to both cycle depth and charge/discharge rates. However, neither of the studies [27, 76, 77], consider the DoD of each cycle.

In contrast, the degradation cost in [28] is calculated using an approximation that links BES lifetime loss with a weighted sum of SoC levels. Authors in [29] also consider SoC level and use Q-learning to approximate the non-convex cycle aging cost. The rainflow algorithm is employed in [75], where the authors prove convexity of the cycle-based degradation cost function provided that the DoD stress function is also convex. Then, they use a subgradient algorithm to approximate the solution of optimal BES dispatch. The loss of lifecycle as a function of DoD is also studied in [30], although the specific DoD related to each cycle is not considered. The authors propose a piecewise linearization of the lifecycle loss function, where the BES sizing of an MG is decided based on the expected degradation associated with the maximum DoD of all cycles. A sensitivity analysis is performed in [78] to define the impact of multiple stress factors on the BES degradation cost. For simplicity, the authors assume that the BES charging and discharging efficiencies are the same.

Unlike most studies, which neglect calendar aging, the authors in [31] incorporate both calendar and cycle aging into a mixed-integer linear programming (MILP) problem considering their dependencies on time elapsed and cumulative throughput, respectively. In order to include calendar aging in the MILP problem, a predefined desired BES lifetime must be entered as a parameter. The impact of SoC is not

evaluated in either cycle or calendar aging.

The BES degradation can be expressed either as loss of available capacity or as increase in the BES resistance. Most of the studies reviewed in this section link the degradation cost with a percentage of the estimated capacity loss. This percentage is multiplied with the initial investment cost of the BES to define a degradation cost term in the objective function. Thus, these studies determine the optimal BES dispatch considering the trade-off between degradation cost and revenue from load shifting. An interesting study on the trade-off between profit and BES degradation investigating the participation of the BES owner in different services can be found in [79]. For a more realistic representation of the BES degradation cost both the decreasing trends in BES replacement costs and the end-of-life retained capacity (the remaining capacity of the BES when it is retired) for grid applications would have to be considered. These were not discussed in the previously mentioned works that linked the degradation cost with BES capacity reduction.

Practical approaches can also be found to calculate the degradation cost, as for example those proposed in [28, 30]. In these works, the BES depreciation was calculated using only data from the manufacturer's performance warranty without utilizing any modeling approach to account for the effect of aging mechanisms on the BES capacity or resistance. In [28], the BES degradation was calculated by estimating the effective cumulative throughput (depending on the SoC levels) of the BES dispatch. Considering the cumulative throughput that the BES can deliver in its lifetime according to the manufacturer's warranty, the BES loss could then be calculated as a percentage of the cumulative throughput that was removed from the total throughput. Authors in [30] calculated degradation as a percentage of lifecycle loss, using manufacturer's data about the maximum number of cycles the BES could deliver at a specific DoD.

The manufacturers of residential, stationary BESs (e.g., Tesla's Powerwall [80], and Samsung's SDI [81]) give a performance warranty of 10 years considering, in addition, an operating limitation in terms of maximum throughput or number of cycles, especially if the end-user combines the BESs with products/applications provided from different vendors. The end-of-life retained BES capacity is 65%-80% for BESs that are coupled with PVs, depending on the geographic location of the BES and PV installation. These applications, however, are relatively new, as these BESs were introduced in the market in 2015, and the BES retirement age and end-of-life retained capacity is not as well determined as in EV applications. Further research is required to more accurately quantify the benefits of using residential, stationary BESs in load shifting applications considering the impact of degradation.

The challenge to accurately assess the impact of degradation on the operation cost of the MG is therefore twofold. First, the employed degradation model should be representative of the main aging factors associated with BES usage without adding unnecessary complexity to the optimal MG energy and flexibility dispatch problem. Secondly, regardless of the followed modeling approach, the assessment should account for factors such as future BES replacement cost and expected BES

retirement age.

2.3.2 BES scheduling models

Up until now, studies on optimal BES dispatch that consider degradation have been using technical BES models, which are built on some simplifying assumptions regarding the BES operation e.g., the charging/discharging energy efficiency and the power limits are considered to be constant and independent of the BES's SoC. The BES scheduling in [32], which is formulated as a Markov decision process (MDP), considered both degradation and effective charging/discharging power dependent on the SoC, resulting in an improved BES model compared to previously mentioned works. Still though, the round-trip efficiency was considered to be constant.

The simplifications of the BES scheduling models can lead to miscalculations and failure to implement the BES schedule e.g., the scheduled BES energy might not be delivered or the BES might fail to reach the scheduled energy storage level. Neglecting the BES power dependency on SoC can actually be a valid assumption, if additional limits on stored energy are considered. Rated power can normally be delivered within the SoC region, which is available by the BES converter i.e., where the storage voltage will not trigger the current limiter function. The benefit of additional SoC limits is twofold: 1) the power output becomes more predictable due to relatively stable voltage values and 2) the BES is protected from high stress. Thus, a BES model with this assumption is not expected to deviate much from the behaviour of an actual BES. However, if the state-of-health (SoH) of the battery has deteriorated, the maximum power levels can be affected leading to decreased accuracy of this modeling approach.

As a way to deal with the issues that arise with the existing BES scheduling models, a few recent works proposed models that can integrate the actual, non-linear behavior of a real BES in linear programming (LP) optimization problems [82, 83]. The authors in [82] provide a piecewise linear approximation of the charging curve to account for the non-constant charging power limits, while simplifications are still applied on BES efficiency. Their BES model was tested for two C-rates, separately. In [83], each state of the BES operation is a linear combination of sampled points of operation taken from measurements. This approach considers dependency of both power and efficiency on SoC. Ref. [82, 83] did not consider BES degradation.

Promising results on the SoC estimation with the use of artificial neural networks (ANNs) have also been presented [84, 85]. Boulmrharj et al. [84] showed that the use of an ANN gave higher accuracy than model-based approaches for SoC estimation (the Coulomb counting method was used as a reference value). The long short-term memory (LSTM) method was deployed in [85] to forecast SoC estimation. Future research could integrate these methods in the optimal BES dispatch problem and investigate whether they could increase the reliability of the BES dispatch solution.

2.4 Demand-side flexibility

The flexibility of the power system was first defined as the ability of the system to deploy its resources in order to respond to changes in the net load which is not supplied by RESs [86]. The flexibility resources were mainly conventional generation sources and flexibility studies evaluated their capabilities to adapt their schedules according to the requirements. The metrics of flexibility aimed to measure the ramping requirements and available resources and identify the impact of additional capacity and changes in the operation of flexibility resources to the operation and planning of the power system. As research in flexibility provision and dispatch progressed, it became obvious that load and RES-based generation, which had been treated as the causes of flexibility requirement, could also act as flexibility resources and become a part of the solution. Focus was also given on small-scale resources and demand-side management for the procurement of local flexibility. In other words, distributed resources such as non-dispatchable and dispatchable distributed generation, energy storage, and DRRs could also be employed as flexibility resources. Energy storage, in particular, has been playing an important role in latest flexibility studies, because it can be coupled with non-dispatchable RES-based sources and essentially turn them into dispatchable generators. Flexibility from non-dispatchable generators can be provided by curtailment of their injected power. As a result, additional flexibility could be available originating from distributed DERs and DRRs depending on the power system's operational policies and the state of each resource at the time instance when flexibility would be needed. Interconnection to other power systems was also suggested as a supplementary flexibility solution.

The demand-side flexibility refers to the ability of the DSOs to draw flexibility from local flexible resources to alleviate congestion or reduce peak imported power from the upstream grid. The concept of LFMs is a current research trend which analyzes how market-based principles can solve grid operation issues in a cost-efficient manner. To demonstrate the benefit of establishing such markets, studies need to investigate methods of quantifying the local flexibility and show that FSs can offer economic value to both the DSOs and the flexibility service providers (FSPs). For this purpose, the ideas of flexibility quantification and demand-side FSs provided from DERs or DERs aggregators such as MG operators have recently gained attention, as is evident by a number of studies e.g., [38, 41–48].

2.4.1 Quantification

The real-time quantification of flexibility, which is critical for modeling and implementing any FS, is a research gap addressed by a few works only e.g., [42, 43]. Ref. [41] presents a rudimentary model of an FS offered by a large heat pump with predetermined cost of activation and discrete steps of flexibility amounts. The MG flexibility bids are assumed to be equal to the predicted power injected to the main grid in the hour-ahead bidding process of [44], where solar irradiance uncertainty is considered in the BES-based MG energy scheduling using a Markov transition matrix and the recursive least-squares method for predictions; the load uncertain-

ties are disregarded. The use of the BES as a buffer to correct hourly mismatches between injected power and bids might require investments on larger capacity or reduce income from other revenue streams, as less capacity is released to provide services. Unlike aforementioned studies, which use model-based approaches, machine learning techniques are proposed in [45] to forecast the longevity of the offered flexibility. Similarly, a regression model is used in [46] to design the incentives that will increase the participation of residential energy hubs in FSs.

2.4.2 Integrating FS models in optimal energy dispatch

Dispatching flexible resources to address the MG's needs i.e., MG energy management, is different from dispatching these resources to address the system's needs. Therefore, for an accurate evaluation of the optimal MG's cost, the models of FSs must be integrated in the optimal energy dispatch problem of an MG that provides an FS to enhance the flexibility of the power system.

Most of the studies reviewed in Section 2.4.1 did not integrate FSs in the optimal energy dispatch problem. The impact of FSs in the economic energy scheduling of MGs was considered in [38,43,47,48]. The concept of the flexibility envelopes is used in [43] to consider the feasibility region of the real-time operational flexibility of an MG in its optimal power dispatch, which is performed in RH. The power exchange with the main grid is assumed to be known per time step, thus the BES flexibility dispatch satisfies the MG needs to avoid the cost of dispatching diesel generators or curtailing load. A scenario-based stochastic optimization (SO) problem is solved for a grid-connected MG in [47, 48], where the problem integrates flexibility limits. In [47] these limits are time-varying and depend on the net consumption of the rest of customers connected to the same distribution feeder as the MG. In [48], these limits are set by the DSO to minimize deviations from the approved power exchange schedule, which is treated as a baseline power profile. Similarly, the scheduled power exchange is used as a baseline reference to define MG flexibility in [38], where a cooperative controller based on model predictive control is used to distribute the flexibility amount among a network of MGs. However, using the MG schedule as a baseline to define MG flexibility can be prone to manipulation [87] and having to agree on a power exchange schedule can be problematic for a real-world implementation of this FS.

Despite its issues the baseline FS model is currently one of the main models to dispatch local flexibility and different methods have been proposed to calculate the baseline reference [87]. In the context of MG energy scheduling, the MG energy schedules can be employed as the baseline references. Another FS model used for local flexibility dispatch is the capacity limitation FS [88], a novel FS model which does not depend on baseline reference profiles. This model defines a capacity limits and the FSP is requested to limit the net power consumption below this limit. Therefore, the flexibility is estimated as the amount of power reduction from the capacity limit instead of the amount that deviates from the baseline.

2.5 Industrial perspectives of MG integration

MG-EMSs are already offered by several manufacturers including ABB [89], Siemens [90], and General Electric [91] among others. Some of these platforms also provide integration with the supervisory control and data acquisition (SCADA) system of the utility through standard industrial protocols. Thus, the technology for both MG deployment and DSO integration is available. The adoption of MGs could benefit both end-users, which could reduce their energy cost, and the operation of the distribution system, which can exploit the energy flexibility offered by MGs. Despite the available technologies and the benefits to different stakeholders the MG integration raises questions from both sides.

In Europe, the development of MGs has not been significantly promoted yet, which is evident by the lack of regulations and policies on this concept [92]. In fact, only 11% of the total MG capacity can be found in Europe [93]. The low implementation can be attributed to the unbundled framework of operation. As the DSOs have generally not been able to own or operate DERs so far, it has been difficult to directly affect the MG integration. Besides, the DSOs deem flexibility services as less reliable compared to grid reinforcement, which reduces their incentive to implement MGs. Therefore, it seems that the general preference from the DSOs' side, especially in high-density urban areas, is a bottom-up integration initiated by the end-users.

The problem is that the bottom-up integration has been highly restricted and hindered by present regulations, perhaps even more so than the deployment which could be realised by the utilities. An example of this is the "over-the-fence" rule [94], which is applied in many US states, including the otherwise very supportive of MG projects, state of California. This regulatory roadblock prevents entities other than utilities to own and operate MGs with assets and customers belonging to more than two neighboring properties. Thus, due to this rule, an MG developed and operated by a small community of people such as a neighborhood is practically made impossible, as the MG would become subject to utility-related regulations, which cannot be managed by a small entity. As a result, the efforts to achieve bottom-up MG integration are left to the end-users that would be interested to develop smaller MGs that would not be affected by the such regulations. The investment on small-scale RESs and BESs is financially supported, however, there are no incentives for the end-users to invest on advanced control functions offered by the MG-EMSs. Furthermore, there are other unresolved issues for the interested parties apart from investments on advanced control systems including communication infrastructure, standardization, grid ownership, cyber security, and data protection.

The regulatory obstacles that dissuade the deployment of MGs by prosumers' initiatives, could be overcome by supporting the formation of citizen energy communities. These energy initiatives were recognized by the EU Directive for the internal electricity market 2019 [95]. As described in the Directive, the operation of the energy communities essentially resembles the operation of MGs, with less emphasis on the geographic contiguity of the assets and more emphasis on the voluntary and open participation of the community members and the primary purpose of the energy

community, which is to fight energy poverty of its members rather than generate financial profits.

Another issue related with the bottom-up MG deployment is the interoperability of MGs and MG components. The integration can be challenging for heterogeneous devices, especially if these are provided by different vendors or manufacturers. Although Internet interface facilitates an easier integration of the control devices, each controllable device or converter-embedded controller might use a different communication protocol on top of the Transmission Control Protocol/Internet Protocol (TCP/IP) protocol. Moreover, not all control functions are available through Internet interface and, therefore, additional interfacing devices might be required, which adds to the complexity of the control system. Unless integration of end-user devices becomes a more standardized procedure, the prosumers will be discouraged to invest on smart devices, which could offer energy flexibility to the grid, or might not be interested on taking full advantage of their capabilities, unless there are very strong incentives from the utility company. Without a high degree of standardization, the widespread adoption of the MG technologies can only be realised by third-party MG developers, as even the development of small MG projects such as residential BMGs will be a very challenging task.

Despite the lack of initiatives from the DSOs' side, their interest in grid-connected MGs and their contribution in the distribution system operation could rise in the future considering the relaxation of the rules about energy storage ownership. Up until now, distribution utilities in Europe were generally not allowed to own and operate energy storages [21] due to the unbundling of network operation and energy supply, as already explained. In the latest report of the Swedish Energy Markets Inspectorate [96], which was published in February 2020, it is clearly stated that DSOs can, as an exception, own and operate energy storage, if it is used to handle unexpected events and as long as the DSOs do not buy or sell energy to the energy or the balance market. With creating MGs in form of clusters of energy storage systems in certain strategic areas the DSO could alleviate congestion or regulate voltage, when needed in a network area. With a large number of energy storage based MGs, the distribution network could even become dispatchable and reduce the effect of uncertainties of RES generation and EV integration. However, excluding the participation to energy and balancing markets reduces the revenue streams from BESs, such as, for example, revenues associated with frequency response services and energy arbitrage. Thus, despite the change in the regulation and despite the services that BESs can offer to the operation of the distribution network, the DSOs' investment in BESs might not be efficiently rewarded.

2.5.1 Business model

A real-world example of innovative grid-connected MG projects is the financing business model that introduces MG as an energy-as-a-service (EaaS) [97, 98]. According to this model, the MG is owned and operated by a third party and the costumers are relieved from risks associated with investment, operation, and maintenance costs. Thus, the MG can own both small-scale (residential) and utility-scale assets and

DERs. The customers, who have an agreement with the third-party MG developer, only pay for the energy services (for the energy provided by the MG) or they might share the energy savings with the MG developer, depending on their power purchase agreement [98, 99]. The energy savings can result from efficient management of the energy portfolio to deliver energy and flexibility services such as for example energy arbitrage and peak demand reduction. This business model enables the MG industry to share its expertise with prospective customers by overcoming complexities that have so far dissuaded prosumers from participating in this market. Thus, it can lead to a faster MG integration and accelerated growth of the energy market at the end-user level.

2.5.2 Demonstrators of MGs

There are many laboratory-scaled MGs that are used for research on MG control, e.g., at the Electric Energy Systems laboratory in National Technical University of Athens [100], in Aalborg University [101] in Denmark, at the KIOS laboratory [102] in Cyprus, the Prince lab microgrid testbed [103] at Polytechnic University of Bari, in Italy and others. Jansen et al. [104] present a survey of smart grid labs, most of which can be found in Europe and many of these labs already implement MGs.

The need to bridge the gap between research and deployment motivated the development of field testbeds, e.g., in Kythnos island [105] of Greece, in Bornholm island [106, 107] of Denmark, at the University of California, San Diego [108] and others. Among them, the Borrego Springs MG [109] in San Diego, California, is a characteristic example of an "unbundled utility MG", where the distribution assets of the MG are owned by the utility, while the DER of the MG are owned by independent producers and the MG customers.

In 2019, there were 4475 identified MG projects globally [93]. These MG projects are either in operation, under development, or under planning and the total MG capacity amounts to about 27 GW. Out of these about 11 GW (42.3%) belong to remote MGs, while the new MG projects that were recorded were mostly remote systems (93.4% of new entries). The projects that are taken into account include grid-connected systems that are capable of operating in island mode or remote systems that display at least one of the following characteristics: 1) RES-based generation, 2) combined heat and power (CHP) generation, 3) energy storage, and 4) control that enables optimal operation of the resources. The leader area in MG capacity is Asia Pacific with 37% of total MG capacity, followed by North America with 33%, Middle East and Africa with 14%, Europe with 11%, and finally Latin America with 5% [93].

In Sweden, there are several local energy systems that can be viewed as platforms for small-scale integration of energy sources and operate as grid-connected MGs. One example is Simris [110, 111], a local energy system comprising a village of 140 households, a 660kW wind turbine, a 440kW solar power plant, and a 800 kWh BES. A diesel generator has also been installed to additionally supply the MG in case it operates in island mode. The back-up diesel generator is power by the hydrogenated vegetable oil Diesel 100, a diesel fuel based 100% on renewable materials coming from

slaughterhouse waste. Another example is the MG on the Arholma island [112]. The MG supplies about 250 residents with the installed PV systems and the two BESs of 1225 kWh total capacity. In case of a power outage, the MG can supply the customers for at least one hour, under normal demand conditions and fully-charged BESs. Other examples can also be found in local energy systems managed by the EnergyHub system provided by Ferroamp [113] such as e.g., the HSB Living Lab building [114, 115], the Brf Viva buildings [116], Fjärås [117], and others. The EnergyHub is a converter-embedded power management system, which integrates PV and BES DC/DC converters. The AC electricity load consumption and the PV generation are monitored by the EnergyHub, which controls the power exchange between the local energy system and the main grid by controlling the BES power.

2.6 Summary of identified research gaps

From the literature review in Sections 2.2-2.4 it was observed that studies on coordinated operation of the MGs and the DSO have exclusively focused on defining the amount of energy trade between the DSO and the MGs often without considering the underlying constraints of the distribution network operation. Thus, not all real-world examples of distribution network operation can be studied by these approaches. The research question RQ-1 that was formulated in Section 1.4 indicates the attempt of this thesis work to assess the impact of MG integration and evaluate the cost of potential MG services considering unbundled network operation.

The role of BES as an energy-flexible resource was discussed in Section 2.3. For efficient BES dispatch and accurate evaluation of the BES utilization, it is important to consider both real-life performance and lifetime degradation of the BES, something which has not been investigated in published literature on optimal MG energy management, as was pointed out. This research gap is highlighted in the question RQ-2, which is addressed in the thesis. The literature survey also identified the drawbacks of the previous studies in realistically representing the BES degradation cost. Overcoming these issues is significant for answering RQ-3 in Section 1.4.

Although the development of forecast models was outside of the scope of the thesis, the effect of short-term and high-resolution load forecasting was evaluated in a comparative study in order to address RQ-4 in Section 1.4. In particular, a comparison of the two main optimization techniques in MG energy management i.e, DO and SO, under different solution approaches for short-term and high-resolution load forecasting was lacking from the literature.

As the literature review in Section 2.4 showed, the optimal MG flexibility dispatch has rarely been integrated in the energy dispatch problem to quantify the economic value of flexibility for the MG. Studies mostly focus on estimating the technically available flexibility or take into account its economic impact to the energy dispatch of the DERs. The technically available flexibility refers to the estimated flexibility amounts that are feasible according to the technical operation of the DERs as in [38,41,43–46,48]. It can also refer to flexibility which is admissible by the network operation [118] and even further restricted to secure the network's reliability [119]

or robustness against uncertainties [120]. It does not, however, consider the "willingness" of the FSP to offer a specific amount of flexibility i.e., the economically viable or optimal flexibility, which can be less than the technically feasible amount.

Even when studies embed FSs into optimal energy scheduling models, the flexibility potential is not explicitly calculated, leading to a lack of quantification and evaluation of the flexibility, especially at distribution level [121]. The flexibility amount that is dispatched solely depends on the operational limits and the grid operator setpoints, which are usually arbitrarily chosen power exchange references. The research question RQ-5 in Section 1.4 stresses the need for insights regarding the economic value of intra-day flexibility in the presence of uncertainties for the FSP. In addition, an integrated MG energy and flexibility dispatch model, such as the proposed MODEFlex model, has not been employed in the coordinated MGs' operation with the DSO. Therefore, the assessment of the local flexibility which is technically and economically feasible to both the MGs and the DSO has not been studied in depth. However, to answer RQ-6 the flexibility value for both the FSPs and the flexibility procurer needs to be considered in the optimization of the flexibility dispatch, which is why the bilevel optimization framework was proposed in the thesis.

Chapter 3

Methodology

This chapter presents the methodology that was used to solve the optimization problems which are formulated based on the comprehensive MODEFlex model presented in Chapter 4 and are solved in the studies of the thesis given in Chapters 5–8. The chapter first gives an overview of the studies and then illustrates the process of building and validating the optimization model used for the solution of the defined optimization problem. Afterwards, the operational framework of the studied MG system is described and the basic structure of a MODEFlex problem is presented. The chapter also discusses the coordination schemes that can be applied utilizing the DMS interface in order to solve the MODEFlex problem. In the final sections, the chapter introduces the test systems and the set-up used in real-life demonstrations.

3.1 Overview of studies

Depending on the entity that solved the MODEFlex problem, the MG resource mix, the optimization method, and the solution approach that was followed, different test cases were built to be studied in the thesis. The studies are presented in Chapters 5–8. Each of these chapters first introduces the aim of the study, then presents the followed study approach including the formulation of the optimization models utilized in the study, and finally analyzes and discusses the study's results.

Table 3.1 summarizes the methodology of each study. The methodologies, which are later described in detail in the respective chapters, were built based on the procedure described in Section 3.2. The methodology characteristics that are highlighted in Table 3.1 are related to the scheme of coordination with the DSO (see Section 3.5), optimization method (deterministic or stochastic), solution approach (DA or RH, see Section 3.4), and the time resolution, where high resolution refers to time intervals of 5-15 minutes and low resolution refers to one-hour time intervals. All studies used a 24-hour time horizon, except for the study of Chapter 6, where the time horizon could be decreased depending on the availability of the forecasts. Note that Table 3.1 only shows the characteristics of the main methodology used in the simulations of each study and not from other methodologies used in comparative analyses.

Table 3.1: Characteristics of the main methodology employed in each study presented in Chapters 5–8.

	Cordination	Optimization method	Solution approach	Time resolution
Chapter 5	✗	DO	DA	High
Chapter 6	✗	SO	RH	High
Chapter 7	✗	DO	DA	Low
Chapter 8	✓	DO	DA	Low

3.2 Building and validating the MODEFlex model

Figure 3.1 presents the process of building the MODEFlex model by selecting its attributes according to the problem that is to be solved. It also describes the steps that are used to build a test case and validate the performance of the MODEFlex model. The detailed procedure of the develoment and validation of the MODEFlex model is as follows:

- First, the optimization problem that will solve the optimal MG dispatch is formulated and a suitable optimization model needs to be selected for its solution. Both the problem and the model formulation are based on the formulation of the comprehensive MODEFlex model, which is given in Chapter 4. The optimization model might be different than the optimization problem, if some mathematical equations and/or inequalities need to be modified to bring the model to a form that facilitates efficient solution by the available solvers.

- The optimization model is built by selecting the optimization method, the coordination scheme, the objective function and the constraints.

- Once the model is built, the solution approach is selected and, afterwards, the time horizon and time resolution for the dispatch of the MG resources were determined. The selection of the optimization method, the solution approach, and the time horizon and resolution are the most important steps of the methodology because they substantially affect the quality of the implemented control. Therefore, these steps are highlighted in the flow diagram of Figure 3.1.

- A test system is selected and a simulation or demonstration test case is defined based on it to prove the effectiveness of the built model to solve the formulated problem. The test case uses input data from the test system and, if not all data are available, input data from external sources can be used provided that they were representative of the test system and test case. Assumptions related to the lack of data or the problem itself are also defined at this stage.

- The final step is to validate the performance of the model using simulations or demonstrations. The simulation and/or demonstration results are analyzed and processed to present the key findings.

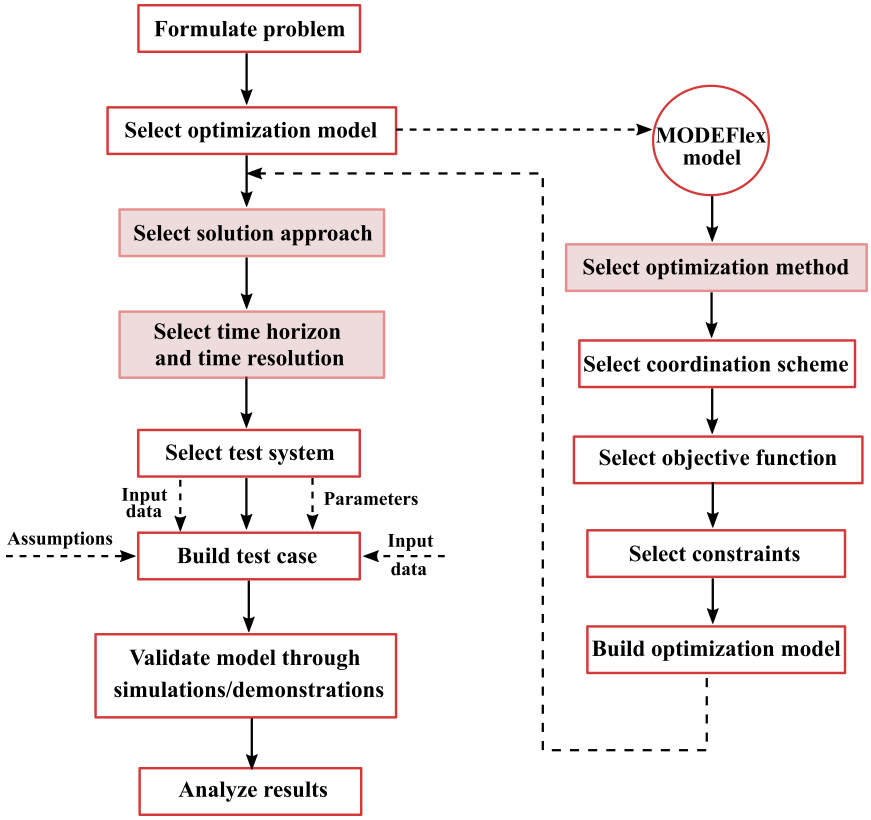

Figure 3.1: Flow diagram of the steps followed to develop and validate the MODEFlex model.

3.3 Description of the MG operational framework

The operational framework of the MODEFlex model assumes that the MG operator is also the owner of the MG's resources and has a contract with an electricity retail provider, which enables energy trading at wholesale electricity market price. Thus, the MG operator can employ ESs to reduce the energy costs of the MG customers performing load shifting and energy price arbitrage. At the same time, the MG operator can have a contract for flexibility provision with a DSO, which purchases and utilizes this flexibility. This contract allows the DSO to request and buy FSs from the MG on a short notice within a day to solve unexpected operation problems or improve operation, utilizing the most recent information (e.g., forecasts). In addition, the DSO can purchase MG flexibility to satisfy balancing needs of the transmission system, although it should be noted that the FSs considered in this thesis are only used by the DSOs. If there are requirements on minimum flexibility amounts that the MG does not meet, the FSs can be offered through an aggregator.

The MODEFlex model can be used in the context of the EaaS business model described in Section 2.5.1 by the third-party MG developer that owns and operates the MG. It can also be used by the operators of privately-owned MGs, which can be prosumers that own flexible resources or building owners and property managers in the case of BMGs. The model can be integrated in an MG-EMS and used for economic dispatch of the flexible MG resources considering participation in ESs or FSs. For this purpose, the MG-EMS solves the MODEFlex problem with or without coordination with the DSO depending on the implemented coordination scheme (see Section 3.4). The solution yields a set of power dispatch set-points that maximize the economic benefits of the MG customers, whose electricity demand is satisfied from the MG resources and the upstream grid connection. Based on these set-points, the MG-EMS controls the MG resources using the values of the electricity price, generation and consumption as inputs. If these inputs are not deterministic, forecasts are used instead. The mix of the MG's resources can include BESs, DRRs, non-dispatchable generation sources (such as PV systems and wind turbines), and dispatchable generation sources such as conventional diesel generators, micro-turbines and micro-CHP plants.

3.4 Structure of the energy and flexibility dispatch problem

The fundamental structure of the MG energy and flexibility dispatch problem is depicted in Figure 3.2. The selection of the look-ahead time horizon depends on the accuracy of the forecast values of load and non-dispatchable generation. The time horizon is discretized and represented by a set of time discretization steps, which can simply referred to as time steps. Thus, the time horizon is divided in time intervals i.e. time periods represented by the time steps. The number of time steps depends on the selected time resolution and usually, although not necessarily, correspond to the frequency update of the dispatched set-points and the resolution of the input

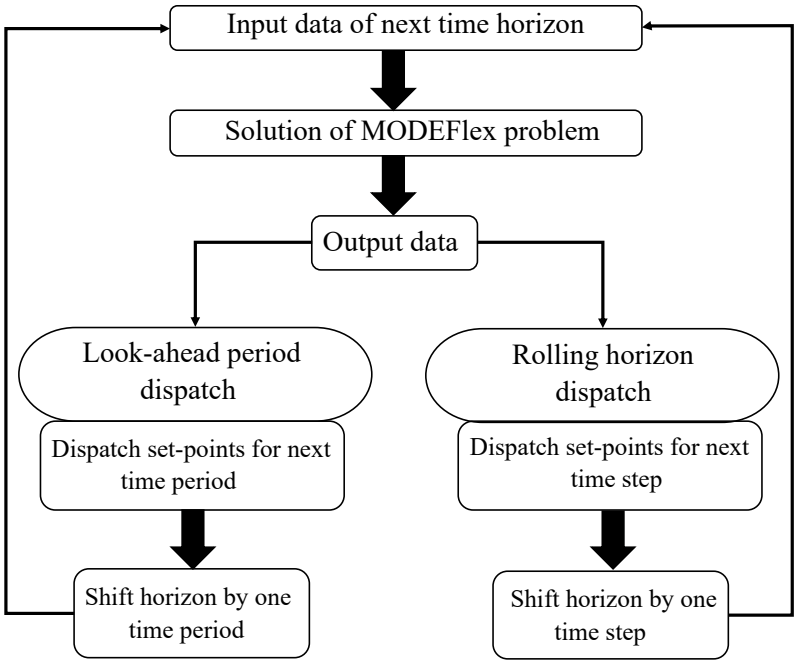

Figure 3.2: The basic structure of the MODEFlex problem.

data. The forecast profiles of load and generation and the uncertainties of their fluctuation should be considered to choose an appropriate time resolution.

There are two solution approaches with regard to how the set-points are dispatched: the look-ahead period dispatch, which can also be called open-loop (OL) dispatch, and the RH dispatch, which can be considered as a closed-loop (CL) dispatch. In both approaches, the optimization is performed for a look-ahead period. In the OL dispatch, all the set-points within the considered time horizon, which are retrieved by the solution of the optimization problem, are dispatched. The look-ahead period can be one hour, one day (i.e., DA dispatch), one week or even a month. In the RH approach (Figure 3.3), there is one simulation for the solution of the MODEFlex problem, before each time interval. The set-points for the first time step are dispatched to the MG resources after each simulation, while the time horizon is shifted forward by one time step for the next simulation. The remaining set-points of each simulation are advisory and can be discarded or used in case of unexpected failures to update them. The input data are updated at each time step to consider values that were outside of the time horizon previous simulation, as the horizon of the new simulation is shifted forward, and potential changes/updates in the forecasts or estimation of network and DERs states. Thus, the MG-EMS can receive feedback from th RH approach which can reduce the impact of forecast errors to the MG's operation cost by both renewing the input values and dynamically adjusting

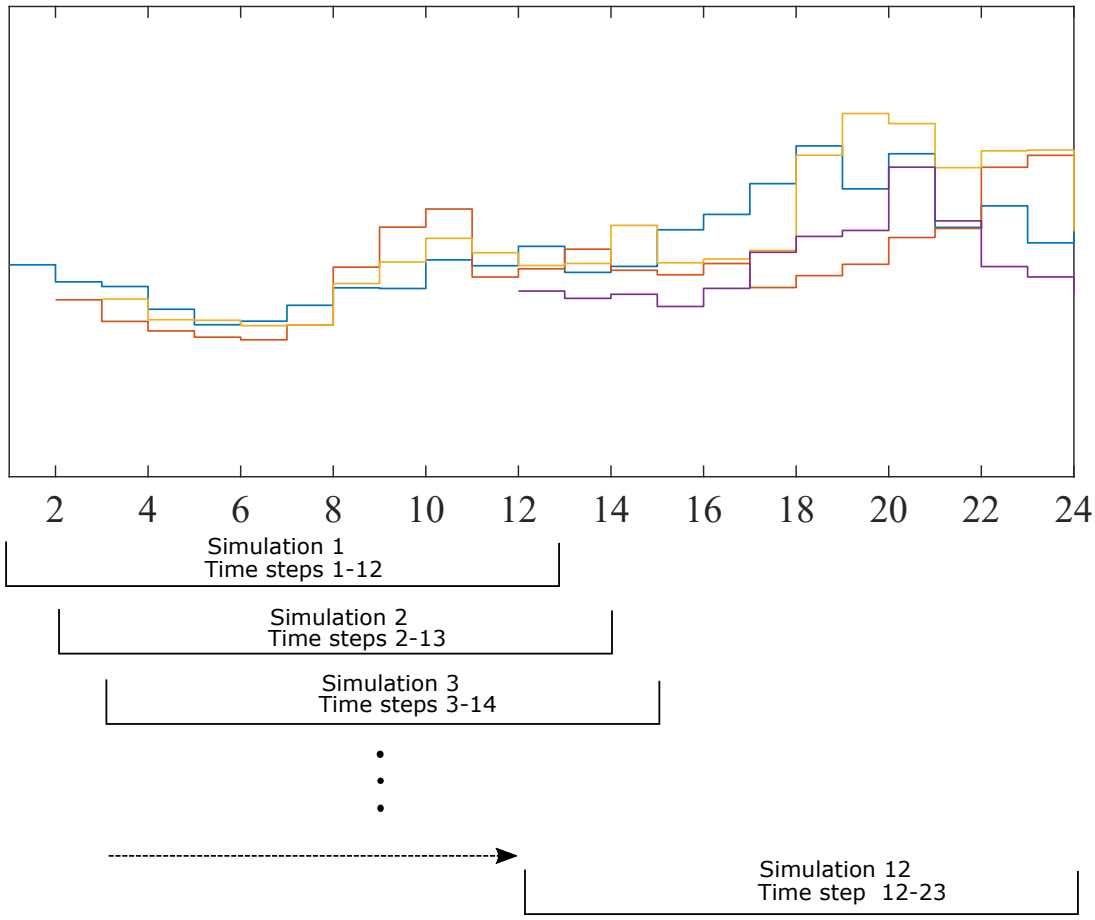

Figure 3.3: The RH approach (each simulation shifts forward in time).

the set-points at each time step. Note that the term RH often appears under the name "model predictive control" in literature [122], typically when the problem is formulated using state-space representation instead of mathematical programming, which will be used for the formulation of the SO model in the thesis.

The RH dispatch be considered as close to real-time dispatch if used with a sufficiently high resolution e.g., 15-minute or smaller time intervals. Energy management schemes with time intervals which are shorter than 5 minutes can be classified as real-time energy management schemes [24, 56] when the RH approach is adopted.

3.5 Coordination schemes

The MG-EMS retrieves the reference set-points, which are obtained from the solution of the MODEFlex problem, and transmits them to the MG resources using the available communication links (see Figure 3.4). The MG-EMS has an interface with the DMS, which is used for the integration of the MG to the distribution system, since the MG operator is a different entity from the DSO.

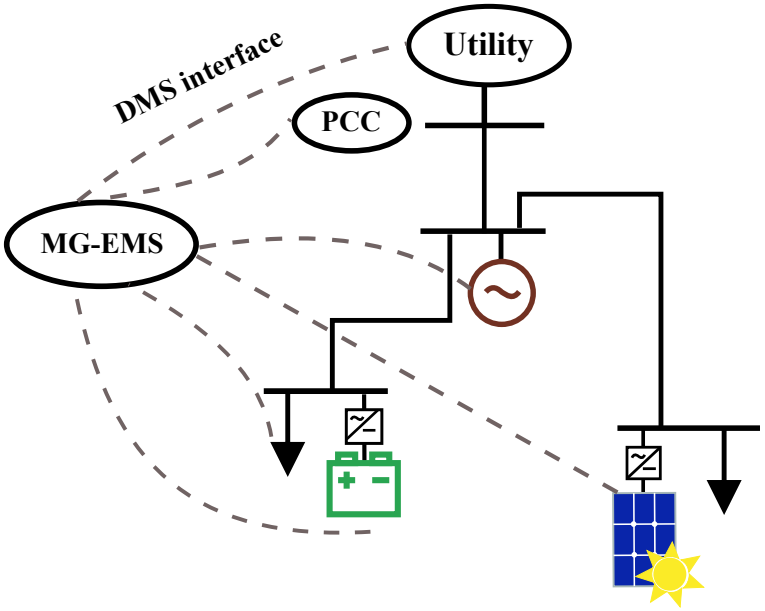

Figure 3.4: The communication infrastructure of the MG-EMS.

The proposed architecture for the integration of the MG to the distribution system can be seen in Figure 3.5, which is a schematic representation of the interface between the MG-EMS and the DMS. Two-ways communication is always assumed between the MG-EMS and the DMS, even if there is no interaction i.e., the decisions or actions of one entity do not affect the decision or actions of the other. No communication or interaction is considered between different MG-EMSs i.e., the MG-EMSs can only interact with the DMS. Three different schemes of coordination between the MG-EMS and the DMS are depicted in Figure 3.5. Coordination is based on interaction between the MG-EMS and the DMS through information exchange which is enabled by the interoperability between these entities. The grid-connected MGs might utilize the same coordination scheme for their interaction with the DSO or each MG might utilize a different scheme, depending on the agreement between the DSO and the MG operator. These coordination schemes, which affect the formulation and solution approach of the energy and flexibility dispatch problem, can be described as follows:

- **No coordination:** The MG-EMS solves the MODEFlex problem and dispatches the MG resources according to this solution.
- **Centralized coordination:** It is assumed that the MG-EMS empowers the DMS to dispatch the MG resources. The MG-EMS receives the reference set-points from the DMS and then transmits them to the MG resources.
- **Decentralized coordination:** The DMS does not directly dispatch the set-points of the MG resources. Instead, it indirectly affects them by transmitting price signals (e.g., flexibility prices, penalties) or the reference values for the desired power exchange at the MG's PCCs. Using this information as an input, the MG-EMS obtains the set-points by solving the MODEFlex problem and

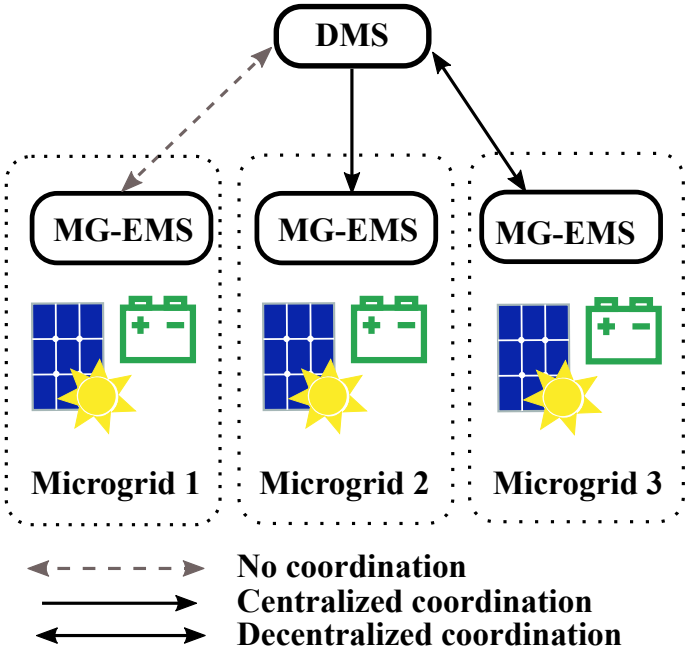

Figure 3.5: The integration of the MG-EMS to the DMS.

transmits them to the MG resources.

The above classification is based on the coordination/interaction with the DSO for the purpose of dispatching the MG resources and, therefore, information exchange for the solution of the MODEFlex problem is not considered. A coordinated operation, whether centralized or decentralized, is assumed when at least one of the following requirements is satisfied: 1) *high amount of shared data*, 2) *high frequency of shared data updates*, and 3) *event-based information exchange*. More than one data update within a day is considered high frequency for this classification. Furthermore, if the DSO requires extended information from within the MG such as resource capacities, technical constraints, network configuration, and forecasts of consumption or generation, then the amount of data exchange is high enough to classify the operation as coordinated even if there is no frequent signal transmission that would require extensive communication infrastructure.

3.6 Test systems

This section presents the test systems that were used in the simulations studies presented in Chapters 5–8. The test systems include two real residential buildings representing BMGs with PV systems and a BES, the real distribution network of the Chalmers University of Technology campus, where network areas were considered as grid-connected MGs, and a 33-bus radial distribution standard network, which has often been used in literature, modified with the addition of grid-connected MGs.

Figure 3.6: The facade of the HSB LL building.

3.6.1 HSB Living Lab

The HSB Living Lab (HSB LL) building [114, 115] is a multi-family residential building (Figure 3.6) of 29 apartments housing 40 residents, which serves as a testbed for sustainable living solutions and is located at the campus of Chalmers University of Technology. A 7.2 kWh BES with 6 kW charging/discharging power limits is installed on the top floor of the building, while solar panels of an 18 kWp PV system are mounted on its rooftop and facade. Figure 3.7 shows the DC/DC converters of the solar strings and the DC/DC converter of the BES, which are connected to the upstream AC grid (400 V) via a converter provided by the Ferroamp company [113].

The grid side converter, which is shown on the top-right side of Figure 3.7, has bi-directional operation, since the solar energy and the BES stored energy can be exported to the upstream AC grid and, in addition, the BES can be charged through both the upstream AC grid and the PV system (see Figure 3.8). The converter-embedded controller, which is called EnergyHub, is coupled with sensors that monitor the DC/DC converters of the solar strings and the BES as well as the building consumption and power exchange with the grid. The measurements of PV generation, BES power, building load, and power exchange with the grid are collected with a time resolution of 1 sec. In 2019, the building electricity consumption was 84.2 MWh (the daily demand ranged from 162 kWh to 384 kWh), and the local energy production of the solar panels was 12.3 MWh, out of which 0.7 MWh was exported to the grid. The peak building consumption (minute average) was 32 kW, while the peak PV power output that was recorded was 13 kW (minute average). The characteristics of the HSB LL BMG are summarized in Table 3.2.

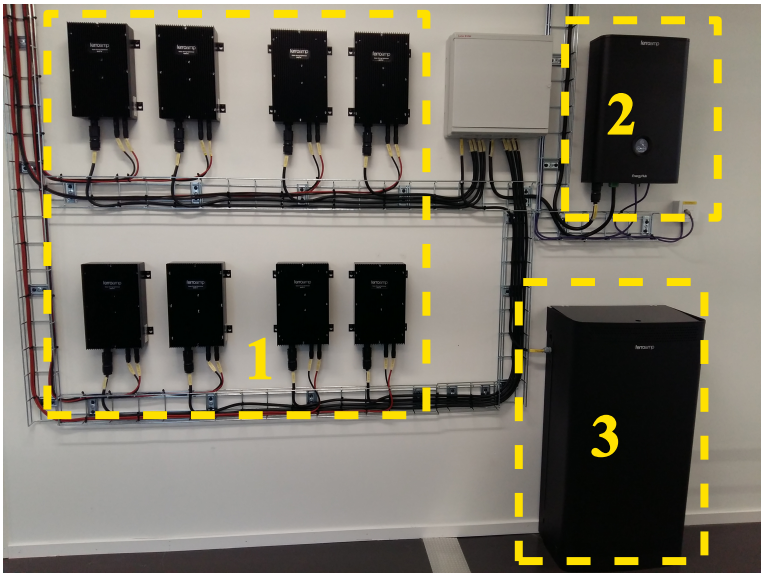

Figure 3.7: The basic components of the HSB LL BMG: 1) the DC/DC converters of the solar strings, 2) the bi-directional grid side converter, and 3) the BES with the integrated DC/DC converter.

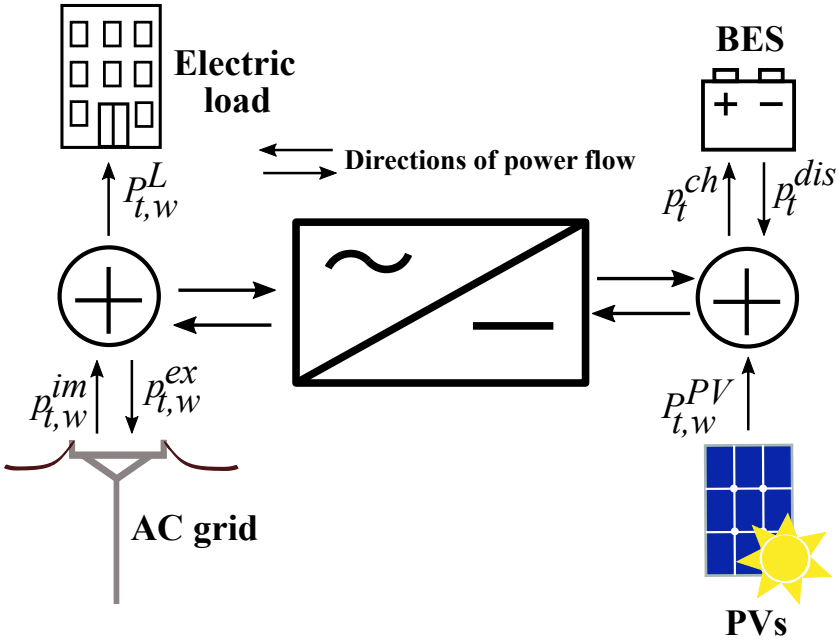

Figure 3.8: Power flow of the BMG.

Table 3.2: Load Demand and DERs of the HSB LL BMG.

BES capacity (kWh)	7.2
BES energy to power ratio (h)	1.2
Daily electricity consumption (kWh)	162-384
PV capacity (kWp)	13
Peak demand (kW)	32

Figure 3.9: The Brf Viva buildings in Guldheden, Gothenburg (photo courtesy of Ulf Celander and Riksbyggen).

3.6.2 Brf Viva

The Brf Viva is a housing association of six buildings (shown in Figure 3.9), which are in Guldheden, an area close to the campus of Chalmers University of Technology. The buildings consist of 132 residences inhabited since 2018 [116].

The study is based on the 170.8 kWp PV system, which has been installed for local electrical energy production and the 14 second-life Li-ion BESs (Figure 3.10), each with a rated capacity of about 14 kWh and a maximum charge/discharge power of 6 kW, which have been installed to increase the PV self-consumption and reduce the peak demand. The BESs have been taken from old electric buses (provided by Volvo Buses). The DC/DC converters of the solar strings and the DC/DC converter of the BESs are connected to the upstream AC grid via a 168 kVA multi-level converter provided by Ferroamp [113]. Similar to the HSB LL building, the grid side converter of the Brf Viva BMG has bi-directional operation and the BESs can be charged through both the upstream AC grid and the PV system. The converter controller i.e., the EnergyHub system, is coupled with sensors and provides measurements of PV generation, power of the 14 BES system, building load, and power exchange with the grid. In 2019, the building electricity consumption was 162 MWh, and the local energy production of the solar panels was 72 MWh, out of which 11 MWh was exported to the grid. The peak building consumption (minute average) was 198 kW, while the peak PV power output that was recorded was 129 kW (minute average).

3.6.3 Electrical distribution system of Chalmers University of Technology

The 12-kV distribution network of Chalmers University of Technology, which will be referred to as "Chalmers" throughout the remaining of the thesis, is illustrated in Figure 3.11. The electrical load demand, which is supplied by the electricity distribution system of Chalmers varies between 2.5 and 6 MW. The load is supplied by

Figure 3.10: The second-life Li-ion batteries of Brf Viva.

importing energy from the upstream distribution grid and, in addition, by electricity generated through a micro-CHP plant and solar panels. The micro-CHP plant has heating power capacity of 9000 kW, while the electrical capacity of the steam turbine is 0.5-1.0 MW (the heating or electrical operational power output depends on the choice of fuel). The micro-CHP plant is out of operation between April-September, as its boilers are primarily scheduled for heating energy production. The total PV capacity is 831 kWp and the majority of the solar panels have been installed on rooftops of the campus's buildings, with only a few solar panels of 16 kWp total capacity mounted on the wall of a building. The network also hosts two BESs with energy capacity of 200 kWh and 100 kWh and 35 PEV charging points at 32 A/22 kW and 16 A/3.7 kW level, located at two different charging stations. The facilities include an advanced metering infrastructure (AMI) system that consists of an ABB MicroSCADA and smart meters. The buildings of Chalmers are also equipped with various energy meters as well as controllable devices that enable the building operator to control the heating, cooling, and ventilation system.

3.6.4 33-bus distribution network

This test system is a 12.6-kV 33-bus radial distribution network first presented in [123]. The 33-bus network was modified to include three grid-connected MGs at the distribution buses 13, 18, and 30, as can be seen in Figure 3.12, and the BESs of these MGs had an energy-to-power ratio of 17.2kWh/14.4kW, 25.9kWh/21.6kW, and 134.9kWh/111.76kW, respectively.

3.7 Real-life demonstrators

The HSB LL and Brf Viva BMGs described in Section 3.6.1 and Section 3.6.2 were also used as demonstrators. A schematic diagram of the communication and control set-up used at each BMG testbed can be seen in Figure 3.13. The Message Queue Telemetry Transport (MQTT) protocol, which runs on top of Transmission Control Protocol/Internet Protocol (TCP/IP), was used for real-time data sharing between the server, where the BMG-EMSs were implemented, and the grid side converter at

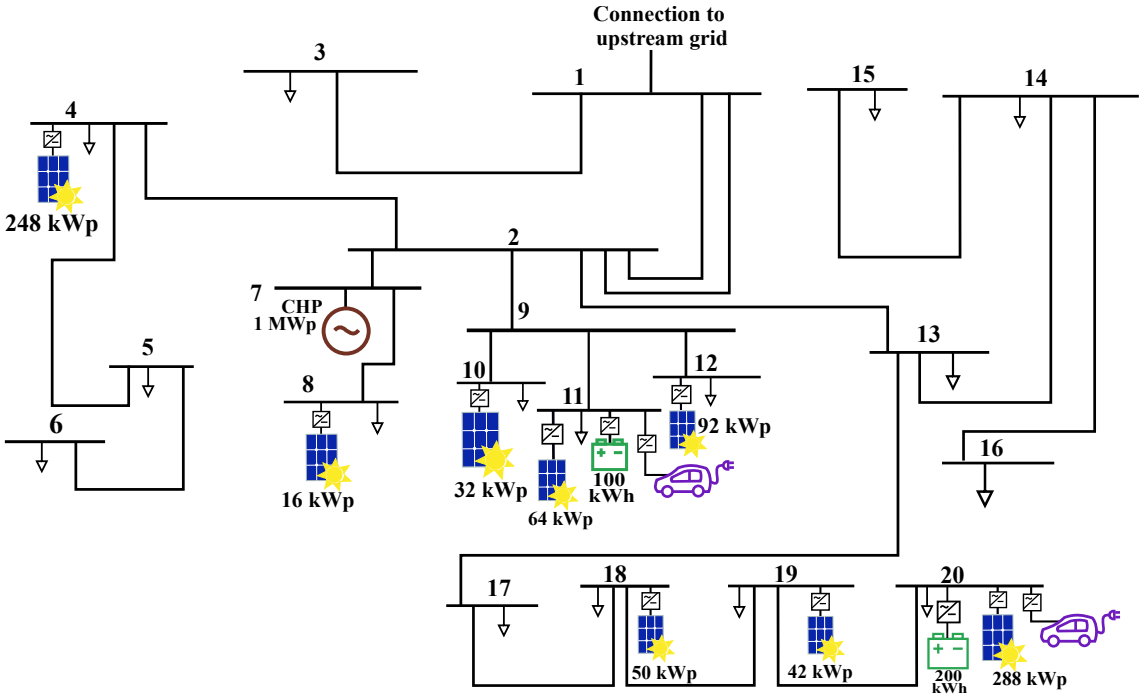

Figure 3.11: The configuration of the distribution network of the Chalmers University of Technology campus.

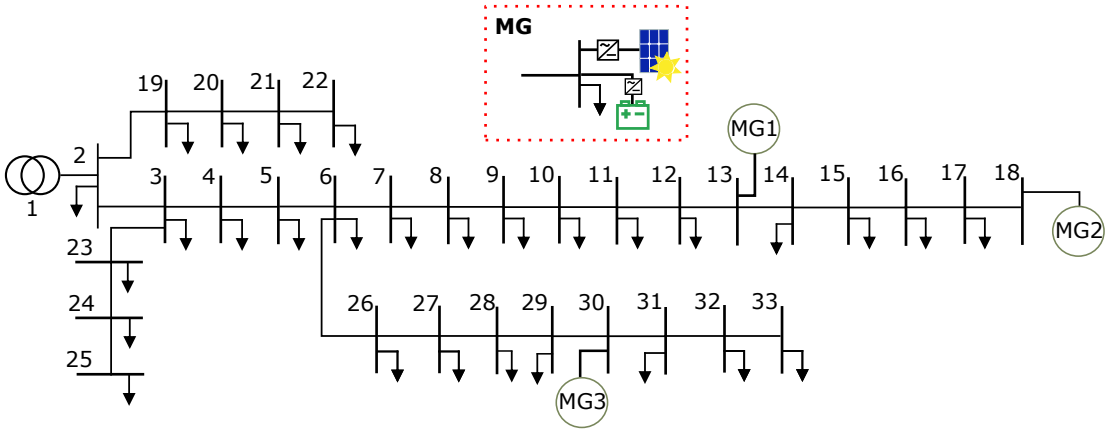

Figure 3.12: The modified 33-bus network with three grid-connected MGs.

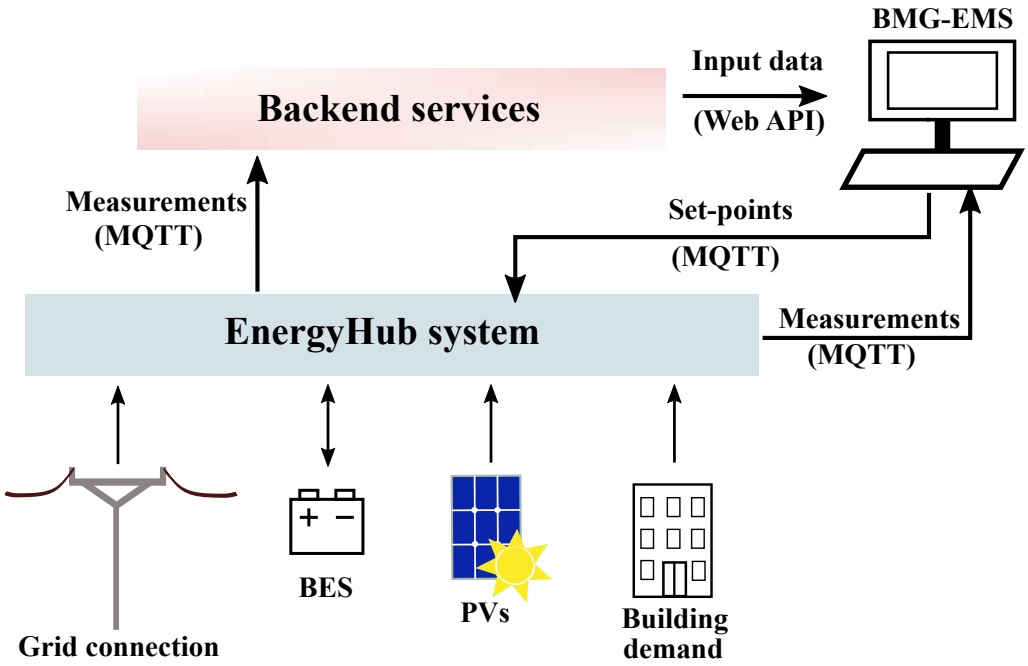

Figure 3.13: Communication and control interface set-up of the BMG.

each demo site. The MQTT protocol is a "machine-to-machine (M2M)/"Internet of Things" connectivity protocol [124], which was designed for lightweight and low power message transport and is therefore very useful for remote control applications. With the MQTT protocol the BMG-EMS could interact with the EnergyHub system at each demonstration site to receive real-time measurements as input for the energy scheduling problem, as well as send commands i.e., BES power set-points.

The server interfaced MATLAB [125] to set up the communication and control interface with the test site. An MQTT publisher/subscriber (also called MQTT client) was built in MATLAB to interact with the MQTT broker run at the controller of each grid side converter. The MATLAB subscriber read real-time measurements that the MQTT broker transmitted in different topics. The MATLAB publisher sent control commands i.e., BES power requests, to the MQTT broker, which would then send these requests to the DC/DC converters of the BESs. The data that the MQTT client and the MQTT broker exchanged were encoded in JSON format. In addition to the MQTT protocol, HTTP requests could be used to retrieve historical data, which were stored in an SQL-database, with the help of a web application programming interface (API). A MATLAB to GAMS [126] interface was used for data exchange with the optimization models and for retrieving the BES scheduling solution, which included the BES power set-points that were dispatched in an online manner. The server interfaces that were employed for the demonstrations can be seen in Figure 3.14.

The data exchange with MQTT is very fast, and the control set-points were received by the broker in about 50-200 msec (from measurements with the HSB LL BMG-EMS the average response was 130 msec). The process of the command by the converter-embedded controller took about 10 sec. After that, the control signal

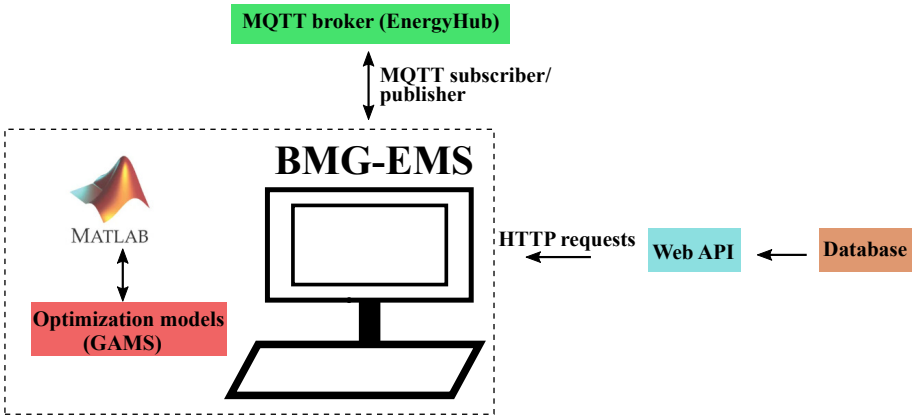

Figure 3.14: The server interfaces that enabled interaction of the BMG-EMS with the grid side converter and the database.

was transmitted to the BES DC/DC converter through power line communication (PLC), which also added a delay to the dispatch of the set-point. Once the battery management system (BMS) was actuated, the desired value was reached in about 10 sec depending on the BES status and the amount of requested power. The results showed a total delay of 30-40 sec to the dispatch of the BES set-point. This delay is acceptable for close to real-time energy management applications, where the time scale is usually 5-15 minutes.

As already explained, interoperability was not the main focus of the thesis. Therefore, in order to replicate the designed interface set-ups at different testbeds, related ontologies developed for standards such as SAREF, OpenADR, DELTA, CIM, etc., can be used to ease the integration with control and measurement systems operating under heterogeneous standards and guarantee the interoperability of these systems [127]. The description of these systems according to these ontologies can be easily incorporated in the backend services platform employed in the demonstrations, which was based on the open-source FIWARE software [128].

Chapter 4

Model Formulation

This chapter presents the comprehensive MODEFlex model i.e., the optimization model developed to solve the problem of energy and flexibility dispatch of grid-connected MGs. The comprehensive MODEFlex model is presented in its stochastic formulation and, therefore, uncertainty modeling approaches are discussed in the beginning of the chapter. The MG's optimization problem is solved by the MG-EMS which integrates an optimization model derived from the MODEFlex model. However, the solution can also be affected or even directly implemented by the DMS of the DSO depending on the level of interaction between the MG and the DSO. Hence, the optimization models employed for the optimal operation of the DSO's grid are also presented separately. At the end of this chapter, the MGs' and the DSO's grid optimization models are used to formulate the bilevel optimization multi-follower problem for the optimal allocation and dispatch of MGs' flexibility. The equivalent single-level optimization problem is also derived.

4.1 Uncertainty modeling

The main uncertainty modeling approaches that have been used in MG energy management studies include [129]: 1) *scenario-based SO and robust optimization (RO)*, where it is assumed that uncertainty is adequately characterized by a set of future event scenarios each of them associated with the probability of occurrence of the event, 2) *adaptive RO and chance-constrained optimization (CCO)*, which use uncertainty sets to constrain the operating points, 3) *Markov decision processes (MDPs)*, where the uncertainty is only modeled for the next-step decision, and 4) *reinforcement learning (RL)*, which observes (instead of explicitly modeling) uncertainty. Depending on the application these approaches can offer advantages regarding computation time, feasibility, and solution cost. Below is the description of the most common uncertainty modeling approaches and their comparison with the scenario-based SO optimization, which was used in the proposed MODEFlex model.

4.1.1 Optimization approaches

The main drawbacks of RO and CCO are the too conservative (and by extent costly) solutions of the former and the arbitrarily chosen constraint violation levels of the latter. On the other hand, one major benefit of RO and CCO against SO is that they can yield simplified equivalent reformulations of the original optimization problem and reduce its complexity. However, the stochastic MODEFlex model presented in this thesis already considerably reduces the size of the problem. This is achieved by eliminating the "wait and see" decision variables which are used in classical SO; the future scheduling plan consists of deterministic control variables and the only stochastic variables are the imported and exported MG power which are affected by the deterministic control variables and the stochastic inputs (load, PV generation), as shown in the mathematical formulation in Section 4.2. In other words, the model considers look-ahead uncertainty thanks to the stochastic formulation and, instead of considering real-time uncertainty realization, control adjustments are dynamically being implemented with the RH approach to deal with close to real-time uncertainty. In addition, the scenario generation and reduction technique which is presented at the end of this section further improves the performance of the model by reducing its size. Therefore, it was computationally efficient to perform SO in RH with the proposed model and, since the performance of RO and CCO is heavily dependent on the underlying characteristics of the probability distribution function [14, 130], their computational advantage would be trivial.

Apart from faster execution, thanks to its deterministic control the proposed SO model also offers certainty of feasible solutions in out-of-sample analysis assuming that the system is properly dimensioned to avoid exceeding the PCC capacity. Therefore, the other advantage of CCO against classical scenario-based SO, which is the guaranteed satisfaction of the problem's constraints for a specific percentage of the scenarios [131] in out-of-sample analysis, is not relevant for the proposed model.

4.1.2 Markov decision process

In this case, the problem is formulated in state-space representation and the system state as well as the control output need to be discretized. This leads to the problem well-known as "curse of dimensionality" i.e., to improve the quality of the control more discrete points must be considered which crucially expands the size and the computation time. Formulating the energy scheduling of an MG as an MDP also enables to solve the problem in RH, as was done in [132], by changing the control strategy or trajectory at each time step depending on the latest forecast information. However, these strategies are pre-determined, whereas solving the SO problem in RH results in a new optimal strategy at each time step.

4.1.3 Reinforcement learning

Built on MDP, the optimal strategies are defined without full knowledge of the uncertainty model [133] (or even the MG system). They are rather defined through observation and, therefore, a lot of information is needed as an input to train the

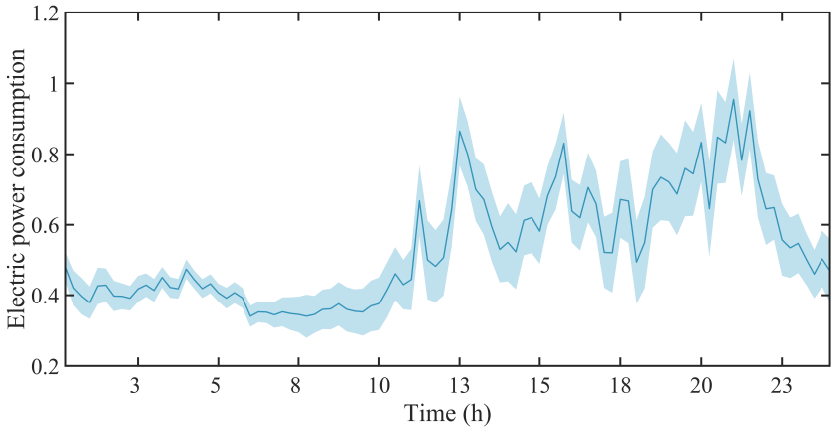

Figure 4.1: Scenarios of electric load (given as ratio of the peak load) over a scheduling period. The base forecast is shown by the dark color line and one standard deviation is shown by the light-shaded areas.

RL models, so that they can choose the best "action" i.e., next-step control decision, "on the go". Similar to MDP, the control actions are pre-determined unless the RL model is trained online, which is typically time-consuming.

4.1.4 Scenario generation and reduction

In order to model stochasticity in scenario-based SO, which is the uncertainty modeling approach used in this thesis, the probability distribution of forecast errors of the variable input data must be known. A common practice employed by many studies e.g., [48, 134], is to assume that these errors follow Gaussian distributions. Other studies use scenario generation algorithms to capture stochasticity and correlations among historical data [135]. To represent the uncertainty associated with the input values in the thesis, the DA forecast errors of PV generation and power consumption are assumed to follow Gaussian distributions. Based on the distributions of forecast errors, a number of scenarios are generated using the Monte Carlo (MC) method i.e., random sampling of the input variables (taken from their most recently updated forecasts) with the added noise to represent the forecast error. The input values are the most recently updated forecast profiles, which have the same time resolution as the time horizon of the simulation i.e., the same number of time discretization steps. The available forecast profiles, which are naturally not perfect, are used as base scenarios and a Gaussian random number generator is used to generate an error for each time step. The values of the base scenarios at each time step are then adjusted according to the generated errors and the outcome is one future event scenario of electricity load and PV generation. This process is then repeated to generate all scenarios. One example of the generated scenarios for a scheduling period can be seen in Fig. 4.1.

After the scenario generation, a scenario reduction technique is used to create a reduced number of scenarios which are not equiprobable i.e., a different probability

of occurrence is assigned to each scenario by the scenario reduction technique. The resulting set of reduced scenarios is representative of the real variability of the input values. Thus, scenario reduction contributes to reducing the size of the SO problem without substantially compromising the accuracy of the results.

4.2 Optimization model for grid-connected MGs

The MG-EMS that integrates the MODEFlex model is designed to control the electrical power supply of the MG loads and the electrical power exchange with the connected main distribution grid. The MG operators seek to optimally schedule the available DERs, while satisfying power balance within the MG and the operational constraints of the resources. The DERs considered in this work include: a bio-fuel based micro-CHP plant, PV systems, BESs and DRRs. Note that the following conventions are used in this section:

- To present the MODEFlex model in a compact form, some equations contain two parts i.e., "a" and "b". Part "a" refers to the equation used in the deterministic MODEFlex model, while part "b" refers to the equation used in stochastic MODEFlex model.
- The definition of the variables is given with all the indices that can be associated to them.
- Expected cost or values only refer to the stochastic MODEFlex model.
- The dual variables λ and μ, which are associated with equality and inequality constraints, respectively, are only given for the constraints that will also be used in the bilevel optimization problem in Section 4.4.3. The inequality constraints that will be used in the bilevel optimization to derive the KKT conditions are described together with their complementarity slackness (CS) conditions. The CS constraints are not part of the primal problem.

4.2.1 Objective functions

In this section, two generic objective functions are formulated depending on the main operational target of the MG owner/operator. The first objective function is cost minimization, which can alternatively be formulated as profit maximization, and is related to economic operation targets. The other objective function is the energy exchange minimization and is related to the desired level of interaction between the MG and the main grid.

The objective function for *(expected) cost minimization* is:

$$\min f_m = c_m^{im} - r_m^{ex} + c_m^{p} + c_m^{DER} - r_m^{flex}, \tag{4.1}$$

$$c_m^{im} = \sum_{t\in\mathcal{H}} (\Lambda_t + C^{im}) p_{tm}^{MG,im} \Delta t, \tag{4.2a}$$

$$c_m^{im} = \sum_{t\in\mathcal{H}} \sum_{w\in\mathcal{W}} \Pi_{wm} (\Lambda_t + C^{im}) p_{wtm}^{MG,im} \Delta t, \tag{4.2b}$$

$$r_m^{ex} = \sum_{t\in\mathcal{H}} (\Lambda_t + C^{ex}) p_{tm}^{MG,ex} \Delta t, \tag{4.3a}$$

$$r_m^{ex} = \sum_{t\in\mathcal{H}} \sum_{w\in\mathcal{W}} \Pi_{wm} (\Lambda_t + C^{ex}) p_{wtm}^{MG,ex} \Delta t, \tag{4.3b}$$

$\forall m \in \mathcal{M}_i$, where $\mathcal{M}_i$ is the set of the MGs' PCCs with the distribution network (assuming that each MG only has one PCC with the distribution network and no PCCs with other MGs), $\mathcal{H}$ is the look-ahead time horizon, and Δt is the time interval. The positive variables $p_{wtm}^{MG,im}/p_{wtm}^{MG,ex}$ denote the MG imported/exported power from/to the upstream network through the PCC at bus m, at time step t and scenario w, while Π_w is the probability of occurrence of scenario w.

In (4.1), the first term (c_m^{im}) is the (expected) cost of the imported energy and the second term (r_m^{ex}) is the (expected) revenue associated with the energy exported to the grid. The term c_m^{DER} refers to variable operation costs associated with the DER owned by the MG (e.g., fuel costs, degradation costs) and r_m^{flex} is the (expected) reward for providing flexibility. Eq. (4.2)–(4.3) analytically present the values of c_m^{im}, r_m^{ex}, and r_m^{flex}. The electricity wholesale market is denoted by Λ_t, while C_i is the grid charge for energy transmission (grid utilization), and C_e is the reimbursement fee paid by the DSO as an incentive to reduce network losses. Finally, c_m^{peak} is the (expected) cost of the peak power drawn from the main grid, which satisfies:

$$c_m^{peak} \geq \Lambda^{peak} p_{tm}^{MG,im}, \ \forall m \in \mathcal{M}_i, \ t \in \mathcal{H}, \tag{4.4a}$$

$$c_m^{peak} \geq \Lambda^{peak} \sum_{w\in\mathcal{W}} \Pi_w p_{wtm}^{MG,im}, \ \forall m \in \mathcal{M}_i, \ t \in \mathcal{H}. \tag{4.4b}$$

In (4.4), Λ^{peak} is the power tariff, which is linked to the (expected) maximum average power of the studied period (measured per Δt).

The objective function for *(expected) energy exchange minimization* is:

$$\min \sum_{t\in\mathcal{H}} (p_{tm}^{MG,ex} + p_{tm}^{MG,im}) \Delta t, \ \forall m \in \mathcal{M}_i, \tag{4.5a}$$

$$\min \sum_{t\in\mathcal{H}} \sum_{w\in\mathcal{W}} \Pi_w (p_{wtm}^{MG,ex} + p_{wtm}^{MG,im}) \Delta t, \ \forall m \in \mathcal{M}_i. \tag{4.5b}$$

An MG that minimizes the energy exchange with the distribution grid aims at increasing the level of autonomy, as zero energy exchange indicates the possibility of off-grid operation provided that the MG has islanding operation and control capability. Besides the capacity and the technical constraints of the MG resources, the choice of time horizon and solution approach i.e., if the scheduling problem is solved one-period ahead or in RH, can also affect the level of autonomy. If the variable $p_{wtm}^{MG,ex}/p_{tm}^{MG,ex}$ is omitted from (4.5), then the MG operator aims to minimize imported energy, which is equivalent to maximizing the use of MG resources. If the variable $p_{wtm}^{MG,im}/p_{tm}^{MG,im}$ is omitted instead i.e., the aim is to minimize exported energy, the objective function becomes equivalent to the *maximization of self-consumption*.

4.2.2 Power balance

An MG connected at bus $m \in \mathcal{M}_i$ must satisfy (4.6)–(4.7) $\forall t \in \mathcal{H}$ to ensure that the electricity consumption of the MG customers is supplied through the MG resources and through the connection with the upstream distribution grid:

$$p_{tm}^{G}+P_{tm}^{PV}+p_{tm}^{dis}+p_{tm}^{DR}-P_{tm}^{L}-p_{tm}^{ch}+p_{tm}^{MG,im}-p_{tm}^{MG,ex}=0, \qquad : \lambda_{tm}^{APB}, \quad (4.6a)$$

$$p_{tm}^{G}+P_{wtm}^{PV}+p_{tm}^{dis}+p_{tm}^{DR}-P_{wtm}^{L}-p_{tm}^{ch}+p_{wtm}^{MG,im}-p_{wtm}^{MG,ex}=0, \qquad : \lambda_{wtm}^{APB}, \ \forall w \in \mathcal{W}, \quad (4.6b)$$

$$q_{tm}^{G} + q_{tm}^{DR} - Q_{tm}^{L} + q_{tm}^{MG,im} - q_{tm}^{MG,ex} = 0 \qquad : \lambda_{tm}^{QPB}, \quad (4.7a)$$

$$q_{tm}^{G} + q_{tm}^{DR} - Q_{wtm}^{L} + q_{wt}^{MG,im} - q_{wtm}^{MG,ex} = 0 \qquad : \lambda_{wtm}^{RPB}, \ \forall w \in \mathcal{W}. \quad (4.7b)$$

Constraint (4.6) defines the active power balance, where the variables p_{tm}^{G}, p_{tm}^{dis}/p_{tm}^{ch}, and p_{tm}^{DR} refer to electrical power output from the CHP plant, BES charging/discharging power, and power from DRRs, respectively, while the parameters P_{wtm}^{PV} and P_{wtm}^{L} refer to active power from PV generation and active load demand, respectively. Note that p_{tm}^{DR} is positive when power consumption from DRRs is curtailed and negative when it is increased. The PV systems are non-dispatchable generation sources and can therefore be viewed as negative loads. They operate at fixed (unitary) power factor and they do not participate in Volt/Var control. Moreover, it is assumed that the BES draws power from both the main distribution grid and the PVs and injects power into both the main grid and the MG's consumption points. Constraint (4.7) defines the reactive power balance, where constant power factor is considered for generation and load (flexible and inflexible). The variables q_{tm}^{G} and q_{tm}^{DR} refer to reactive power from the CHP plant and reactive power of DRRs, respectively, while parameter Q_{wtm}^{L} refers to reactive power of load demand.

4.2.3 Combined heat and power plant

A CHP plant is a source of heat and electrical power. It is considered that the micro-CHP used in this thesis is primarily scheduled for heating energy production.

When there is generation of heat, the electrical power output of the CHP plant can be controlled and is constrained by

$$P_m^{G,min} \leq p_{tm}^G \leq P_{tm}^H R_m^{CHP},\ m \in \mathcal{M}_i,\ \forall\ t \in \mathcal{H}, \tag{4.8}$$

where $P_m^{G,min}$ is the minimum electrical power output and P_{tm}^H is the heating output, which is treated as a parameter. Constraint (4.8) is only effective, when there is generation of heating power. The parameter R_m^{CHP} is the ratio of electrical power to heating power output, which depends on the type of fuel and the operating point of the electric generator.

When the micro-CHP plant is a part of the MG's resource mix, the term C_m^{CHP} is added as part of the term c_m^{DER} in (4.1), where

$$C_m^{CHP} = \sum_{t \in \mathcal{H}} C_m^f P_{tm}^H,\ m \in \mathcal{M}_i \tag{4.9}$$

and C_m^f refers to the fuel cost of the CHP plant. Although C_m^{CHP} is not affected by the solution of the MODEFlex problem, the cost of the MG is affected by the electrical power output of the CHP, since the power exchange with the grid and potentially the peak imported power are also modified.

4.2.4 Demand response

The model for load flexibility is equivalent to a generic energy storage model and is described by the constraints on the energy that is available for DR:

$$e_{tm}^{DR} = \begin{cases} E_m^{DR,init},\ \forall m \in \mathcal{M}_i,\ t = 1, \\ e_{m,t-1}^{DR} + p_{m,t-1}^{DR} \Delta t,\ \forall m \in \mathcal{M}_i,\ \forall t \in \mathcal{H} \setminus \{1\}, \end{cases} \tag{4.10}$$

$$e_m^{DR,end} = e_{tm}^{DR} + p_{tm}^{DR} \Delta t, m \in \mathcal{M}_i,\ t = T, \tag{4.11}$$

$$0 \leq e_{tm}^{DR} \leq P_{tm}^{L,r},\ m \in \mathcal{M}_i,\ \forall t \in \mathcal{H}, \tag{4.12}$$

$$-K_m^{DR} P_{tm}^{L,r} \leq p_{tm}^{DR} \leq K_m^{DR} P_{tm}^{L,r},\ m \in \mathcal{M}_i,\ \forall t \in \mathcal{H}, \tag{4.13}$$

$$e_m^{DR,end} = E_m^{DR,init},\ m \in \mathcal{M}_i. \tag{4.14}$$

In the above formulas, e_{tm}^{DR} is the part of energy available from DRRs that has already been curtailed at time step t, while $e_{tm}^{DR,end}$ is the DR energy that has been curtained by the end of the time horizon. The parameter $E_{tm}^{DR,init}$ denotes the DR

energy already curtailed at the beginning of the time horizon. The value of the maximum energy capacity of the DRRs is related to the available responsive load $P_{tm}^{L,r}$ and K_m^{DR} is the power to energy ratio, which depends on the technology of the DRRs [136]. Note that (4.14) may only be used in OL dispatch to set identical conditions at the beginning and at end of the time horizon.

4.2.5 BES dispatch

This section presents two BES dispatch models that have been used in the optimization problems that were defined in the thesis. The first model is the conventiontal BES model, which has most frequently been used in relevant literature on optimal MG energy management. The other model, is a measurement-based model, which more accurately represents the behavior of a real BES, as it can capture non-ideal BES operation.

Since the BES throughput is calculated in Wh instead of Ah in the proposed optimization model, the term state-of-energy (SoE) is used instead of the SoC [82]. The SoE level is not affected by fluctuations of the BES voltage in contrast with SoC. However, the term SoC is still used, for the experimental BES measurements presented in the thesis. This thesis also defines DoD as the discharged energy from 100% SoE i.e., $DoD = 1 - SoE$.

4.2.5.1 Conventional model

The BES model that has been most frequently used in the latest literature on BES scheduling (e.g., [26, 27, 33, 34]) assumes that the SoE of the BES at each time step is linearly dependent on the cumulative BES throughput of the previous time steps. The charging/discharging energy efficiency and the power limits are considered to be constant and independent of the SoE level. This model is described by (4.15)–(4.21):

$$soe_{tm} = \begin{cases} SoE_m^{init}, & \forall m \in \mathcal{M}_i,\ t = 1 \\ soe_{t-1,m} + \eta_m^{ch} \frac{p_{t-1,m}^{ch} \Delta t}{E_m^{max}} - \frac{p_{t-1,m}^{dis} \Delta t}{\eta_m^{dis} E_m^{max}}, & \forall m \in \mathcal{M}_i,\ \forall t \in \mathcal{H} \setminus \{1\} \end{cases} \tag{4.15}$$

$$soe_m^{end} = soe_{tm} + \eta_m^{ch} \frac{p_{tm}^{ch} \Delta t}{E_m^{max}} - \frac{p_{tm}^{dis} \Delta t}{\eta_m^{dis} E_m^{max}}, \qquad \forall m \in \mathcal{M}_i,\ t = T \tag{4.16}$$

$$SoE_m^{min} \leq soe_{tm} \leq SoE_m^{max}, \qquad \forall m \in \mathcal{M}_i,\ \forall t \in \mathcal{H}, \tag{4.17}$$

$$0 \leq p_{tm}^{ch} \leq K_m^{BES} E_m^{max}, \qquad \forall m \in \mathcal{M}_i,\ \forall t \in \mathcal{H}, \tag{4.18}$$

$$0 \leq p_{tm}^{dis} \leq K_m^{BES} E_m^{max}, \qquad \forall m \in \mathcal{M}_i,\ \forall t \in \mathcal{H}, \quad (4.19)$$

$$p_{tm}^{ch} \leq z_{tm}^{BES} M, \qquad \forall m \in \mathcal{M}_i,\ \forall t \in \mathcal{H}, \quad (4.20)$$

$$p_{tm}^{dis} \leq (1 - z_{tm}^{BES}) M, \qquad \forall m \in \mathcal{M}_i,\ \forall t \in \mathcal{H}, \quad (4.21)$$

$$soe_m^{end} = SoE_m^{init}, \qquad \forall m \in \mathcal{M}_i. \quad (4.22)$$

In the above formulation, K_m^{BES} denotes the power to energy ratio, which determines the maximum charging/discharging power according to the specifications of the BES manufacturer. Moreover, η_m^{ch}/η_m^{dis} respectively refer to the charging/discharging efficiency, E_m^{max} is the installed capacity and soe_{tm} is the SoE, which must lie between the lower and upper limit (SoE_m^{min} and SoE_m^{max}, respectively). The binary variable z_{tm}^{BES} indicates if the BES is charging or discharging and M is a very large number, which is necessary for the linearization of this BES model. The linearization technique used in this case is called the Fortuny-Amat approach, which is also known as the "Big-M" approach [137]. Note that (4.22) may be considered in OL dispatch because, in this case, the SoE at the end is often set to be equal [138] or very close [139] to the initial SoE.

4.2.5.2 Measurement-based model

The assumptions that simplify the battery operation i.e., the constant charging/discharging efficiencies and maximum power limits can be seen in (4.15)–(4.16) and (4.18)–(4.19). Depending on the application and the BES's state-of-health (SoH), these assumptions may lead to mismatches between the estimated and actual SoE or the BES may fail to deliver the rated power. Therefore, a sampling-based approach, which was first presented in [83], is used to derive a model that captures more accurately the behavior of an actual BES by utilizing underlying patterns that exist in the charging/discharging data. This measurement-based model uses sample data from charging/discharging curves and satisfies (4.23)–(4.39), where $\mathcal{N}$ ($\mathcal{K}$) denotes the set of discharging (charging) data and the positive variables p_{tm}^{-}/p_{tm}^{+} respectively represent power output/input from/to the battery cells, before/after battery losses have been taken into account:

$$soe_{tm} = \begin{cases} SoE_m^{init}, & : \lambda_{tm}^{start},\ \forall m \in \mathcal{M}_i,\ t = 1 \\ soe_{t-1,m} + \frac{p_{t-1,m}^{+} \Delta t}{E_m^{max}} - \frac{p_{t-1,m}^{-} \Delta t}{E_m^{max}} & : \lambda_{tm}^{BES},\ \forall m \in \mathcal{M}_i,\ \forall t \in \mathcal{H} \setminus \{1\} \end{cases} \quad (4.23)$$

$$soe_m^{end} = soe_{tm} + \frac{p_{tm}^{+}\Delta t}{E_m^{max}} - \frac{p_{tm}^{-}\Delta t}{E_m^{max}}, \qquad : \lambda_{tm}^{BES,end},\ \forall m \in \mathcal{M}_i,\ t = T \quad (4.24)$$

$$0 \geq SoE_m^{min} - soe_{tm} \quad \perp \quad \underline{\mu}_{tm}^{SoE} \geq 0, \qquad \forall m \in \mathcal{M}_i,\ \forall t \in \mathcal{H}, \quad (4.25)$$

$$0 \geq soe_{tm} - SoE_m^{max} \quad \perp \quad \overline{\mu}_{tm}^{SoE} \geq 0, \qquad \forall m \in \mathcal{M}_i,\ \forall t \in \mathcal{H}, \quad (4.26)$$

$$p_{tm}^{-} = \sum_{n \in \mathcal{N}} P_{mn}^{-} x_{tmn}, \qquad : \lambda_{tm}^{-},\ \forall m \in \mathcal{M}_i,\ \forall t \in \mathcal{H}, \quad (4.27)$$

$$p_{tm}^{dis} = \sum_{n \in \mathcal{N}} P_{mn}^{dis} x_{tmn}, \qquad : \lambda_{tm}^{dis},\ \forall m \in \mathcal{M}_i,\ \forall t \in \mathcal{H}, \quad (4.28)$$

$$p_{tm}^{+} = \sum_{k \in \mathcal{K}} P_{mk}^{+} y_{tmk}, \qquad : \lambda_{tm}^{+},\ \forall m \in \mathcal{M}_i,\ \forall t \in \mathcal{H}, \quad (4.29)$$

$$p_{tm}^{ch} = \sum_{k \in \mathcal{K}} P_{mk}^{ch} y_{tmk}, \qquad : \lambda_{tm}^{ch},\ \forall m \in \mathcal{M}_i,\ \forall t \in \mathcal{H}, \quad (4.30)$$

$$0 \geq -p_{tm}^{ch} \quad \perp \quad \mu_{tm}^{ch} \geq 0, \qquad \forall m \in \mathcal{M}_i,\ \forall t \in \mathcal{H}, \quad (4.31)$$

$$0 \geq -p_{tm}^{dis} \quad \perp \quad \mu_{tm}^{dis} \geq 0, \qquad \forall m \in \mathcal{M}_i,\ \forall t \in \mathcal{H}, \quad (4.32)$$

$$0 \geq -p_{tm}^{+} \quad \perp \quad \mu_{tm}^{+} \geq 0, \qquad \forall m \in \mathcal{M}_i,\ \forall t \in \mathcal{H}, \quad (4.33)$$

$$0 \geq -p_{tm}^{-} \quad \perp \quad \mu_{tm}^{-} \geq 0, \qquad \forall m \in \mathcal{M}_i,\ \forall t \in \mathcal{H}, \quad (4.34)$$

$$soe_{tm} = \sum_{n \in \mathcal{N}} SoE_{mn}^{dis} x_{tmn} + \sum_{k \in \mathcal{K}} SoE_{mk}^{ch} y_{tmk} \qquad : \lambda_{tm}^{SoE}, \forall m \in \mathcal{M}_i,\ \forall t \in \mathcal{H}, \quad (4.35)$$

$$\sum_{n \in \mathcal{N}} x_{tmn} = 1, \qquad : \lambda_{tm}^{x},\ \forall m \in \mathcal{M}_i,\ \forall t \in \mathcal{H}, \quad (4.36)$$

$$0 \geq -x_{tmn} \quad \perp \quad \mu^x_{tmn} \geq 0, \qquad \forall n \in \mathcal{N},\ \forall m \in \mathcal{M}_i,\ \forall t \in \mathcal{H}, \tag{4.37}$$

$$\sum_{k \in K} y_{tmk} = 1, \qquad : \lambda^y_{tm},\ \forall m \in \mathcal{M}_i,\ \forall t \in \mathcal{H}, \tag{4.38}$$

$$0 \geq -y_{tmk} \quad \perp \quad \mu^y_{tmk} \geq 0, \qquad \forall k \in \mathcal{K},\ \forall m \in \mathcal{M}_i,\ \forall t \in \mathcal{H}, \tag{4.39}$$

$$soe^{end}_m = SoE^{init}_m, \qquad : \lambda^{end}_m, \forall m \in \mathcal{M}_i. \tag{4.40}$$

Eq. (4.23) calculates the BES's SoE at each time step. Similar to (4.15), the SoE depends on the cumulative BES throughput and the SoE at the previous time step. Unlike the conventional model, the dependency of maximum charging/discharging rates on SoE levels is considered in the measurement-based model. That is because the feasibility regions of BES power and SoE in the measurement-based model are not independent from each other. Instead, a 3-dimensional feasibility region is defined by (4.27)–(4.28), (4.32), and (4.34)–(4.37) using the discharging sample data $(SoE^{dis}_{mn}, P^-_{mn}, P^{dis}_{mn})$ to constrain the values of the variables soe_{tm}, p^-_{tm}, and p^{dis}_{tm}, which are dependent to each other, during discharging. Similarly, (4.29)–(4.31), (4.33), (4.35), and (4.38)–(4.39) define the feasibility region of the variables soe_{tm}, p^+_{tm}, and p^{ch}_{tm} during charging using the charging sample data $(SoE^{ch}_{mk}, P^+_{mk}, P^{ch}_{mk})$. In other words, the sample data form the convex hull of the feasible region for the BES operation points. Thus, the variables soe_{tm}, p^+_{tm}, p^{ch}_{tm}, p^-_{tm}, and p^{dis}_{tm} can be written as convex combinations of the sample measurements. Each convex combination (BES operation point) depends on the positive variables x_{tmn} and y_{tmk}, which are associated respectively with the choice of discharging or charging sample data. No binary variables are required in this model, provided that the sample data include the BES state where the BES is an open-circuit as well as the state where the BES is an open-circuit and fully charged or fully discharged [83]. Similar to the conventional BES model, (4.40) may be considered in OL dispatch.

It can easily be seen that the measurement-based model also incorporates the variable (with respect to BES power and SoE) charging/discharging efficiencies (both internal BES losses and DC/DC converter losses are considered), which are given by $\eta^{ch}_{tm} = \frac{p^+_{tm}}{p^{ch}_{tm}}$ and $\eta^{dis}_{tm} = \frac{p^{dis}_{tm}}{p^-_{tm}}$, respectively, $\forall m \in \mathcal{M}_i,\ \forall t \in \mathcal{H}$ [83]. As the efficiencies are correlated with the model's decision variables, the efficiency values (at each BES power and SoE level) depend on the feasible combinations of x_{tmn} and y_{tmk}, which determine the choice of p^{dis}_{tm} and p^-_{tm} (or p^{ch}_{tm} and p^+_{tm} during charging periods).

4.2.6 BES degradation

The BES degradation can be expressed as loss of available capacity or increase in the BES resistance and is linked in a non-linear manner to many factors [77, 140]. Degradation is caused when the BES is cycled as well as during resting periods i.e., when the BES is an open-circuit. Different mechanisms are in effect in each case. Degradation is more prominent with high C-rates (C-rate of 1C indicates discharging at nominal discharging current, C-rate of 2C indicates discharging at twice the nominal current, etc. [83]), frequent cycling with high DoD, high operating temperatures, and resting periods at high SoC [140, 141]. The temperature in residential, stationary BES applications can easily be controlled and is therefore considered to be constant for the BES degradation models that are presented below. Each of these BES degradation models calculates the BES degradation cost c_m^B. If this cost is considered in the MODEFlex model, it can be added in (4.1) as a part of the term c_m^{DER}.

4.2.6.1 Cycle aging (dependency on cumulative throughput)

The degradation model presented in [142] and modified in [31, 143] is used to model the dependency of cycle aging on cumulative throughput:

$$Q_m^l = B_1 e^{B_2 I_c} \sum_{t \in \mathcal{H}} (p_{tm}^- + p_{tm}^+) \Delta t \ , \qquad \forall m \in \mathcal{M}_i. \ (4.41)$$

In (4.41), Q_m^l represents the cycle-based BES capacity loss in %, while the pre-exponential and exponential factors B_1 and B_2 can be obtained from empirical fitting of experimental data. The daily average C-rate I_c is entered as a parameter and thus (4.41) becomes linear. The BES degradation cost is calculated as:

$$c_m^B = \frac{C_m^{B,0} Q_m^l}{100\% - H\%}, \qquad \forall m \in \mathcal{M}_i, \ (4.42)$$

where $C_m^{B,0}$ is the purchase (or replacement) cost of the BES and H is the end-of-life retained capacity percentage i.e., the percentage of retained capacity, when the BES is retired. Depending on the manufacturer, the end-of-life retained capacity can range from 65% to 80% [80, 81].

4.2.6.2 Cycle aging (dependency on DoD)

Another degradation model that can be used to define a cost associated with cycle-based degradation is the one presented in [144], which estimates cycle aging taking into account the maximum DoD of each cycle. Given a function of lifecycle percentage loss for one cycle of a specific DoD, the cycle-based BES degradation cost according to this model is given by

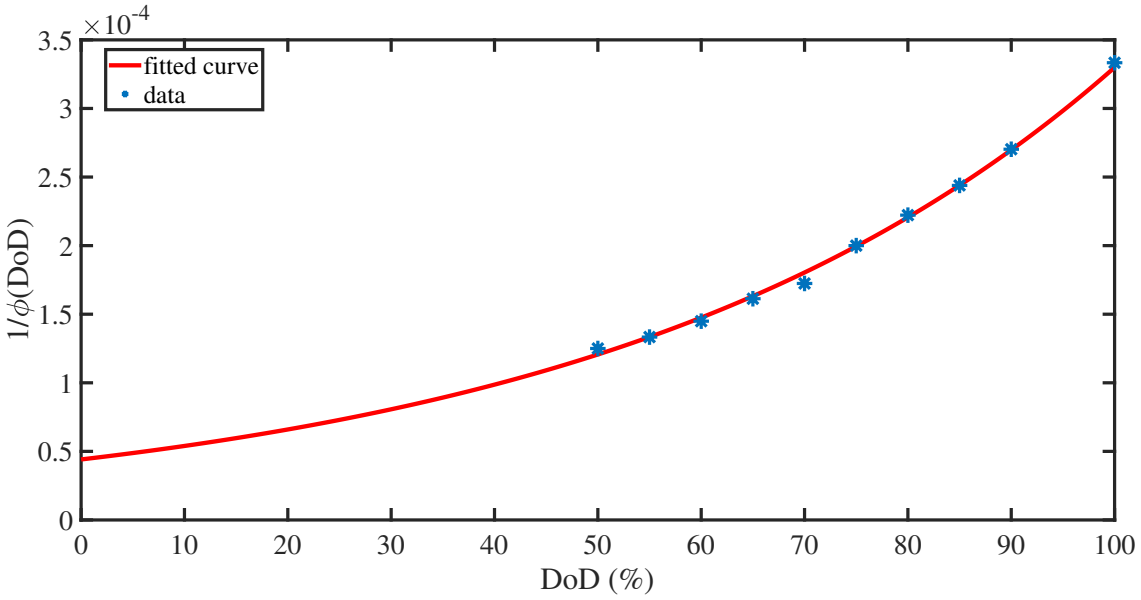

Figure 4.2: The percentage of lifecycle loss as a function of one cycle at a specific DoD.

$$c_m^B = \sum_{t \in \mathcal{H}} c_{tm}^{DoD}, \qquad \forall m \in \mathcal{M}_i, \quad (4.43)$$

where c_{tm}^{DoD} is the cycle aging cost per time step t given by

$$c_{tm}^{DoD} = \max\{0, (\rho_{tm} - \rho_{t-1,m}) C_m^{B,0}\}, \qquad \forall m \in \mathcal{M}_i. \quad (4.44)$$

This cost is related to the percentage of lifecycle loss $\rho_{tm} = 1/\phi(DoD)$ for one cycle at a specific DoD, where $\phi(DoD)$ refers to the lifecycle as a function of DoD. An example of the loss of lifetime as a function of DoD derived from data of a Li-ion BES can be seen in Fig. 4.2 (based on data from [30]).

In (4.44), ρ_{tm} is greater than $\rho_{t-1,m}$ only when the BES is discharging, since the loss of BES lifetime increases, when the DoD increases. Thus, the aging cost is added for every discharging half-cycle, while it is zero during charging. The degradation model can be piecewise linearized according to (4.45)–(4.50):

$$dod_{tm} = \sum_{p \in \mathcal{P}} DoD_{mp} \xi_{tmp}, \qquad \forall m \in \mathcal{M}_i, \quad (4.45)$$

$$\rho_{tm} = \sum_{p \in \mathcal{P}} \widehat{\rho}_{mp} \xi_{tmp}, \qquad \forall m \in \mathcal{M}_i, \quad (4.46)$$

$$\sum_{p}^{P} \xi_{tmp} = 1, \qquad \forall m \in \mathcal{M}_i, \quad (4.47)$$

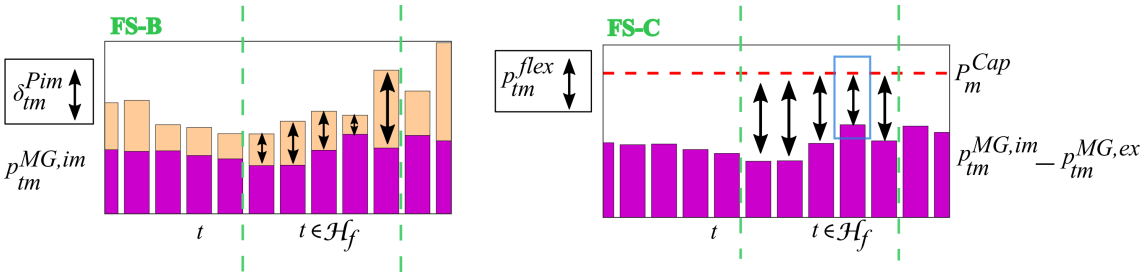

Figure 4.3: The baseline (left) and capacity limitation (right) FSs.

$$0 \leq \xi_{tmp} \leq 1, \qquad \forall m \in \mathcal{M}_i,\ \forall t \in \mathcal{H}, \quad (4.48)$$

$$\begin{bmatrix} \xi_{tm1} \\ \xi_{tm2} \\ \vdots \\ \xi_{tmP} \end{bmatrix} \leq \begin{bmatrix} \boldsymbol{H} \end{bmatrix} \begin{bmatrix} b_{tm1} \\ b_{tm2} \\ \vdots \\ b_{tmP-1} \end{bmatrix}, \qquad \forall m \in \mathcal{M}_i, \quad (4.49)$$

$$\sum_{p=1}^{P-1} b_{tmp} = 1, \qquad \forall m \in \mathcal{M}_i. \quad (4.50)$$

In (4.45)–(4.46), $\mathcal{P}$ denotes the set of sample points of the BES lifecycle loss function, while DoD_{mp} and $\widehat{\rho}_{mp}$ respectively refer to the sample points of DoD (dod_{tm}) and lifecycle loss percentage (ρ_{tm}), which are used for the piecewise linearization of the lifecycle loss function curve (Fig. 4.2). The positive variable ξ_{tmp} is related to the choice of sample point $p \in \mathcal{P}$. Eq. (4.49)–(4.50) are adjacency constraints, where $\boldsymbol{H}$ is the adjacency matrix. The binary variable b_{tmp} is used to ensure interpolation of the decision variables dod_{tm} and ρ_{tm} between consecutive sample points.

4.2.7 Models of FSs

Two models of FSs were considered for integration to the MODEFlex model: FS-B and FS-C. These are illustrated in Fig. 4.3. The FS-C model is used for the flexibility that is offered as a capacity limitation product and the FS-B model is used for the flexibility that is offered as a baseline product.

4.2.7.1 FS-B

When FS-B is integrated in the MODEFlex problem the term r_m^{flex} of (4.1) becomes

$$r_m^{flex} = \sum_{t \in \mathcal{H}_f} \pi_{tm}^{fl,ex} \delta_{tm}^{Pex} + \pi_{tm}^{fl,im} \delta_{tm}^{Pim}, \quad (4.51)$$

while the MG imported and exported power in (4.6) are replaced according to (4.52)–(4.53) during the flexibility activation period $\mathcal{H}_f \subseteq \mathcal{H}$:

$$p_{tm}^{MG,im} = p_{tm}^{im} + \delta_{tm}^{Pim}, \qquad \forall t \in \mathcal{H}_f,\ \forall m \in \mathcal{M}_i, \quad (4.52)$$

$$p_{m,t}^{MG,ex} = p_{m,t}^{ex} + \delta_{tm}^{Pex}, \qquad \forall t \in \mathcal{H}_f,\ \forall m \in \mathcal{M}_i. \quad (4.53)$$

To incorporate the FS-B model to the MODEFlex model the following constraints are added:

$$0 \geq -p_{tm}^{im} \quad \perp \quad \mu_{tm}^{im,+} \geq 0 \qquad \forall t \in \mathcal{H}_f, \forall m \in \mathcal{M}_i, \quad (4.54)$$

$$0 \geq -p_{tm}^{ex} \quad \perp \quad \mu_{tm}^{ex,+} \geq 0 \qquad \forall t \in \mathcal{H}_f, \forall m \in \mathcal{M}_i, \quad (4.55)$$

$$0 \geq \delta_{tm}^{Pim} \quad \perp \quad \mu_{tm}^{fl,im+} \geq 0 \qquad \forall t \in \mathcal{H}_f, \forall m \in \mathcal{M}_i, \quad (4.56)$$

$$0 \geq -\delta_{tm}^{Pex} \quad \perp \quad \mu_{tm}^{fl,ex+} \geq 0 \qquad \forall t \in \mathcal{H}_f, \forall m \in \mathcal{M}_i, \quad (4.57)$$

$$0 \geq -p_{tm}^{im} - \delta_{tm}^{Pim} \quad \perp \quad \mu_{tm}^{fl,im} \geq 0 \qquad \forall t \in \mathcal{H}_f, \forall m \in \mathcal{M}_i, \quad (4.58)$$

$$0 \geq -p_{tm}^{ex} - \delta_{tm}^{Pex} \quad \perp \quad \mu_{tm}^{fl,ex} \geq 0 \qquad \forall t \in \mathcal{H}_f, \forall m \in \mathcal{M}_i, \quad (4.59)$$

where the positive variables $\pi_{tm}^{fl,im}, \pi_{tm}^{fl,ex}$ are the flexibility prices and the variables $\delta_{tm}^{Pim}/\delta_{tm}^{Pex}$ are the procured flexibility amounts. In FS-B, the amount of flexibility provided δ_{tm}^{Pim} or δ_{tm}^{Pex} is the deviation from the baseline power exchange profile. In this thesis, it is assumed that the baseline profile corresponds to the optimal MG energy dispatch $(p_{tm}^{ex} - p_{tm}^{im})$ computed as the solution of the optimal MG energy management problem when no FS is considered.

4.2.7.2 FS-C

When FS-C is integrated in the MODEFlex problem the term r_m^{flex} of (4.1) becomes

$$r_m^{flex} = \sum_{t \in \mathcal{H}_f} \pi_{tm}^{fl,Cap} p_{tm}^{flex} = \sum_{t \in \mathcal{H}_f} \pi_{tm}^{fl,Cap} (P_m^{Cap} - p_{tm}^{fl,p}), \quad (4.60)$$

while the MG imported and exported power in (4.6) are replaced according to (4.61)–(4.62) during the flexibility activation period $\mathcal{H}_f \subseteq \mathcal{H}$:

$$p_{tm}^{MG,im} = p_{tm}^{im}, \qquad \forall t \in \mathcal{H}_f,\ \forall m \in \mathcal{M}_i, \quad (4.61a)$$

$$p_{wtm}^{MG,im} = p_{wtm}^{im}, \qquad \forall t \in \mathcal{H}_f,\ \forall m \in \mathcal{M}_i, \forall w \in \mathcal{W}, \quad (4.61b)$$

$$p_{tm}^{MG,ex} = p_{tm}^{ex}, \qquad \forall t \in \mathcal{H}_f,\ \forall m \in \mathcal{M}_i, \quad (4.62a)$$
$$p_{wtm}^{MG,ex} = p_{wtm}^{ex}, \qquad \forall t \in \mathcal{H}_f,\ \forall m \in \mathcal{M}_i, \forall w \in \mathcal{W}. \quad (4.62b)$$

To incorporate the FS-C model to the MODEFlex model (4.63) is added:

$$0 \geq p_{tm}^{im} - p_{tm}^{ex} - p_{tm}^{fl,p} \quad \perp \quad \mu_{tm}^{fl,Cap} \geq 0, \qquad \forall t \in \mathcal{H}_f, \forall m \in \mathcal{M}_i, \quad (4.63a)$$
$$0 \geq -p_{tm}^{fl,p} + \sum_{w \in \mathcal{W}} \Pi_w (p_{tmw}^{im} - p_{tmw}^{ex}) \quad \perp \quad \mu_{tm}^{fl,Cap} \geq 0, \qquad \forall t \in \mathcal{H}_f, \forall m \in \mathcal{M}_i. \quad (4.63b)$$

The positive variable p_{tm}^{flex} denotes the procured amount of active power flexibility (average value over Δt), $\pi_{tm}^{fl,Cap}$ is the flexibility price, and $p_{tm}^{fl,p}$ is the expected imported power per time step of the flexibility activation period $\mathcal{H}_f \subseteq \mathcal{H}$. The amount of flexibility is calculated in terms of power capacity reduction. When this FS is activated, the MG resources modify their schedule to guarantee that the imported power will not exceed the "new" capacity $P_m^{Cap} - p_{tm}^{flex}$ provided by FS-C. The parameter P_m^{Cap} should be based on a value that the DSO and the MG operator can easily agree upon such as e.g., the capacity at the grid connection point, so that the flexibility can be quantified in a reliable manner.

In FS-C, the flexibility amount can also be evaluated and dispatched over the entire activation period instead of per time step of this period. In this case, the term r_m^{flex} of (4.1) becomes

$$r_m^{flex} = \pi_m^{fl,Cap} p_m^{flex} = \pi_m^{fl,Cap} (P_m^{Cap} - p_m^{fl,p}). \quad (4.64)$$

while (4.65)–(4.66) are added to MODEFlex model to incorporate the FS-C model:

$$p_m^{fl,p} \geq p_m^{Max,net}, \qquad \forall t \in \mathcal{H}_f, \forall m \in \mathcal{M}_i, \quad (4.65a)$$
$$p_m^{fl,p} \geq \sum_{w \in \mathcal{W}} \Pi_w p_{wm}^{Max,net}, \qquad \forall t \in \mathcal{H}_f, \forall m \in \mathcal{M}_i, \quad (4.65b)$$

$$p_m^{Max,net} \geq (p_{tm}^{im} - p_{tm}^{ex}), \qquad \forall w \in \mathcal{W}, \forall t \in \mathcal{H}_f, \forall m \in \mathcal{M}_i, \quad (4.66a)$$
$$p_{wm}^{Max,net} \geq (p_{wtm}^{im} - p_{wtm}^{ex}), \qquad \forall w \in \mathcal{W}, \forall t \in \mathcal{H}_f, \forall m \in \mathcal{M}_i. \quad (4.66b)$$

The amount of flexibility p_m^{flex} i.e., the peak power capacity reduction, is highlighted in Fig. 4.3 enclosed within a rectangle. In (4.65), $p_m^{fl,p}$ is the (expected) peak imported power during the flexibility activation period, whereas the variable $p_{wm}^{Max,net}$ in (4.66) is the net peak power of scenario w during the flexibility activation period.

4.3 Optimization model for the DSO

Generally, the DSOs are not allowed to own or operate DERs. The distribution network's DERs, which belong to the MGs, can be dispatched by the DSO, only if s/he is allowed to have full knowledge of the MG constraints and, in addition,

is empowered to control the MG resources. Alternatively, the DSO can treat the MGs as dispatchable resources, since they are represented as controllable entities connected at a PCC. For this purpose, there must be proper coordination between the DMS and the MG-EMS.

The optimal dispatch of the MG resources by the DSO, whether it is performed directly through centralized coordination or indirectly through decentralized coordination and control of power exchanges at the PCCs, is formulated as an AC OPF problem. The dispatch of MGs and network controllable devices must satisfy the grid technical constraints, while serving the specific operational targets of the DSO. The DSO may aim to minimize the grid connection charges paid to the transmission system operator (TSO) in order to achieve a more economic operation. These charges include the energy transmission fee paid for the imported energy from the TSO's grid and the subscription fee, which is related to the peak imported power.

4.3.1 Objective functions

Two objective functions that can be used to improve the economic operation of the distribution grid are formulated for the DSO's optimization model. One objective function is the *minimization of the grid charges paid to the TSO*:

$$\min \sum_{i \in \mathcal{S}} \sum_{t \in \mathcal{H}} p_{ti}^{SS} C^{im,SS} \Delta t + \sum_{i \in \mathcal{S}} c_i^{SS,peak}, \tag{4.67}$$

where $\mathcal{S} \subseteq \mathcal{D}$ is the subset of substation buses. These are the boundary buses with connection (physical interface) to the upstream network i.e., the buses with TSO-DSO interface. These buses belong to the set of distribution network buses $\mathcal{D}$ which also includes all the MG buses. In the case of a radial distribution grid, the subset $\mathcal{S}$ has only one element. The grid charges refer to the costs paid by the DSO to the TSO and are associated with the cost of imported energy and the cost of peak imported power, which are respectively shown by the first and the second term in (4.67). The variables p_{ti}^{SS} and $c_i^{SS,peak}$ represent the active power and the cost of the peak power through the boundary substation at bus i, respectively, while the parameter $C^{im,SS}$ is the imported energy transmission grid tariff. The other objective function is the *minimization the peak power cost considering the procurement of local FSs*:

$$\min \sum_{i \in \mathcal{S}} c_i^{SS,peak} + c^{flex}. \tag{4.68}$$

This objective, which can be used to reduce the subscription fee paid to the TSO, sums the peak power cost paid to the TSO and the cost of procuring flexibility from local FSPs. In this thesis, it is assumed that the grid-connected MGs are the only local FSPs and the cost of purchasing local flexibility from them is denoted by c^{flex}. The peak power cost in (4.67)–(4.68) is constrained by:

$$c_i^{SS,peak} \geq \Lambda^{SS,peak} p_{ti}^{SS}, \qquad \forall i \in \mathcal{S},\ t \in \mathcal{H}, \tag{4.69}$$

where $\Lambda^{SS,peak}$ is the imported peak power grid tariff. If the MGs offer the flexibility product FS-B, the term c^{flex} of (4.68) becomes

$$c^{flex} = \sum_{t \in \mathcal{H}_f} \sum_{m \in \mathcal{M}_i} -\pi_{tm}^{fl,im} \delta^{Pim} + \pi_{tm}^{fl,ex} \delta^{Pex}, \tag{4.70}$$

whereas if the MGs offer the flexibility product FS-C and assuming that the flexibility is calculated and dispatched per time step of the flexibility activation period, the term c^{flex} of (4.68) becomes

$$c^{flex} = \sum_{t \in \mathcal{H}_f} \sum_{m \in \mathcal{M}_i} \pi_{tm}^{fl,Cap} p_{tm}^{flex} = \pi_{tm}^{fl,Cap} (P_m^{Cap} - p_{tm}^{fl,p}). \tag{4.71}$$

4.3.2 Network power flow

The AC power flow of the distribution network is described by the branch flow model (BFM). The BFM is a relaxed model of the original non-convex OPF problem [145], which applies angle relaxation to eliminate the phase angles of voltages and currents. This relaxation is exact only for radial distribution networks and, therefore, the obtained solution for a meshed network might not be globally optimal i.e., there might be other feasible solutions that yield a better objective function value. The AC power flow of the radial network is described by a set of equations, also known as DistFlow equations, which was first presented in [123].

Below is the derivation of the linearized BFM as given in [145]for a radial distribution network represented by a set of buses $\mathcal{D}$.

4.3.2.1 Branch flow model

The BFM, which is derived after the angle relaxation, is given by [145]:

$$p_j = \sum_{i:j \sim i} p_{ji} - \sum_{i:i \sim j} (p_{ij} - R_{ij} \frac{p_{ij}^2 + q_{ij}^2}{|\nu_i|^2}) + G_i |\nu_i|^2, \qquad \forall j \in \mathcal{D}, \tag{4.72}$$

$$q_j = \sum_{i:j \sim i} q_{ji} - \sum_{i:i \sim j} (q_{ij} - X_{ij} \frac{p_{ij}^2 + q_{ij}^2}{|\nu_i|^2}) + B_i |\nu_i|^2, \qquad \forall j \in \mathcal{D}, \tag{4.73}$$

$$|\nu_j|^2 = |\nu_i|^2 - 2(R_{ij} p_{ij} + X_{ij} q_{ij}) + (R_{ij}^2 + X_{ij}^2) \frac{p_{ij}^2 + q_{ij}^2}{|\nu_i|^2}, \quad \forall (i,j) \in \mathcal{F}, \ \forall i,j \in \mathcal{D}, \tag{4.74}$$

where $j \sim i$ represents a line between bus j and bus i i.e., either $(j,i) \in \mathcal{F}$ or $(i,j) \in \mathcal{F}$ (but not both), where $\mathcal{F}$ is the set of distribution network lines (also called branches). In (4.72)–(4.74), p_j/q_j denote the active/reactive power injection at bus j, p_{ji}/q_{ji} denote the active/reactive power flow from bus j to bus i, and $|\nu_i|$ refers to the voltage magnitude. Moreover, R_{ij} and X_{ij} respectively denote the resistance and reactance of line $i-j$, while G_i and B_i respectively refer to shunt conductance and shunt susceptance from bus i to ground.

The relaxed model is still non-convex. Neglecting the capacitance of the lines and the quadratic terms that represent the power losses, which are much smaller compared

to the power flows, the linearized BFM (also known as LinDistFlow equations) is derived:

$$p_j = \sum_{i:j\sim i} p_{ji} - \sum_{i:i\sim j} p_{ij}, \qquad \forall j \in \mathcal{D}, \tag{4.75}$$

$$q_j = \sum_{i:j\sim i} q_{ji} - \sum_{i:i\sim j} q_{ij}, \qquad \forall j \in \mathcal{D}, \tag{4.76}$$

$$v_j = v_i - 2(R_{ij}p_{ij} + X_{ij}p_{ij}), \qquad \forall (i,j) \in \mathcal{F},\ \forall i,j \in \mathcal{D}, \tag{4.77}$$

where $v_i = |\nu_i|^2$. The linearized BFM has extensively been used in literature for power flow calculations in radial distribution networks [63, 146]. In fact, the approximations that derive this model only introduce a small relative error of about 1% [147], while they simplify the network state calculation by reducing it to the following three variables: voltage magnitude, active power and reactive power injections.

4.3.2.2 Distribution network power flow equations

The AC power flow equations for a distribution network with grid-connected MGs according to the linearized BFM are given by:

$$-\sum_{m\in\mathcal{M}_i}(p_{tm}^{MG,im} - p_{tm}^{MG,ex}) - P_{ti}^{L} + \sum_{i\in\mathcal{S}} p_{ti}^{SS} + \sum_{j:i\sim j}(p_{tji} - p_{tij}) = 0, \qquad \forall i \in \mathcal{D}\setminus\mathcal{M},\ \forall t \in \mathcal{H}, \tag{4.78}$$

$$-\sum_{m\in\mathcal{M}_i}(q_{tm}^{MG,im} - q_{tm}^{MG,ex}) - Q_{ti}^{L} + \sum_{i\in\mathcal{S}} q_{ti}^{SS} + \sum_{j:i\sim j}(q_{tji} - q_{tij}) = 0, \qquad \forall i \in \mathcal{D}\setminus\mathcal{M},\ \forall t \in \mathcal{H}, \tag{4.79}$$

$$v_{tj} = v_{ti} - 2(R_{ij}p_{tij} + X_{ij}q_{tij}), \qquad \forall (i,j)\in\mathcal{F},\ \forall i,j \in (\mathcal{D}\cup\mathcal{M}_i)\setminus\mathcal{M},\ t\in\mathcal{H}, \tag{4.80}$$

$$p_{tij} = 0, \qquad \forall (i,j) \notin \mathcal{F},\ \forall i,j \in (\mathcal{D}\cup\mathcal{M}_i)\setminus\mathcal{M},\ \forall t \in \mathcal{H}, \tag{4.81}$$

$$q_{tij} = 0, \qquad \forall (i,j) \notin \mathcal{F},\ \forall i,j \in (\mathcal{D}\cup\mathcal{M}_i)\setminus\mathcal{M},\ \forall t \in \mathcal{H}, \tag{4.82}$$

$$p_{tij} + p_{tji} = 0, \qquad \forall (i,j) \in \mathcal{F},\ \forall i,j \in (\mathcal{D}\cup\mathcal{M}_i)\setminus\mathcal{M},\ \forall t \in \mathcal{H}, \tag{4.83}$$

$$q_{tij} + q_{tji} = 0, \qquad \forall (i,j) \in \mathcal{F},\ \forall i,j \in (\mathcal{D} \cup \mathcal{M}_i) \setminus \mathcal{M},\ \forall t \in \mathcal{H}, \quad (4.84)$$

$$v_{ti} = V^{SB}, \qquad \forall i \in \mathcal{S},\ \forall t \in \mathcal{H}, \quad (4.85)$$

$$V_{min} \leq |\nu_{ti}| \leq V_{max}, \qquad \forall i \in (\mathcal{D} \cup \mathcal{M}_i) \setminus \mathcal{M},\ \forall t \in \mathcal{H}. \quad (4.86)$$

In (4.78)–(4.86), q_{ti}^{SS} is the reactive power through the boundary substation at bus i and the parameters P_{ti}^{L}/Q_{ti}^{L} denote the active/reactive power load at the distribution bus i. The square of voltage at the distribution grid's boundary buses, which represent controlled voltage buses, must remain constant and equal to the reference value denoted by V^{SB} as seen in (4.85), while (4.86) constraints the voltage magnitude within statutory limits. The equations are defined for all the network buses except for the buses that belong to the MGs, i.e., the DSO does not have knowledge of the network structure that belongs to the MGs. The network buses where MGs are connected i.e., the PCCs, which represent the physical interface between the MGs and the main distribution network, are considered in the network power flow equations. If it could be assumed that the DSO has full knowledge of the MGs' network and the technical constraints of the MG resources, then (4.78)–(4.80) could be re-written as:

$$p_{ti}^{G} + P_{ti}^{PV} + p_{ti}^{dis} + p_{ti}^{DR} - p_{ti}^{ch} + -P_{ti}^{L} + \sum_{i \in \mathcal{S}} p_{ti}^{SS} + \sum_{j:i \sim j} (p_{tji} - p_{tij}) = 0, \qquad \forall i \in \mathcal{D},\ \forall t \in \mathcal{H}, \quad (4.87)$$

$$q_{ti}^{G} + q_{ti}^{DR} - Q_{ti}^{L} + \sum_{i \in \mathcal{S}} q_{ti}^{SS} + \sum_{j:i \sim j} (q_{tji} - q_{tij}) = 0, \qquad \forall i \in \mathcal{D},\ \forall t \in \mathcal{H}, \quad (4.88)$$

$$v_{tj} = v_{ti} - 2(R_{ij} p_{tij} + X_{ij} q_{tij}), \qquad \forall (i,j) \in \mathcal{F},\ \forall i,j \in \mathcal{D},\ t \in \mathcal{H}, \quad (4.89)$$

$$p_{tij} = 0, \qquad \forall (i,j) \notin \mathcal{F},\ \forall i,j \in \mathcal{D},\ \forall t \in \mathcal{H}, \quad (4.90)$$

$$q_{tij} = 0, \qquad \forall (i,j) \notin \mathcal{F},\ \forall i,j \in \mathcal{D},\ \forall t \in \mathcal{H}, \quad (4.91)$$

$$p_{tij} + p_{tji} = 0, \qquad \forall (i,j) \in \mathcal{F},\ \forall i,j \in \mathcal{D},\ \forall t \in \mathcal{H}, \quad (4.92)$$

$$q_{tij} + q_{tji} = 0, \qquad \forall (i,j) \in \mathcal{F},\ \forall i,j \in \mathcal{D},\ \forall t \in \mathcal{H}, \quad (4.93)$$

$$v_{ti} = V^{SB}, \qquad \forall i \in \mathcal{S},\ \forall t \in \mathcal{H}, \quad (4.94)$$

$$V_{min} \leq |\nu_{ti}| \leq V_{max}, \qquad \forall i \in \mathcal{D},\ \forall t \in \mathcal{H}. \quad (4.95)$$

4.4 Bilevel optimization model for coordinated operation of DSO and MGs

To represent the coordinated operation of the DSO grid and the MGs, a bilevel optimization problem is defined following the developing research trend of utilizing bilevel programming to model interactions between resource aggregators (or MGs) and prosumers [148, 149], as well as interactions between grid or market operators and aggregators, MGs or prosumers [150, 151]. The bilevel problem is transformed into an equivalent single-level mixed integer programming (MIP) problem by replacing the LL problem with its Karush–Kuhn–Tucker (KKT) conditions and adding them to the UL problem.

4.4.1 DSO (UL): Optimal network operation problem

The DSO purchases the FSs offered by the grid-connected MGs i.e., the FSPs, in order to minimize the peak power cost of the distribution grid. The formulation of the UL problem depends on the type of the offered FS. In case of:

- **FS-B**, the UL problem is given by (4.68) s.t. (4.52)–(4.53), (4.69), (4.78)–(4.86), and (4.70).
- **FS-C**, the UL problem is given by (4.68) s.t. (4.61)–(4.62), (4.69), (4.78)–(4.86), and (4.71).

4.4.2 MGs (LL): Optimal energy and flexibility dispatch

The MGs offer FSs to reduce their cost given by (4.1). The LL optimization problems are formulated as DO problems and their formulation depends on the type of the offered FS. In case of:

- **FS-B**, the LL problem is given by (4.1) s.t. (4.2)–(4.4), (4.6), (4.23)–(4.39), and (4.51)–(4.59), $\forall m \in \mathcal{M}$, where the terms c_m^p and c_m^{DER} are ignored.
- **FS-C**, the LL problem is given by (4.1) s.t. (4.2)–(4.4), (4.6), (4.23)–(4.39), and (4.60)–(4.63), $\forall m \in \mathcal{M}$, where the terms c_m^p and c_m^{DER} are ignored.

4.4.3 Bilevel optimization: DSO and MGs

To formulate the bilevel problem as a single-level equivalent problem the KKT conditions of the LL problem are added to the DSO's UL problem. The KKT conditions comprise all the equality and inequality conditions of the LL problem (along with the CS conditions of the LL inequalities) and the equality constraints derived from the partial derivatives of the LL Lagrangian function, w.r.t. the LL primal variables (the derivatives must be equal to zero). These equalities are given by (4.96)–(4.112) for **FS-B** as well as (4.96)–(4.108), and (4.113)–(4.114) for **FS-C**, $\forall m \in \mathcal{M}_i$, where T is the last time step of the time horizon. Note that all the primal and dual

variables of the LL problem become primal variables of the single-level equivalent problem.

$$\frac{\partial \mathcal{L}}{\partial p^{ch}_{tm}} = 0 = -\lambda^{APB}_{tm} + \lambda^{ch}_{tm} - \mu^{ch}_{tm}, \qquad \forall t \in \mathcal{H}, \ (4.96)$$

$$\frac{\partial \mathcal{L}}{\partial p^{dis}_{tm}} = 0 = \lambda^{APB}_{tm} + \lambda^{dis}_{tm} - \mu^{dis}_{tm}, \qquad \forall t \in \mathcal{H}, \ (4.97)$$

$$\frac{\partial \mathcal{L}}{\partial x_{tmn}} = 0 = -P^{-}_{mn}\lambda^{-}_{mt} - P^{dis}_{mn}\lambda^{dis}_{tm} - SoE^{dis}_{mn}\lambda^{SoE}_{tm} - \lambda^{x}_{tm} - \mu^{x}_{tmn}, \quad \forall t \in \mathcal{H}, \ \forall n \in \mathcal{N}, \ (4.98)$$

$$\frac{\partial \mathcal{L}}{\partial y_{tmk}} = 0 = -P^{+}_{mk}\lambda^{+}_{tm} - P^{ch}_{mk}\lambda^{ch}_{tm} - SoE^{ch}_{mk}\lambda^{SoE}_{tm} - \lambda^{y}_{tm} - \mu^{y}_{tmk}, \quad \forall t \in \mathcal{H}, \ \forall k \in \mathcal{K}, \ (4.99)$$

$$\frac{\partial \mathcal{L}}{\partial soe_{tm}} = 0 = -\lambda^{BES}_{tm} + \lambda^{start}_{m} + \lambda^{SoE}_{tm} + \overline{\mu}^{SoE}_{tm} - \underline{\mu}^{SoE}_{tm}, \qquad t = 1, \ (4.100)$$

$$\frac{\partial \mathcal{L}}{\partial soe_{tm}} = 0 = \lambda^{BES}_{t,m} - \lambda^{BES}_{t+1,m} + \lambda^{SoE}_{tm} + \overline{\mu}^{SoE}_{tm} - \underline{\mu}^{SoE}_{tm}, \qquad \forall t \in \mathcal{H} \setminus \{1, T\}, \ (4.101)$$

$$\frac{\partial \mathcal{L}}{\partial soe_{tm}} = 0 = \lambda^{BES}_{tm} - \lambda^{BES,end}_{m} + \lambda^{SoE}_{tm} + \overline{\mu}^{SoE}_{tm} - \underline{\mu}^{SoE}_{tm}, \qquad t = T, \ (4.102)$$

$$\frac{\partial \mathcal{L}}{\partial p^{im}_{tm}} = 0 = (\Lambda_t + C^{im})\Delta t + \lambda^{APB}_{tm} + \mu^{im,+}_{tm} - \mu^{fl,im}_{tm}, \qquad \forall t \in \mathcal{H}_f, \ (4.103)$$

$$\frac{\partial \mathcal{L}}{\partial p^{ex}_{tm}} = 0 = -(\Lambda_t + C^{ex})\Delta t - \lambda^{APB}_{tm} + \mu^{ex,+}_{tm} - \mu^{fl,ex}_{tm}, \qquad \forall t \in \mathcal{H}_f, \ (4.104)$$

$$\frac{\partial \mathcal{L}}{\partial p^{+}_{tm}} = 0 = -\frac{\Delta t}{E^{max}_{m}}\lambda^{BES}_{t+1,m} + \lambda^{+}_{tm} - \mu^{+}_{tm}, \qquad \forall t \in \mathcal{H} \setminus \{T\}, \ (4.105)$$

$$\frac{\partial \mathcal{L}}{\partial p^{+}_{tm}} = 0 = -\frac{\Delta t}{E^{max}_{m}}\lambda^{BES,end}_{t,m} + \lambda^{+}_{tm} - \mu^{+}_{tm}, \qquad t = T, \ (4.106)$$

$$\frac{\partial \mathcal{L}}{\partial p^{-}_{tm}} = 0 = -\frac{\Delta t}{E^{max}_{m}}\lambda^{BES}_{t+1,m} + \lambda^{-}_{tm} - \mu^{-}_{tm}, \qquad \forall t \in \mathcal{H} \setminus \{T\}, \ (4.107)$$

$$\frac{\partial \mathcal{L}}{\partial p^{-}_{tm}} = 0 = -\frac{\Delta t}{E^{max}_{m}}\lambda^{BES,end}_{t,m} + \lambda^{-}_{tm} - \mu^{-}_{tm}, \qquad t = T, \quad (4.108)$$

$$\frac{\partial \mathcal{L}}{\partial \delta^{Pim}_{tm}} = 0 = (\Lambda_t + C^{im})\Delta t + \pi^{fl,im}_{tm} + \lambda^{PB}_{tm} + \mu^{fl,im+}_{tm} - \mu^{fl,im}_{tm}, \qquad \forall t \in \mathcal{H}_f, \quad (4.109)$$

$$\frac{\partial \mathcal{L}}{\partial \delta^{Pim}_{tm}} = 0 = (\Lambda_t + C^{im})\Delta t + \lambda^{PB}_{tm} + \mu^{fl,im+}_{tm} - \mu^{fl,im}_{tm}, \qquad \forall t \in \mathcal{H} \cap \mathcal{H}'_f, \quad (4.110)$$

$$\frac{\partial \mathcal{L}}{\partial \delta^{Pex}_{tm}} = 0 = -(\Lambda_t + C^{ex})\Delta t - \pi^{fl,ex}_{tm} - \lambda^{APB}_{tm} - \mu^{fl,ex+}_{tm} - \mu^{fl,ex}_{tm}, \qquad \forall t \in \mathcal{H}_f, \quad (4.111)$$

$$\frac{\partial \mathcal{L}}{\partial \delta^{Pex}_{tm}} = 0 = -(\Lambda_t + C^{ex})\Delta t - \lambda^{APB}_{tm} - \mu^{fl,ex+}_{tm} - \mu^{fl,ex}_{tm}, \qquad \forall t \in \mathcal{H} \cap \mathcal{H}'_f, \quad (4.112)$$

$$\frac{\partial \mathcal{L}}{\partial p^{fl,p}_{tm}} = 0 = \pi^{fl,Cap}_{tm} - \mu^{fl,+}_{tm} - \mu^{fl,Cap}_{tm}, \qquad \forall t \in \mathcal{H}_f, \quad (4.113)$$

$$\frac{\partial \mathcal{L}}{\partial p^{fl,p}_{tm}} = 0 = -\mu^{fl,+}_{tm} - \mu^{fl,Cap}_{tm}, \qquad \forall t \in \mathcal{H} \cap \mathcal{H}'_f, \quad (4.114)$$

4.4.3.1 Linearization of CS constraints

As in Section 4.2.5.1, the Fortuny-Amat approach is used to linearize the CS constraints. Since this approach introduces binary decision variables, the equivalent single-level optimization problem is formulated as an MILP problem. For example, the non-linear (4.25) will be replaced by (4.115)–(4.116) in the single-level problem, where $z^{SoE,min}_{tm}$ and $M^{SoE,min}_{min}$ denote the binary variable and "Big-M" parameter associated with the CS constraint of inequality (4.25). The same process is repeated for all inequalities of the CS constraints.

$$-SoE^{min}_{m} + soe_{tm} \leq z^{SoE,min}_{tm} M^{SoE,min}_{min}, \qquad \forall m \in \mathcal{M}_i, \ t \in \mathcal{H}, \quad (4.115)$$

$$\underline{\mu}^{SoE}_{tm} \leq (z^{SoE,min}_{tm} - 1) M^{SoE,min}_{min}, \qquad \forall m \in \mathcal{M}_i. \quad (4.116)$$

4.4.3.2 Linearization of the UL objective function

Irrespective of the choice of the FS, the objective function of the equivalent single-level problem is non-linear. When **FS-C** is used, the objective function contains the product of the variables $\pi^{fl,Cap}_{tm}$ and $p^{fl,p}_{tm}$. When the **FS-B** is used, the objective function includes the product of the variables $\pi^{fl,im}_{tm}$ and δ^{Pim}_{tm}, as well as the product of the variables $\pi^{fl,ex}_{tm}$ and δ^{Pex}_{tm}. The UL objective functions are linearized using the strong duality theorem [152].

Chapter 5

Deterministic Energy Scheduling

This chapter is based on Paper I and Paper IV and presents results from optimal energy scheduling applied in two BMGs that used BES as the main flexible resource considering the energy market-based participation of the buildings. First, the chapter describes the problem that is addressed by the chapter's study and presents the study approach, the formulated DO problems, the considered parameters and the assumptions. Then, simulation results illustrate the comparison of different BES dispatch and degradation models that can be incorporated in the optimal energy management models. Results from demonstrations on the BMG testbeds, which were set up at real residential buildings, validate the accuracy of the BES dispatch models. At the end of this chapter, the effects of load forecasting errors on the BMG's operation costs are analyzed comparing different optimization methods and solution approaches.

5.1 Aim of study

As highlighted by the literature review in Section 2.3, there is a need to improve the accuracy in the assessment of the economic benefits for customers of BMGs using the BES as an energy-flexible resource. This can be achieved by utilizing BES dispatch models tailor-made for each BES to capture their real-life characteristics and, in addition, by investigating the impact of the degradation cost on the BMG's energy scheduling solution.

The aim of this chapter's study was to validate the proposed BMG energy management model, which considered real-life BES behavior and the cost of degradation, with multiple simulation and demonstration test cases, including test cases for long-term evaluation of the energy cost and BES degradation cost. The study also aimed to analyze the impact of different factors to these costs. For this purpose, different SoE limits and BES replacement costs were tested. The effects of the load forecasting errors on the BMG's operation cost was also investigated analyzing the different forecasting models and solution approaches that deal with these errors.

5.2 Study approach

As can be seen in Figure 5.1, which presents the study's approach, four different energy management models have been defined depending on whether the mathematical model of the BES incorporates real-life performance characteristics (measurement-based model) and the impact of cycle-based degradation. These models, which are formulated in Section 5.2.1, utilized the deterministic formulation of the MODEFlex model, without considering participation in FSs, and were used to perform DA optimal energy management. Model-1 incorporates the simplified BES scheduling model typically used in MG energy management, while Model-2 makes use of a measurement-based BES scheduling model that can capture a more realistic BES operation performance. The impact of degradation is not considered in the BES scheduling decisions according to these two models. Instead, Model-3 and Model-4 consider the impact of cycle-based degradation and they incorporate both the measurement-based BES scheduling model and different cycle aging models to account for degradation cost.

Either of the four models can be used to apply RH or DA dispatch and the acquired dispatch decisions can be used to assess the operation cost of the BMG and the BES utilization and degradation. In addition, they can be used to control the BES during demonstrations by dispatching its power and scheduling its stored energy levels. The initial SoC used as an input in the optimization problem was read from the BES during demonstrations, whereas in simulation test cases, it was obtained from the solution of the optimization problem in each simulation (and arbitrarily set before the first simulation).

Simulations were carried out for all four models, while demonstrations were carried out for Model-1 and Model-2 in order to validate their incorporated BES scheduling models and compare their performance. The four models were evaluated in a long-term operation of a BMG by simulating the optimal DA energy management of the HSB LL building over a year. Model-1 and Model-2 were demonstrated in both the HSB LL and the Brf Viva test systems. The optimal BMG energy management was performed in RH during the demonstrations, as shown in Figure 5.1.

Although this study employed deterministic energy scheduling assuming perfect forecasts, a comparative analysis was carried out to evaluate the effect of load forecast errors on the BMG's operation cost. For this purpose, Model-3 was employed to obtain the energy scheduling solution and calculate the operation cost of the HSB LL BMG. The analysis compared the deterministic and stochastic formulations of Model-3 in the following simulation test cases:

1. SO and DA dispatch (SO-DA)
2. SO and dispatch in RH (SO-RH)
3. DO and DA dispatch (DO-DA)
4. DO and dispatch in RH (DO-RH)

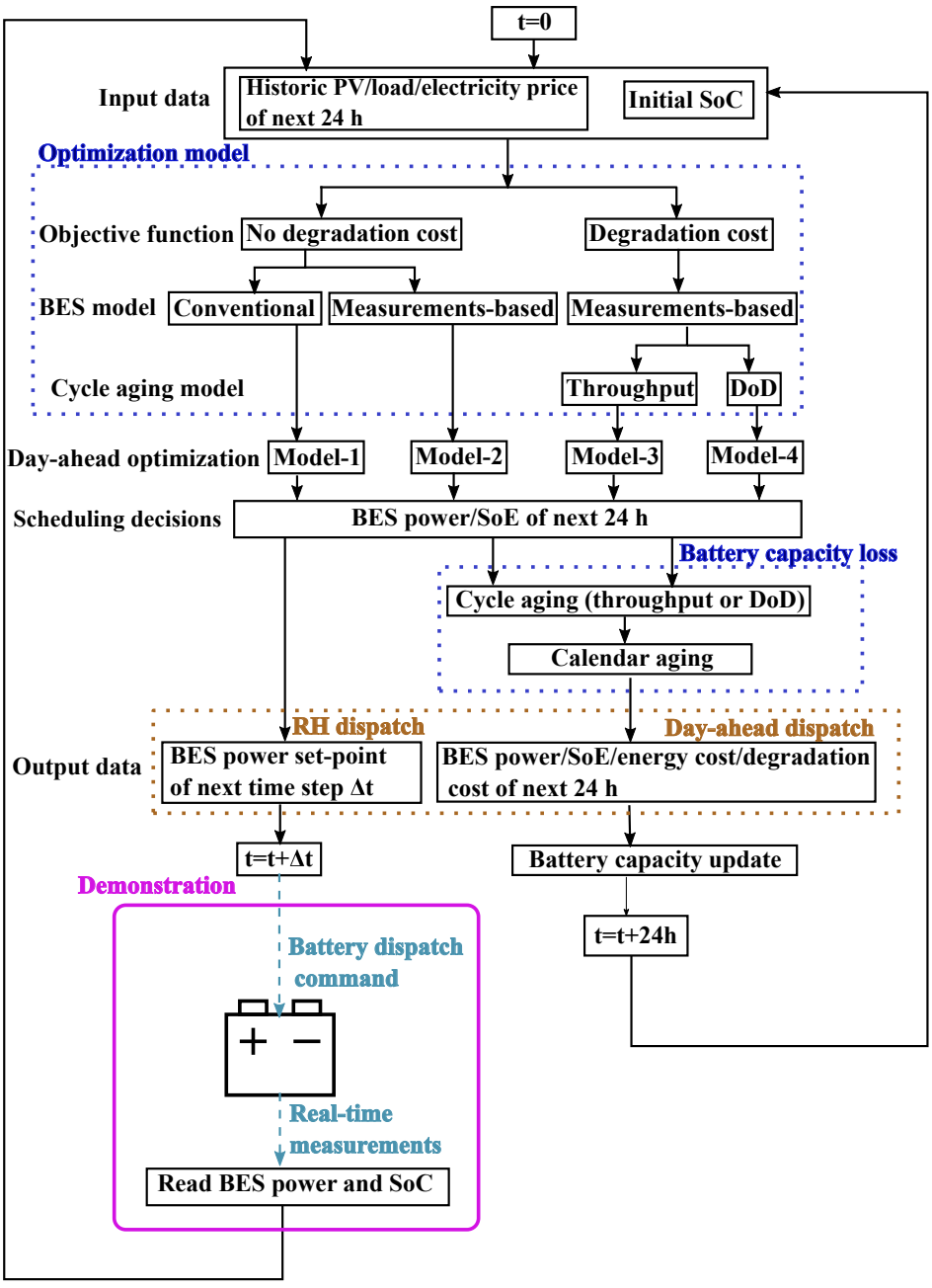

Figure 5.1: The flow diagram presenting the simulation and demonstration set-up of the deterministic BMG energy management model.

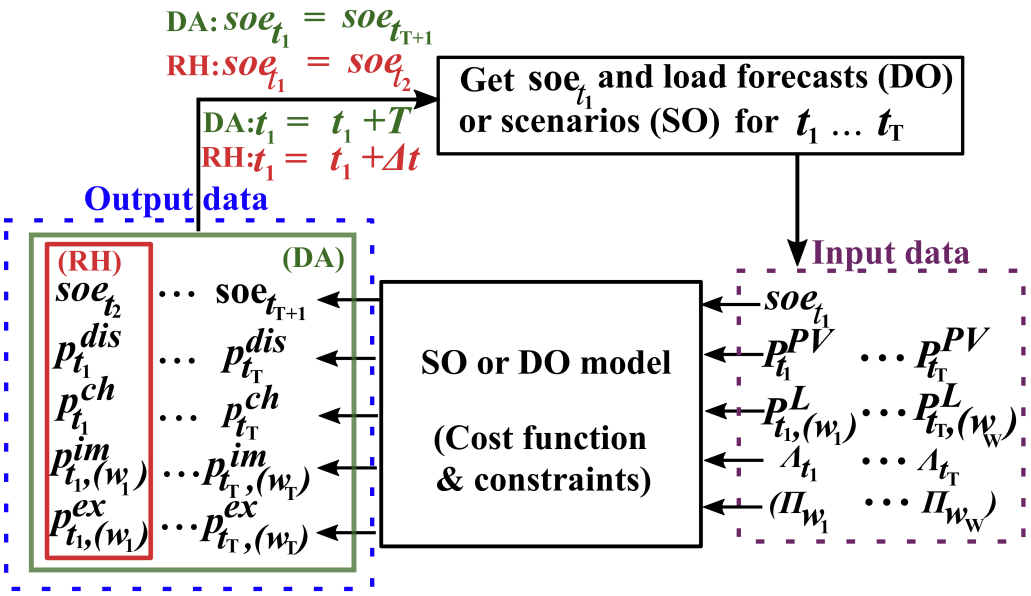

Figure 5.2: Illustrative diagram of the optimal deterministic and stochastic BMG energy dispatch implemented in RH and DA.

Figure 5.2 depicts in detail the input and output data related to the BMG optimal energy scheduling performed in these test cases, which used input values from load profiles acquired from different forecasting ML models [153]. The simulation and demonstration test cases in this chapter had a high time granularity ranging from 5 to 15 minutes and a short look-ahead period, which was typically 24 hours. Therefore, the comparative analysis also used short-term and high-resolution load forecasts. The dispatch time horizon and time resolution in the analysis was adjusted to fit the time horizon and time resolution of the available forecast profiles.

For a detailed characterization of the uncertainty in the SO problems of the comparative analysis, different probability distributions were used for each time step of the time horizon. Thus, instead of having a maximum percentage of uncertainty over the entire time horizon, there were different levels of uncertainty at each time step of the horizon. Specifically, the parameters of the Gaussian distributions depended on the time when the forecast results were acquired, the time when the predicted load values would occur, and the predicted time step ahead. The parameters were obtained from testing the forecasting models with historical data of the HSB LL building and implementing curve fittings. After the time horizon would be shifted either by a look-ahead period in DA dispatch or by Δt in RH dispatch both the load forecast profiles and the distributions of forecast errors would be updated and used as an input to the optimization model.

5.2.1 Formulation of the optimization problems

Four optimization models for the deterministic energy scheduling of a BMG m were defined based on the choice of cost function and the employed BES dispatch and BES degradation models:

- *Model-1*: The conventional BES scheduling model (Section 4.2.5.1) is used, while degradation cost is neglected. The terms c_m^{DER} and r_m^{flex} are omitted from (4.1). The formulated MILP problem is given by (4.1) s.t. (4.2a)–(4.4a), (4.6a), and (4.15)–(4.21).

- *Model-2*: A measurement-based BES scheduling model (Section 4.2.5.2) is used, which was validated with experimental values taken from the real residential building used as a BMG test system. As in Model-1, aging is neglected and the terms c_m^{DER} and r_m^{flex} are omitted from (4.1). The formulated LP problem is given by (4.1) s.t. (4.2a)–(4.4a), (4.6a), and (4.23)–(4.39).

- *Model-3*: The measurement-based model is combined with the cycle aging model with dependency on throughput, which was presented in Section 4.2.6. The formulated LP problem is given by (4.1) s.t. (4.2a)–(4.4a), (4.6a), (4.23)–(4.39), and (4.41)–(4.42). The term r_m^{flex} is omitted from (4.1), while $c_m^{DER}{=}c_m^B$.

- *Model-4*: The measurement-based model is combined with the cycle aging model with dependency on DoD, which was presented in Section 4.2.6. The formulated MILP problem is given by (4.1) s.t. (4.2a)–(4.4a), (4.6a), (4.23)–(4.39), and (4.43)–(4.50). The term r_m^{flex} is omitted from (4.1), while $c_m^{DER}{=}c_m^B$.

These optimization models can be employed to simulate the performance of a BMG's operation and they can also be integrated to a BMG-EMS, like the ones designed for the BMG testbeds which were employed for the demonstrations of this thesis.

5.2.2 Simulation set-up

The values of the buildings' electricity consumption and PV generation as well as the Nordpool spot market prices for bidding area 3 of Sweden [154] were used as inputs to BMG energy management models in simulations and demonstrations. For the HSB LL BMG, the 2018 building load and PV power output were used as inputs in order to run 365 DA energy scheduling simulations. Historical load demand and PV generation data were also used in the demonstrations and were treated as perfect forecasts. The input data for the simulations of the HSB LL BMG can be found in Appendix C.3, while the input data for the simulations of the Brf Viva BMG can be found in Appendix C.4. The actual grid tariffs and reimbursement fee, which have been taken from the website of the local DSO [155] and can be found in Appendix C.1, were also used for the corresponding parameters of the MODEFlex model. The characteristics of the two BMGs were described in Section 3.6.1 and Section 3.6.2. Note, however, that only 5 out of 14 BESs were considered in the study corresponding to the number of BESs that were available during the demonstrations of the BMG energy scheduling solutions in Brf Viva.

The main parameters used in the study's simulations and demonstrations are given in Table 5.1. The time horizon was 24 hours and the time discretization step was $\Delta t = 5$ minutes, except for the demonstrations at the HSB LL building, where the time step was $\Delta t = 15$ minutes. Considering the uncertainty in the future price of residential, stationary BESs [22], a sensitivity analysis was performed with three

Table 5.1: Parameters used in the simulations and demonstrations of deterministic energy scheduling applied on the HSB LL and Brf Viva BMGs.

H	80%
η^{ch}/η^{dis} (HSB LL)	91%/98%
η^{ch}/η^{dis} (Brf Viva)	97%/97%
SoE_{min}/SoE_{max} (Scenario-1)	30%/80%
SoE_{min}/SoE_{max} (Scenario-2)	10%/90%
BES installation prices (\$/kWh)	\$100, \$290, \$500
I_c	0.3 (HSB LL)
B_1	0.0013
B_1	0.3534

prices, i.e., \$100, \$290, and \$500 per kWh, for the BES installation cost. These approximately correspond to a best-case, likely, and worst-case scenario. Moreover, two scenarios of SoE limits were investigated: 30%-80% in Scenario-1 and 10%-90% in Scenario-2. The initial SoE of each simulation in DA dispatch and the first simulation of RH dispatch was set to 50%, while the end-of-life retained capacity was assumed to be $H = 80\%$. The parameters for the measurement-based models were obtained from sample data of tests on the BES systems at each BMG. The values of the charging and discharging efficiencies η^{ch}/η^{dis} used in Model-1 corresponded to the average values that were recorded during those tests, which were performed in April 2019 for the HSB LL BMG and December 2019 for the Brf Viva BMG. Since the measurement-based model is used in Model-2, Model-3, and Model-4 the charging and discharging efficiencies in these models were variable and dependent on SoE and power rate. The Li-ion cycle aging parameters of Model-3 were taken from [142], while the BES lifecycle loss function $\rho_t = 1/\phi(DoD)$, which is used in Model-4, was derived from Li-ion BES data provided in [30]. For the parameter I_c in (4.41), which is included in Model-3, the daily average C-rate was used for the HSB LL BMG, which was found to be 0.3 for the charging/discharging profiles of all four models over the 365 DA simulations.

In the long-term simulation of the HSB LL operation, the BES capacity was updated after each DA optimization, as shown in the flow diagram in Figure 5.1 showed. First, the percentage of capacity loss due to cycle aging given by $c^B(100\% - H)\%/C^{B,0}$ was calculated using one of the models presented in Section 4.2.6 (dependency on throughput or DoD), where the real-time C-rate was used in (4.41). Afterwards, this loss was subtracted from the capacity that the BES had at the beginning of the day. Finally, a linear model dependent on time elapsed was used to evaluate the BES capacity loss due to calendar aging:

$$Q^r = Q^{r,0} - A^c \Delta t. \tag{5.1}$$

The capacity loss that was calculated according to (5.1) was subtracted from the remaining BES capacity for every t of the simulation time horizon that was an open-circuit period for the BES. In (5.1), Q^r is the percentage of retained capacity after the rest period, $Q^{r,0}$ is the capacity percentage at the beginning of the rest period,

and A^c is a parameter dependent on SoC level. The values for A^c were derived from linear interpolation of the calendar aging data given in [141]. As mentioned in Section 4.2.6, the temperature in stationary BESs can easily be controlled and was therefore considered to be constant ($T = 298K$).

The same parameters presented in Table 5.1 were also used in the test cases of the comparative analysis. The time horizon and time resolution of the energy dispatch was set to be identical to the time horizon and time resolution of the available forecasts. Thus, for this analysis, the time horizon was 24 hours and the time step was $\Delta t = 15$ minutes. In addition, (4.40) with $SoE_m^{init} = 0.5$ was added to the formulation of Model-3 for the test cases with DA dispatch. The PV power output was deterministic in the SO models i.e., a perfect PV generation forecast was assumed, to focus on evaluating the effect of the load forecasting errors on the BMG costs. The simulations for all the test cases of the comparative analysis were performed for a week in December, 2018 using the historical load profile as the base scenario for SO and as the realized scenario for DO. In the studied week, there was minimal PV production to effectively eliminate the impact of the approximation due to the perfect PV forecast assumption and enhance the accuracy of the results.

5.2.3 Rule-based BES dispatch

The BMG-EMS could also dispatch the BES using a rule-based algorithm representing the BAU BES operation. This algorithm can be used to reduce the peak load consumption as well as to even out the aggregated load profile as seen by the DSO at the PCC. The BES dispatch under the rule-based algorithm was demonstrated for comparison with the BES dispatch solutions obtained from the optimization models.

This rule-based algorithm tries to constrain the power exchange with the grid between a peak and a low load threshold (P_{peak} and P_{low}, respectively), which can be externally set by the BMG operator. The algorithm updates the BES charging/discharging power output set-point per iteration c (p_c^{ch}/p_c^{dis}) based on the SoC (soc_c) and the average PCC power exchange (p_c^{PCC}) of the previous iteration loop, which are the input values to the rule-based algorithm. The duration of each iteration loop depends on the choice of Δt. The number of iterations N^{it} depends on the scheduling period. To avoid deep discharges/charges of the BES, the SoE (soe) limits are considered (SoE_{min}, SoE_{max}).

Algorithm 1 describes the rule-based algorithm and the interaction between the BMG-EMS and the controlled system via the Message Queue Telemetry Transport (MQTT) protocol. As can be seen, the conventional BES model (see Section 4.2.5) with constant charging/discharging power limits P_{max}^+/P_{max}^- is used for the calculation of the charging/discharging BES power requests p_c^{ch}/p_c^{dis}. The rule-based algorithm can easily be adjusted to incorporate dependency of power limits to the SoE by utilizing BES measurements. It cannot be expected that the applied BES scheduling will be as accurate as when the measurement-based model is used, however, the BES control can become more effective, which can be useful, if BES requests calculated with the conventional BES model are not fully met.

Algorithm 1: Rule-based BES dispatch algorithm

Connect to the MQTT broker.
Subscribe to the available topics.
while $c \leq N^{it}$ **do**
    Read p_c^{PCC} and soc_c;
    Calculate p_c^{ch}/p_c^{dis} so that $P_{low} \leq p_c^{PCC} \leq P_{peak}$;
    if $p_c^{ch}/p_c^{dis} > P_{max}^{+}/P_{max}^{-}$ **then**
        $p_c^{ch}/p_c^{dis} = P_{max}^{+}/P_{max}^{-}$;
    end if
    if $(soe_{c+1} > SoE_{max}) \vee (soe_{c+1} < SoE_{min})$ **then**
        Reduce p_c^{ch}/p_c^{dis} so that $SoE_{min} \leq soe_{c+1} \leq SoE_{max}$;
    end if
    Publish p_c^{ch}/p_c^{dis};
end while

5.3 Results and discussions

This section presents the simulation and demonstration results that validated the performance of the BMG energy dispatch model. The factors affecting the cost of the energy dispatch and the utilization of the BMG's BES are analyzed and discussed.

5.3.1 Assessment of cost and degradation

Figure 5.3–5.4 present the annual assessment metrics of the energy dispatch in the HSB LL BMG according to the four models presented in Section 5.2.1 in the two scenarios of SoE limits given in Table 5.1. The calculation of cycle aging and the respective cost is presented for both approaches (dependency on throughput/DoD) for comparison. The assessment of the models was performed according to the measurement-based BES model. Thus, the maximum feasible charging/discharging power was chosen, when the BES power set-points of Model-1 were infeasible with respect to the measurement-based model. Figure 5.5 shows an example of one DA simulation, where the measurement-based model gives a different estimation of the SoE profile, when the set-points of Model-1 are used as an input.

5.3.1.1 Scenario-1

As Figure 5.3 shows, Model-3 and Model-4 yielded the most economic operation at all prices. The total cost for either model was not higher than \$4401 at \$100, while Model-4 yielded the lowest cost at \$290 and \$500, which was not higher than \$4591 and \$4795, respectively. Even though the energy cost was increased in these models, the total capacity loss was lower than in Model-1 and Model-2, which did not include the cycle aging cost in their objective functions and gave a total cost of at least \$4408 at \$100, \$4616 at \$290, and \$4847 at \$500. Comparing with the highest cost of either Model-1 or Model-2, a reduction of up to 0.4%, 0.6%, and 1.2% could be observed for Model-3 at the price of \$100, \$290, and \$500, respectively.

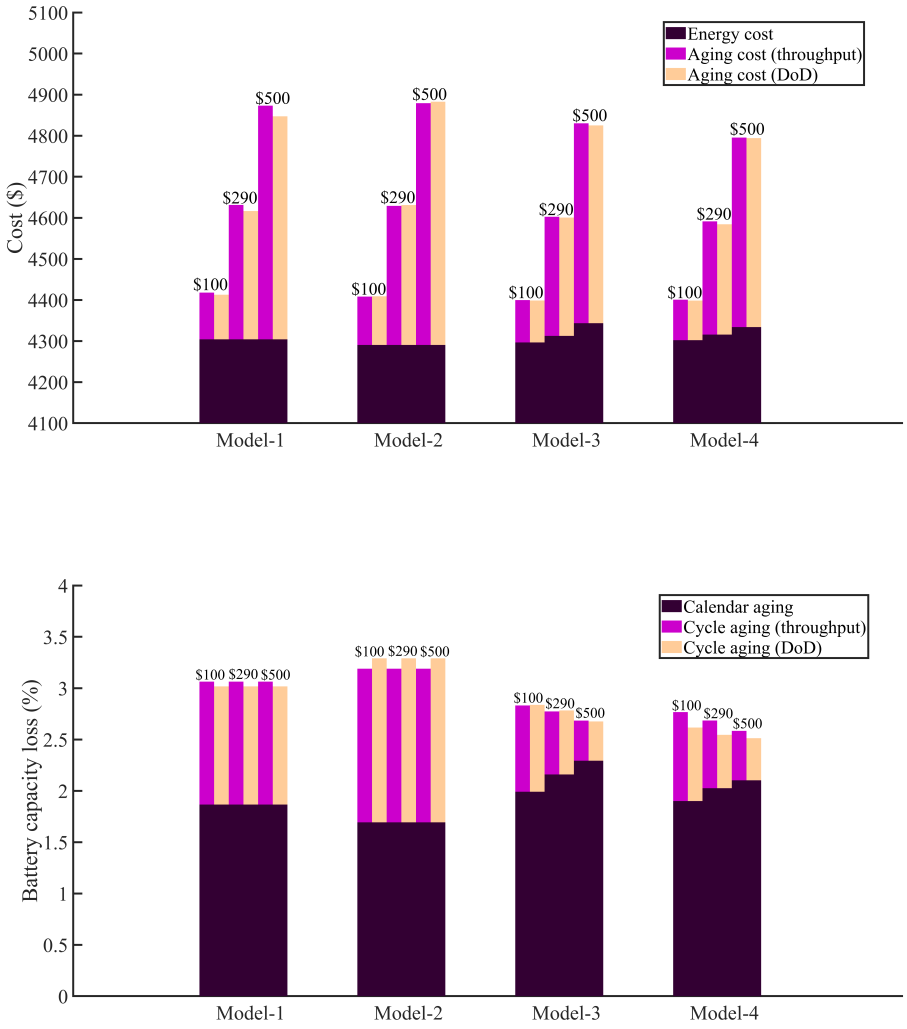

Figure 5.3: The assessment metrics of the energy dispatch in the HSB LL BMG for Scenario-1 (SoE limits of 30%-80%), where the considered BES installation price is indicated on top of the bars representing the total cost or the total capacity loss.

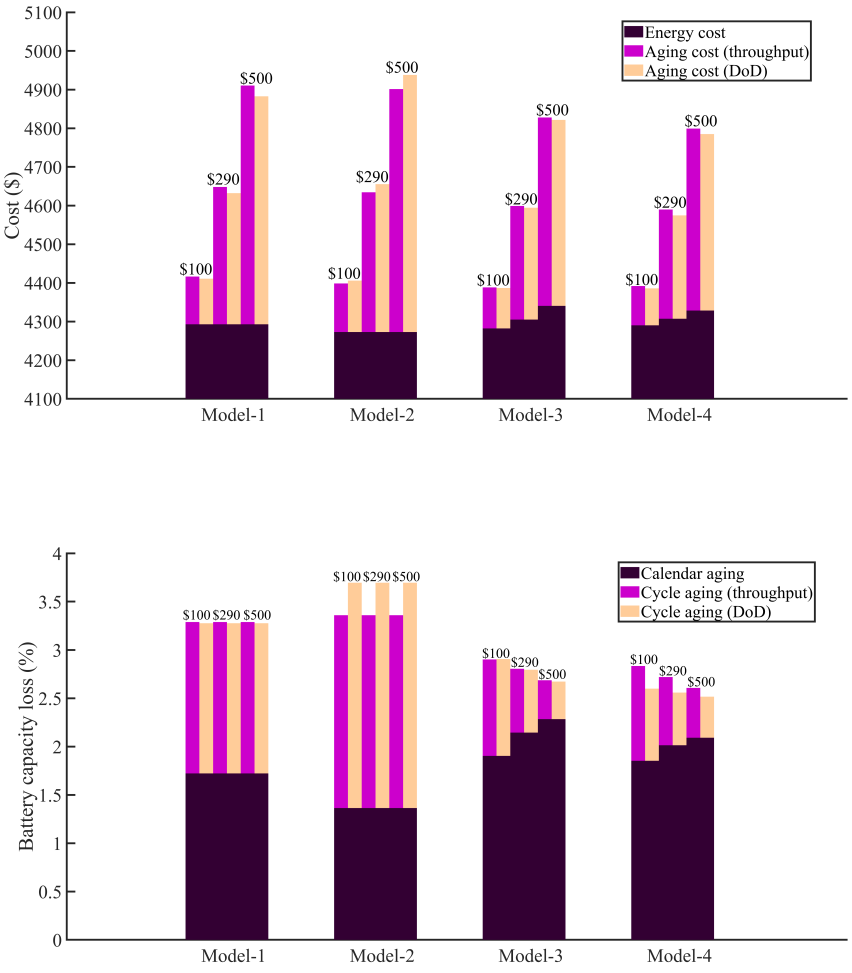

Figure 5.4: The assessment metrics of the energy dispatch in the HSB LL BMG for Scenario-2 (SoE limits of 10%-90%), where the considered BES installation price is indicated on top of the bars representing the total cost or the total capacity loss.

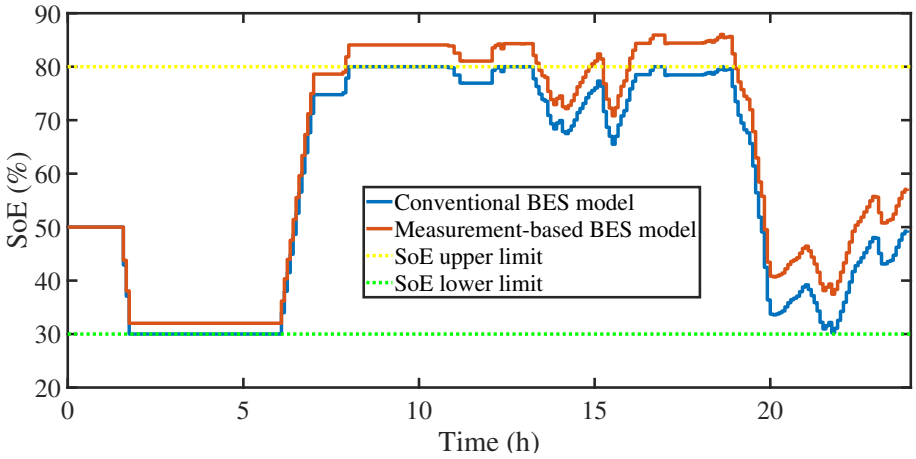

Figure 5.5: The difference in the SoE estimation of the BES at HSB LL BMG, when the solution (BES power set-points) of Model-1 (conventional BES model) is used as an input to the measurement-based model.

Similarly, a reduction of up to 0.4%, 1.0%, and 1.8% could be observed for Model-4 at the price of \$100, \$290, and \$500, respectively. As the BES prices increase, the cycle aging decreases for Model-3 and Model-4. At the same time, calendar aging increases, as the BES is cycled less. Model-4 caused the lowest capacity loss among all models, which was not higher than 2.8% (at \$100). Interestingly, Model-2 caused the highest capacity loss due to cycle aging (at least 1.5%), which was even higher than in Model-1. Apparently, the less accurate SoE estimation of Model-1 led to slower cycle aging. However, Model-2 could yield a lower total cost than Model-1, especially at lower BES prices, because it caused the lowest calendar aging (1.7%) and, more importantly, yielded the lowest energy cost (\$4290) out of all models.

5.3.1.2 Scenario-2

Similar trends with Scenario-1 can be observed among the models and across the three BES prices in Scenario-2, Figure 5.4. The economic performance of Model-3 and Model-4 was enhanced in Scenario-2, where the total cost of either model was not higher than \$4392 at \$100. Again, Model-4 yielded the lowest cost at \$290 and \$500, which was not higher than \$4590 and \$4799, respectively. Apart from the lower energy cost in Scenario-2, the calendar aging also decreased, as lower values of SoE helped the BES retain more capacity during rest periods. This is why these models achieved the best economic performance in Scenario-2 as well.

In contrast, Model-1 and Model-2 gave higher total costs in Scenario-2 at all prices and under both assessments of cycle aging. Again, comparing with the highest cost of either Model-1 or Model-2, a reduction of up to 0.7%, 1.3%, and 2.3% could be observed for Model-3 at the price of \$100, \$290, and \$500, respectively, Similarly, a reduction of up to 0.7%, 1.7%, and 3.1% could be observed for Model-4 at the price of \$100, \$290, and \$500, respectively. Model-2 gave the lowest energy cost (\$4273) and the lowest capacity loss due to calendar aging (1.4%) out of all models. At the same time, however, it caused the highest cycle-based capacity loss (at least 2%)

leading to the largest BES degradation, while Model-4 gave the lowest capacity loss in total, which was not higher than 2.8% at \$100.

5.3.1.3 Discussion on energy and degradation cost

The evaluation of Model-3 and Model-4 highlighted the importance of including both energy and degradation cost in the objective functions that determine the BES dispatch. These models, which combined the measurement-based model with cycle aging models dependent on throughput (Model-3) or DoD (Model-4), could reduce the annual energy and degradation cost by up to 3.1% under the considered pricing scheme compared to when cycle aging cost was neglected in the BES scheduling. Ideally, the cost of calendar aging should also be included in the optimization model to obtain the most economic BES schedule and it can be considered in a future study. As shown by the results, there is a trade-off between cycle and calendar aging and thus, a BES schedule that induces lower cycle aging causes higher calendar aging and vice versa. Nevertheless, Model-3 and Model-4 always yielded the lowest degradation. In particular, the capacity loss was found to be lowest in Model-4. Model-4 also yielded the lowest cost for the BES prices of \$290 and \$500.

5.3.1.4 Discussion on degradation models

In both scenarios, Model-4 gave the lowest total cost at \$290 and \$500 irrespective of the deviation between the two different assessments of cycle aging. Either Model-3 or Model-4 could achieve the most economic operation at \$100. Comparing this two models, Model-4 caused a lower calendar aging (despite directly forcing the BES to higher SoE values), which contributed to a reduced degradation cost, especially when it was a larger part of the total cost. On the other hand, Model-3 gave lower energy cost, which contributed to the reduction of its total cost, when the degradation cost was a less significant part of it. When cycle aging was omitted from the cost function, there was no clear advantage of using the more accurate BES dispatch model i.e., the measurement-based model (Model-2) instead of the conventional one (Model-1).

The accuracy of the aging models can vary depending on the BES chemistry. The aging models used in this study might not be applicable to all Li-ion BESs. Moreover, it can be hard to obtain reliable aging parameters for each installed stationary BES, if aging models that are derived from empirical fitting are to be used, such as, for example, the cycle aging model with dependency on cumulative throughput, which was presented in Section 4.2.6.1 and the calendar aging model.

The cycle aging model with dependency on DoD which was presented in Section 4.2.6.2, on the other hand, is a more practical modeling approach, as it uses a degradation cost function derived by data provided by the manufacturer, which also adds reliability to the cost of the implemented BES scheduling solution. It should be noted, however, that not all manufacturers provide such detailed data regarding the impact of each cycle to the BES lifetime (often only a maximum number of cycles or throughput is given). Rainflow counting could also be used instead of the half-cycle counting used with this model, however, as explained in [75], the cost

function would not be continuously differentiable, and it could therefore not be used in an LP problem formulation. Furthermore, the results (calculated capacity loss after each DA optimization) based on half-cycle counting agreed with the results based on rainflow counting (obtained by the *rainflow* function in MATLAB [125]), thus validating the half-cycle counting approach used in the cycle aging model with dependency on DoD.

5.3.1.5 Discussion on SoE limits

Model-3 and Model-4 could be used with either conservative SoE limits or with less strict SoE limits, as both scenarios resulted in almost equal economic benefits for the BMG owner and the residents in the building. On the other hand, if degradation is neglected in the BES scheduling, it is suggested that conservative limits should be applied to prolong the BES lifetime, unless high economic benefits that can offset the degradation cost can be guaranteed. Test with scenarios of different SoE limits are suggested to investigate if the obtained results can be further improved. The choice of optimal SoE limits depends on the possible economic benefit from load-shifting, which is affected e.g., by price fluctuation or PV generation within a day. If the revenue can compensate for the degradation cost, then a larger SoE window can be used.

5.3.1.6 Discussion on battery retirement

The degradation cost in this study is related with H, which is used to evaluate the remaining useful lifetime of the BES and serves as a termination (retirement) criterion [156]. It is assumed that, when the BES capacity is reduced to $H\%$ of its initial value, the BES is replaced. However, storing electricity generated from RES is a less demanding function than powering EVs. This is also the motivation behind using retired EV BESs as second-life BESs in load shifting applications [157]. BESs with reduced capacity could still be used in energy management, which could potentially lead to an overestimation of the degradation cost, if the BES is ultimately replaced at a capacity, which is lower than H. In practice, the BES needs to be replaced after a certain part of its initial capacity is lost, as the benefit of using the BES for load shifting is reduced and the overall BES performance deteriorates. The choice of H, however, is still an open question, as there are relatively few research studies and applications of residential, stationary BESs

5.3.1.7 Discussion on revenue streams

The motivation for focusing on energy arbitrage as the main revenue stream in this study is twofold: 1) operational policies that reduce degradation have a more severe impact on the profit from energy arbitrage than the profit from balancing services [79], which makes the contribution of the measurement-based model in reducing the energy cost more important, and 2) there are strong indications that energy arbitrage would be the preferred revenue stream for residential BES owners, who consider protection against high electricity prices as one of the main motives for installation of residential BESs [158].

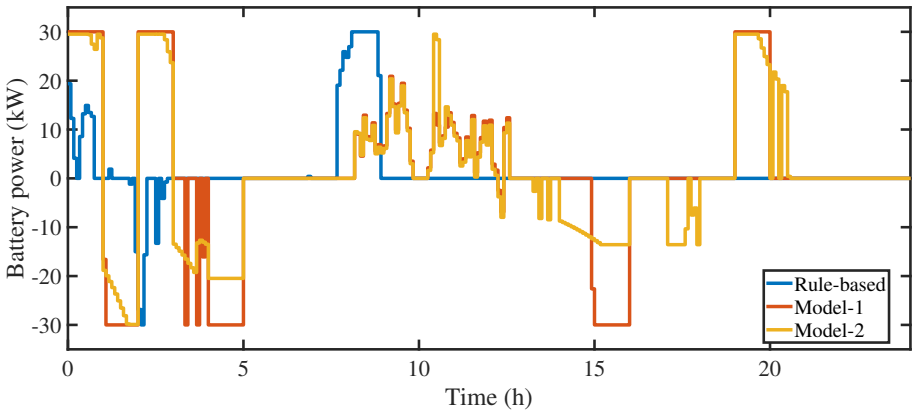

Figure 5.6: The BES power dispatch at the Brf Viva BMG according to the rule-based algorithm, Model-1, and Model-2.

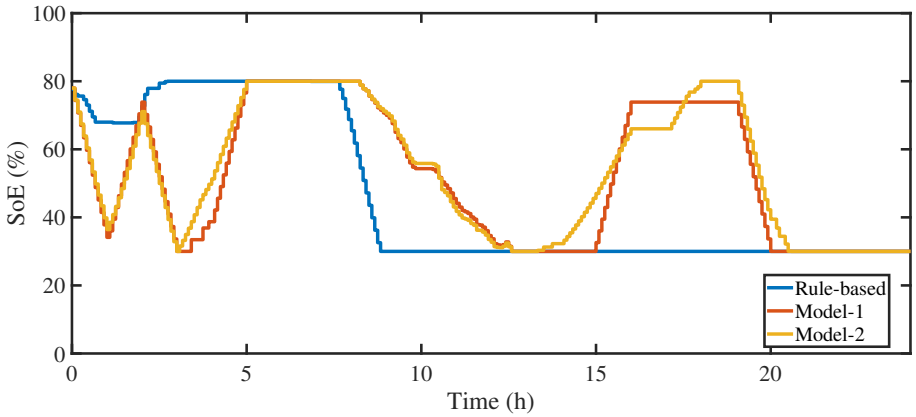

Figure 5.7: The SoE estimation of the BES at the Brf Viva BMG according to the rule-based algorithm, Model-1, and Model-2.

5.3.2 Comparison of BES power and SoE profiles

A comparison of the daily BES power dispatch and SoE the profile obtained from Model-1, Model-2, and Model-4, which were presented in Section 5.2.1, as well as the rule-based algorithm, which was presented in Section 5.2.3, can be seen in Figure 5.6–5.9 for the Brf Viva BMG. The BES dispatch was performed in RH to allow for comparison of the simulation results with the corresponding results from the demonstrations at Brf Viva (see Section 5.3.3.2).

The BES power dispatch in Figure 5.6 and the SoE profile in Figure 5.7 show that the BES was cycled more when the BES was used to minimize energy cost (Model-1 and Model-2), as the BES power followed the fluctuations of the spot price. Small variations in the BES power e.g., between hour 8 and hour 13, can be attributed to the fact that, in each simulation, the forecast of the load and the PV generation was updated, which made the BMG-EMS re-adjust the charging or discharging rate. Bigger variations in BES power were a result of the spot price difference, since the BMG-EMS tried to maximize the profit through energy arbitrage. This can be observed e.g., in the first four hours of the simulation, where there were big

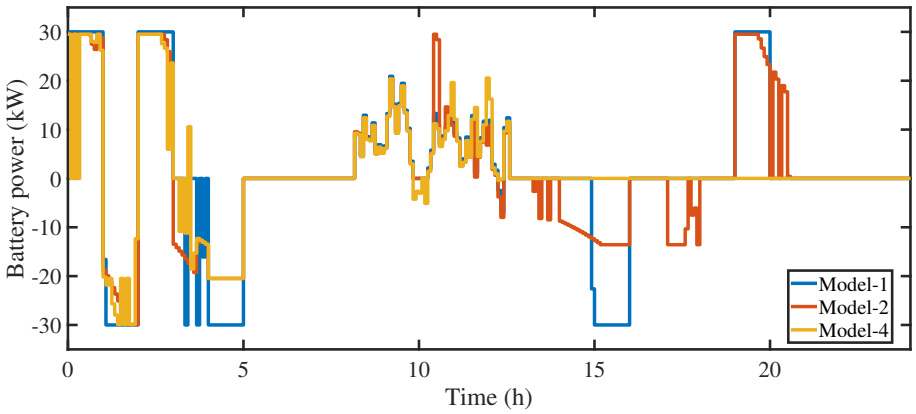

Figure 5.8: The BES power dispatch at the Brf Viva BMG according to Model-1, Model-2, and Model-4.

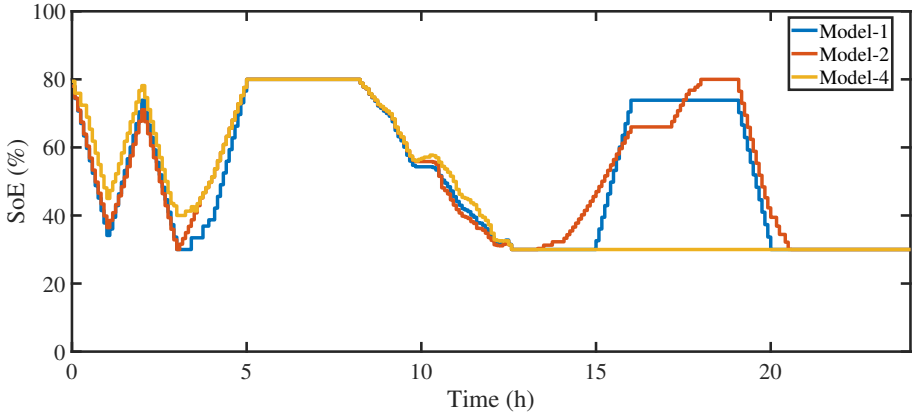

Figure 5.9: The SoE estimation of the BES at the Brf Viva BMG according to Model-1, Model-2, and Model-4.

changes in the electricity price of each hour. Between the BES scheduling according to Model-1 and the BES scheduling according to Model-2 there were only small differences, as can be seen from their SoE profiles.

When BES degradation was considered, however, there was a trade-off between the minimization of energy cost through load shifting and the minimization of BES degradation cost. The cost of cycle aging, which is considered in Model-4, penalizes both the number of cycles and deep discharges resulting in the BES dispatch and SoE profile seen in Figure 5.8–5.9. As can be seen, even when the BES was cycled in the first hours (Figure 5.8), it did not reach the low SoE value that Model-1 and Model-2 yielded (Figure 5.9). In addition to this, the BES was not cycled during the second half of the scheduling period as it happened with Model-1 and Model-2 because the profit from energy arbitrage was very small and did not compensate for the cost of lifecycle loss of the BES. This profit was in fact that small, that the daily BMG energy cost (including peak power cost) was practically similar among the optimization models (about $70).

When the rule-base algorithm was applied, the daily BMG energy cost was higher (about $72), although that could be different depending on the choice of the peak and low load threshold. The rule-based algorithm, however, uses the BES in a non-optimal way and it is hard to capture and reduce the peak power. Since the future load and PV generation profiles are not considered, the energy storage levels might be depleted, when the daily peak power occurs. This problem can be observed in Figure 5.6–5.7, where there is big discharge power rate applied by the rule-based algorithm starting around hour 8, whereas the optimization models (Model-1, Model-2, and Model-4) apply a more conservative BES scheduling, saving energy for the expected peak power. Therefore, the rule-based algorithm results in a peak load of 152.2 kW, while the peak power according to the optimization models ranges from 131.9 to 132.9 kW.

5.3.3 Demonstration results

The designed BMG-EMSs implemented remote control of the buildings' BESs at each demonstration test site. The BMG-EMSs integrated optimization models formulated in Section 5.2.1 and utilized the in-built measurements and control systems of the bi-directional grid side converter installed at each building.

5.3.3.1 HSB LL

The demonstrations with the HSB LL BES showed that the BES dispatch, which was implemented on a 15-minute time scale, could not follow the schedule obtained with Model-1 as well as it followed the schedule obtained with Model-2. The same input data (including initial SoC measured at $t = 0$) were used for both demonstrations to allow for comparison of their results. Figure 5.10 and Figure 5.11 respectively show the BES response during a 24-hour demonstration of Model-1 and Model-2 at HSB LL building. In Figure 5.10, it can clearly be observed that the dispatched power did not match the big charging request.

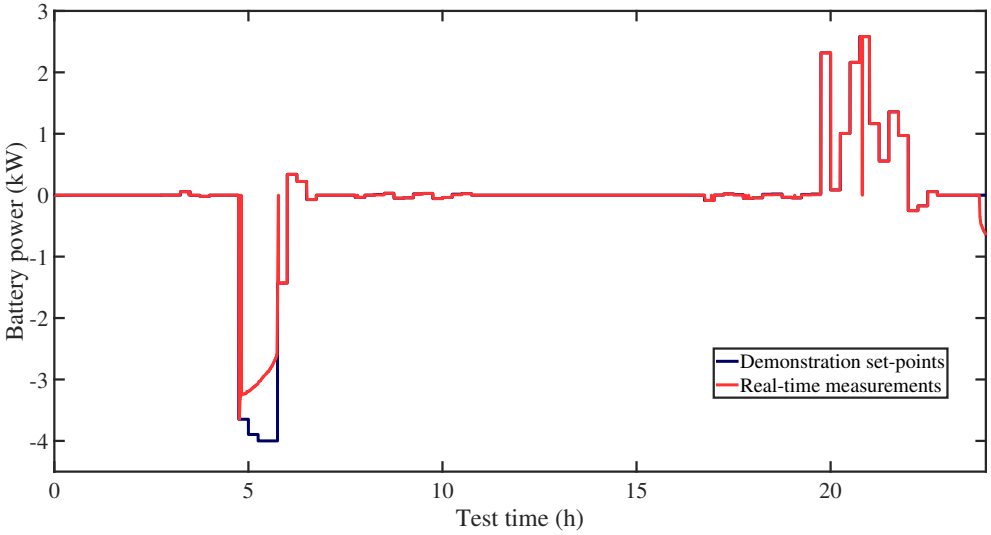

Figure 5.10: The set-points and the real-time measurements of the BES power (demonstration of Model-1 at HSB LL building).

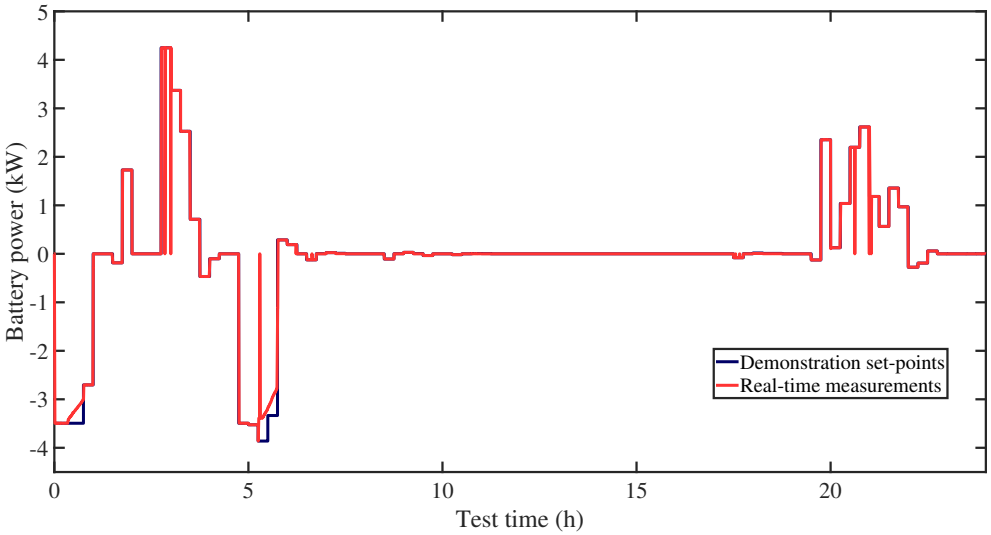

Figure 5.11: The set-points and the real-time measurements of the BES power (demonstration of Model-2 at HSB LL building).

As explained in Section 4.2.5.2, SoE mismatches or SoH issues can lead to deviations from the expected BES performance. These deviation are caused by the current limiter function of the battery management system which is activated to protect the BES from undesired operating conditions e.g., high temperatures or over/under-voltages (caused by too high/low SoC or degraded BES cells, as was the case in HSB LL). To mitigate this issue with Model-1 one would have to apply stricter operation limits in upper/lower SoE and BES power. This is, however, a rule-based solution approach that would considerably reduce the energy flexibility that can be provided by the BES. An alternative solution can be found in the measurement-based model. As seen in Figure 5.11, the BES response was significantly improved in the demonstration of Model-2 without implementing additional, non-optimal limits. This is because any dependency of the efficiencies and delivered BES power on the SoE that has been captured by the discharging/charging sample data has been considered in the parameterization of this model.

The comparison of Model-1 and Model-2 showed that the BES was cycled more when the accuracy of the BES model was improved. This confirms what was indicated by the simulation results, as Model-2 gave a higher cycle aging. Moreover, the total mismatch in delivered charging and discharging BES energy over the requested BES energy was 3.7% and 13.3% in the demonstration of Model-2 and Model-1, respectively. This validates the enhanced accuracy of the measurement-based model and, by extent, the reliability of the BES scheduling solution in the simulation results of Section 5.3.1, since the measurement-based model was incorporated in Model-2, Model-3, and Model-4 and the assessment of Model-1 was performed using the measurement-based model.

Figure 5.12–5.13 show the estimated on a 15-minute time scale SoE according to Model-1 and Model-2, respectively. These values are compared with the SoC measurements (updated per 5 seconds) provided by the converter controller and the SoE limits (as were defined by the BMG operator). Both models provided an accurate SoE estimation on a 15-minute time scale, while the violations of the SoE limits were negligible. To evaluate the accuracy of the SoE quality the following index was defined:

$$q^{idx} = \frac{||soe_t - soc_t||}{soe_t}. \tag{5.2}$$

The quality index q^{idx} gives the percentage value of the difference between the estimated SoE and the measured SoC of one time step. The average quality index for Model-1 and Model-2 was 0.5% and 1.2%, respectively. Model-1 had a better performance in terms of SoE estimation, however, the two models gave a different BES scheduling and SoE profile, as the BES performed more cycles with Model-2.

5.3.3.2 Brf Viva

The results from the demonstration of the BES dispatch at the Brf Viva BMG showed that both the conventional and the measurement-based BES scheduling

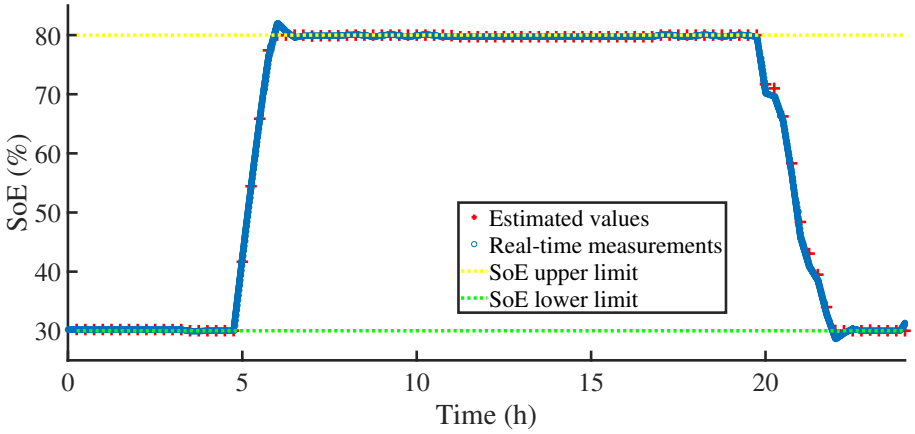

Figure 5.12: The estimated SoE of the BES dispatch model during the demonstration of Model-1 at HSB LL building and the real-time value of SoC as measured by the converter (updated per 5 seconds).

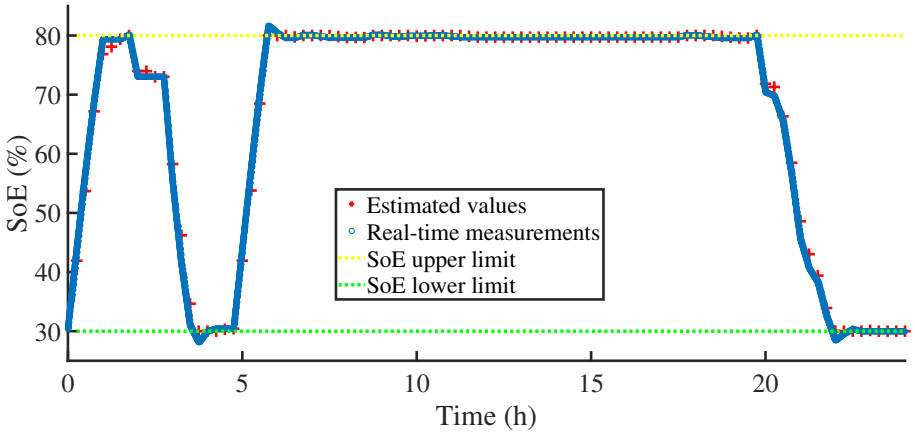

Figure 5.13: The estimated SoE of the BES dispatch model during the demonstration of Model-2 at HSB LL building and the real-time value of SoC as measured by the converter (updated per 5 seconds).

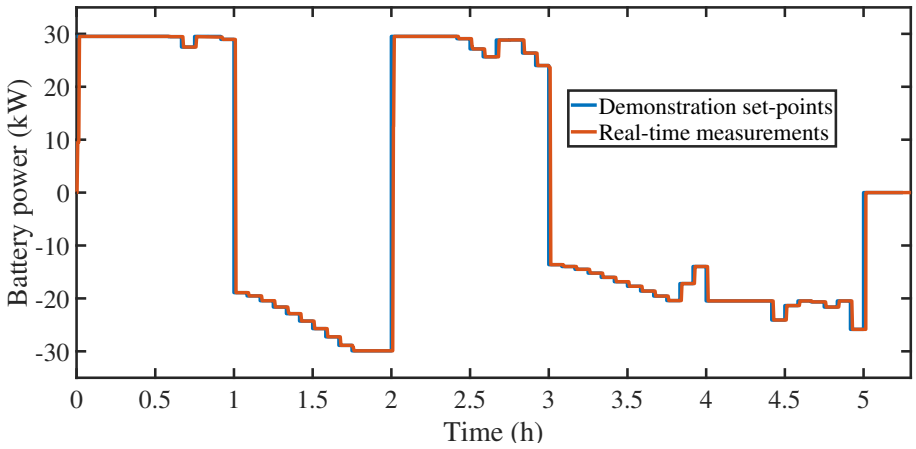

Figure 5.14: The dispatched set-points of Model-2 and the real-time power measurements (demonstration with the system of BESs at Brf Viva).

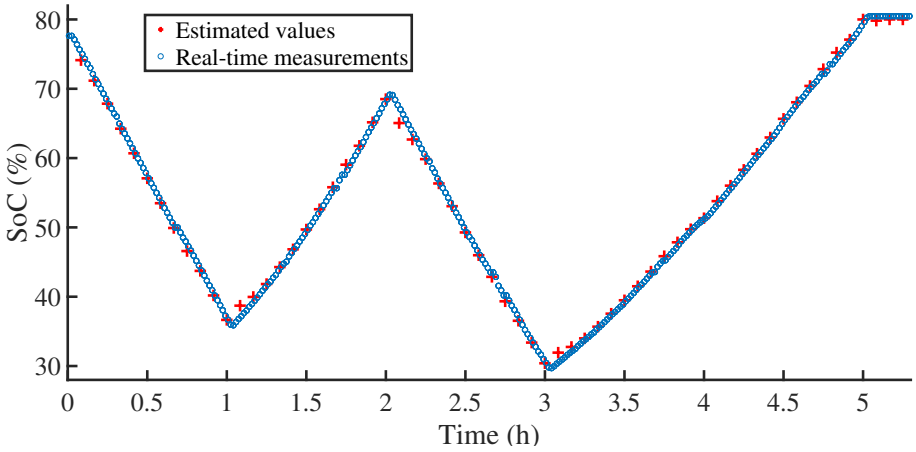

Figure 5.15: The estimated SoC during the demonstration of BES scheduling under Model-2 and the real-time value of SoC (updated per minute) of the system of BESs at Brf Viva.

model had acceptable accuracy and the BES dispatch followed the schedule. Moreover, the demonstration results matched the simulation results, which were presented in Section 5.3.2. The same input data (including initial SoC measured at $t = 0$) were used both for demonstrations and simulations to allow for comparison of their results. As an example, Figure 5.14–5.16 present the results from the demonstration of the BES scheduling obtained by Model-2.

The demonstration results validated the accuracy of Model-2, as the response of the system of BESs matches the requests from the BMG-EMS in Figure 5.14. Moreover, the estimated on a 5-minutes time scale SoE according to this model matches the (updated per minute) SoC measurements provided by the converter controller, as can be seen in Figure 5.15. Thus, the results prove that Model-2, and by extent the proposed Model-3 and Model-4, can be used for close to real-time BMG energy management. Small deviations in the power dispatch compared to the simulated BES scheduling (see Figure 5.16) are attributed to the fact that in the demonstration,

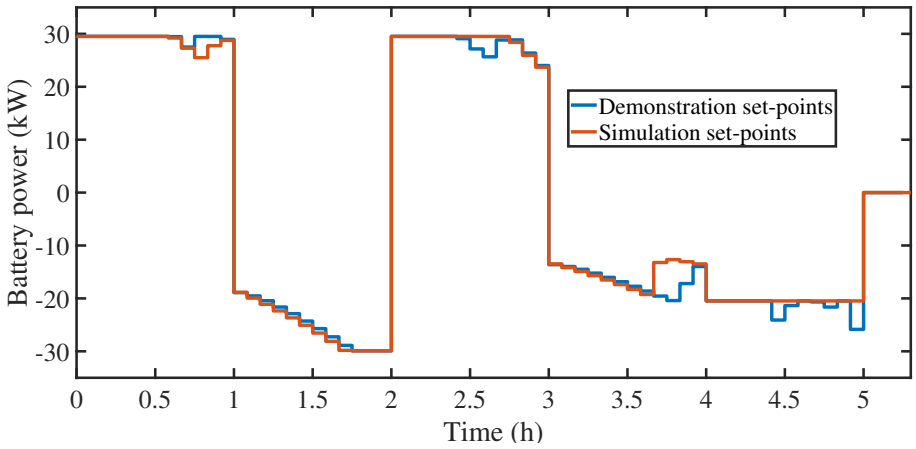

Figure 5.16: The BES power set-points of simulated and demonstrated BES scheduling of the system of BESs at Brf Viva under Model-2.

the measured SoC was entered as an input to the algorithm, whereas simulations used the estimated SoE levels as inputs. The average quality index for Model-1 and Model-2 was 1.5% and 1%, respectively, suggesting a slightly improved performance of the BMG energy management model, when the measurement-based BES scheduling model was used.

5.3.4 Effect of load forecasting errors on the operation cost of the BMG

This section analyzes the effect of short-term and high-resolution load forecast errors on the BMG's operation cost by presenting and discussing the results of the test cases described in Section 5.2. The ML load forecasting models are also presented in this section and their performance is compared.

5.3.4.1 ML load forecasting models

The ML models used and tested for the load forecasting were: 1) a linear regression (LR) [58,159–161] model, 2) an artificial NN (ANN) [162] with backpropagation, and a long short-term memory (LSTM) model [60, 61, 163], which is a type of artificial recurrent NN. For the development of these models only time-series historical electric load data were used. These data, which had a time resolution of 15 minutes, were taken from the HSB LL [115].

The performance of the ML models was evaluated using the mean absolute percentage error (MAPE). The average MAPE over the 24-hour time horizon was found to be approximately 12% for all three ML models [153]. Table 5.2 shows the MAPE of each model for the first four quarters of the forecast's time horizon. These MAPEs were computed over all of prediction tests i.e., a prediction test was run for each time step amounting to a total of 365x96 tests for each ML model. The models were also compared with a base line model i.e., a naive and empirical approach which assumes that the coming four quarters maintain the load value of the current quarter.

Table 5.2: MAPEs for the ML and the base line models over the first four quarters. The MAPEs were calculated on all prediction tests of the HSB LL BMG's load.

Model	15 min	30 min	45 min	60 min
Linear Regression	7.79%	9.63%	10.25%	10.60%
Artificial Neural Network	8.10%	9.77%	10.25%	10.06%
Long Short-term Memory	8.93%	9.98%	10.45%	10.73%
Base Line	8.28%	11.14%	12.43%	12.26%

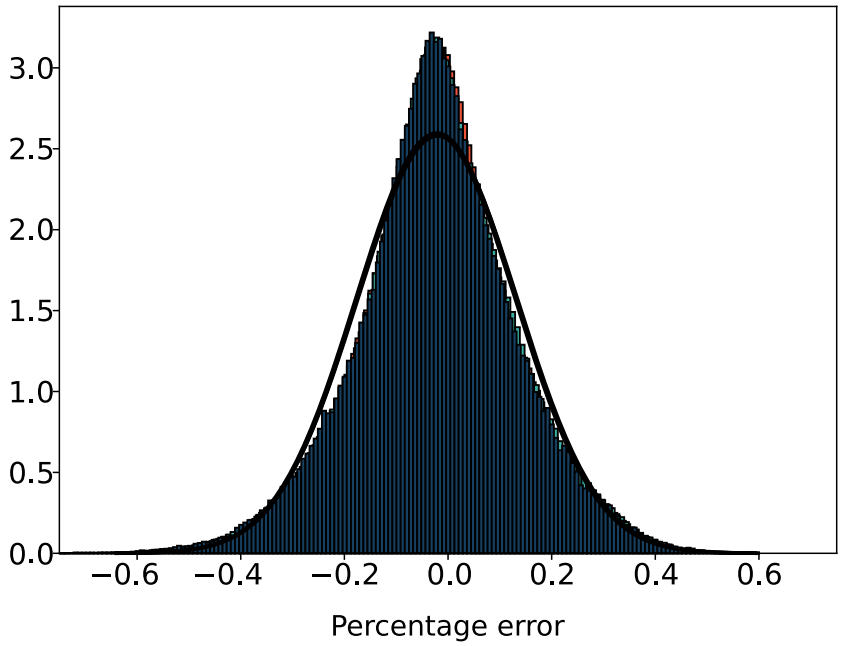

Figure 5.17: Histogram of percentage error for all prediction tests of the HSB LL BMG's load demand. The solid line is a Gaussian distribution fitted to the data.

To corroborate the common assumption that the probability distribution of the load forecast error takes a Gaussian form the errors for each prediction test of the ML models were recorded and presented as a histogram in Figure 5.17. As can be seen, the results verified that the probability distribution of the error can be well approximated by a Gaussian distribution. In summary, the load forecast error normally ranged between about 10%-15% while it was unlikely to be more than 60%. As for the dependencies of these errors on the factors described in Section 5.2, these can be visualized in Figure 5.18. The big deviation between the values of MAPE recorded at the first time steps of the look-ahead horizon and the values of MAPE throughout the rest of the time horizon demonstrates the need to have different probability distribution at each time step. A big deviation is also observed when comparing the values of MAPE between the hours 00:00 and 06:00 to the values of MAPE recorded at different hours, which demonstrates the dependency on the time of occurrence of the predicted load value irrespective of how far ahead the value is found within the look-ahead horizon.

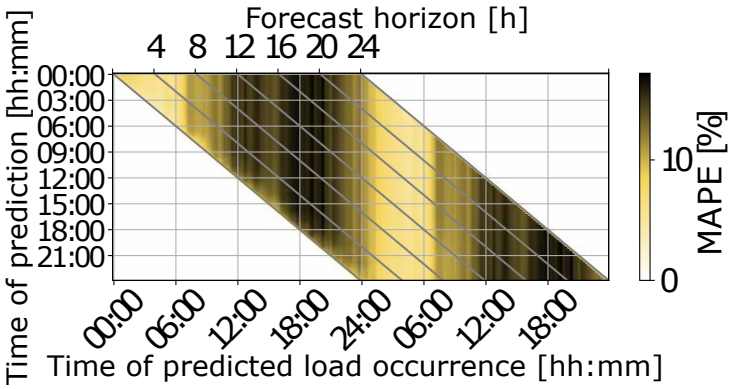

Figure 5.18: Color chart of MAPE in relationship with time of prediction (y-axis) and time of the load value occurrence (x-axis) [153]. The slanted lines through the chart show the time ahead.

5.3.4.2 Effect of forecast error

The costs related to the BMG energy dispatch can be seen in Table 5.3, where all three ML models were used to give input to each test case. As can be seen from the total cost f, similar results were achieved with DO and SO and the same was observed comparing DA and RH dispatch. These were perhaps counter-intuitive outcomes. As Figure 5.19 shows, the forecast errors were non-negligible. In fact, significant variations were recorded in phase i.e., timing, and especially amplitude between the actual and the forecast load demand. Therefore, judging from Figure 5.19, one would expect worse performance from the test cases that employed DO and implemented DA dispatch. Still, all the solutions based on forecasts did not deviate more than 1% from the solution in the ideal case of DO assuming perfect forecast. Based on this, it can be concluded that the generated forecasts for that week were sufficiently good to be used in DO. Note, however, that DO might not perform as well as SO, if different realized scenarios are considered.

The higher cost of the test cases that used forecasts in comparison to the ideal case was mainly due to the BMG's peak power cost (c^{peak}), which accounted for about 8% of the total cost f and was increased up to 20.2%. This can be explained by the difficulty of the ML models to accurately predict the value or the time of occurrence of the daily peak load (see Figure 5.20) and by the low potential for energy arbitrage, which, combined with the low PV output, led to minimal variations in the energy costs.

The value of SO and the effect of the forecast error can also be assessed by two stochastic metrics which use DO as a comparison benchmark [164]: the expected value of perfect information (EVPI) and the expected cost of ignoring uncertainty (ECIU). Defining $f_w^{DO,PI}$ as the cost obtained by DO assuming perfect forecast i.e., perfect knowledge of the load profile of scenario w, the value of the EVPI is obtained by subtracting the expected cost computed as the weighted sum of the costs $f_w^{DO,PI}$

Table 5.3: Cost [$] of the HSB LL BMG's energy dispatch for a week.

	f	$c^{im} - r^{ex}$	c^{peak}	c^{B}
SO-DA (LR)	145.58	134.17	11.24	0.17
SO-DA (ANN)	145.52	134.17	11.24	0.10
SO-DA (LSTM)	145.50	134.18	11.23	0.09
SO-RH (LR)	145.31	133.93	11.24	0.15
SO-RH (ANN)	145.26	133.87	11.24	0.16
SO-RH (LSTM)	145.26	133.86	11.24	0.16
DO-DA (LR)	145.47	134.18	11.24	0.05
DO-DA (ANN)	145.51	134.18	11.24	0.09
DO-DA (LSTM)	145.44	134.18	11.23	0.03
DO-RH (LR)	145.35	133.96	11.24	0.15
DO-RH (ANN)	145.34	133.96	11.24	0.15
DO-RH (LSTM)	145.35	133.96	11.24	0.16
DO-DA (perfect forecast)	143.40	134.04	9.35	1.39
DO-RH (perfect forecast)	144.30	133.92	10.38	0.27

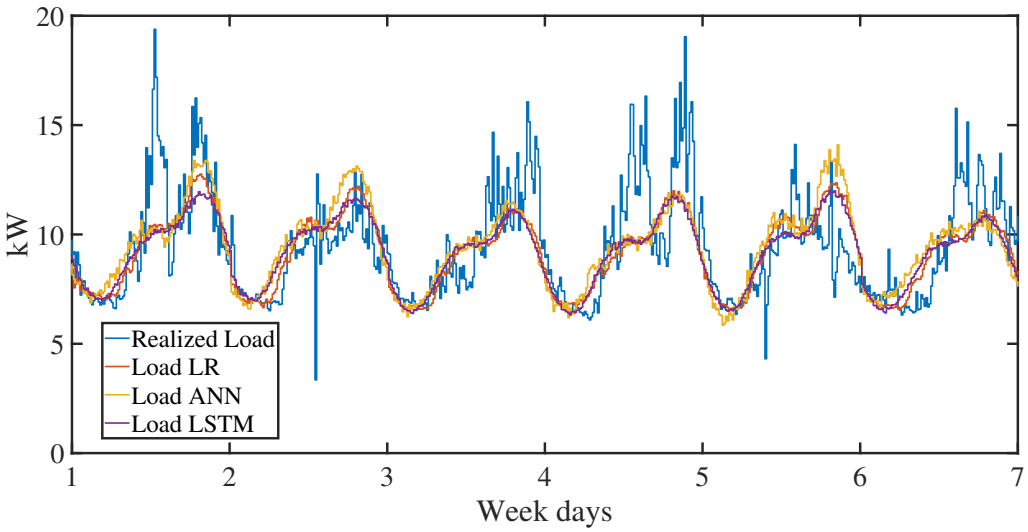

Figure 5.19: The load forecasts obtained by the ML models.

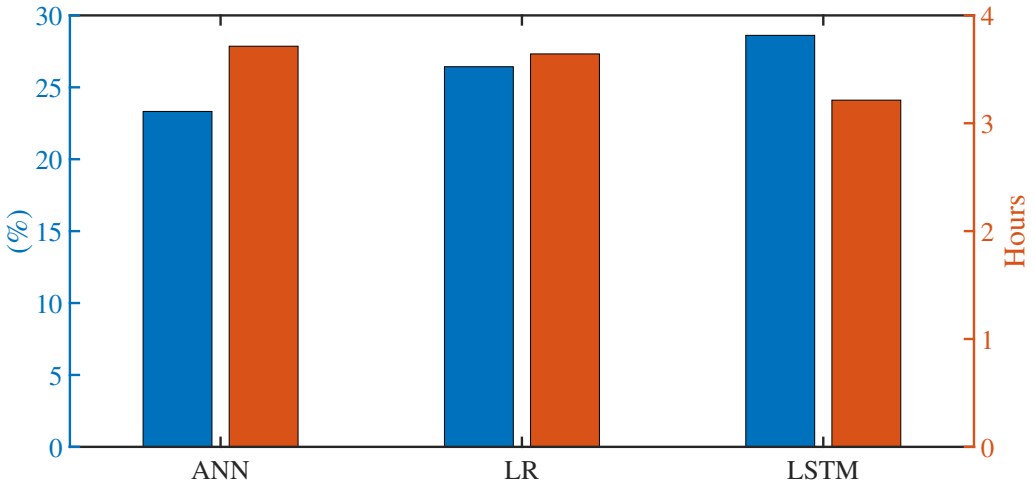

Figure 5.20: The average error of the peak load's predicted value (left y-axis) and time of occurrence (right y-axis) over the simulated week for each ML model.

Table 5.4: SO assessment metrics for the optimal energy dispatch implemented day-ahead at the HSB LL BMG.

ML model	EVPI	ECIU
LR	3.13%	0.29%
ANN	3.19%	0.32%
LSTM	5.69%	0.30%

over all scenarios from f^{SO} :

$$EVPI = f^{SO} - \Pi_\omega \sum_{w \in \mathcal{W}} f_w^{DO,PI}. \tag{5.3}$$

The ECIU value is obtained by the weighted sum of the difference between the cost of the SO solution and the cost of the DO solution f_w^{DO} for each scenario w, where the forecast is naively treated as perfect information ignoring uncertainties:

$$ECIU = \Pi_\omega \sum_{w \in \mathcal{W}} (f_w^{DO} - f^{SO}), \tag{5.4}$$

Assuming that only one of these scenarios is realized, the deterministic cost will be higher than the expected cost over some of the scenarios. An example of these metrics for the DA energy scheduling is given in Table 5.4.

The EVPI and ECIU are given in % of the total cost of DO-DA with perfect forecast and have been calculated for all ML models assuming that the base scenario was realized for the calculation of ECIU. The almost similar costs of SO and DO in DA or RH solution approaches (see Table 5.3) indicated that there was very little cost of ignoring uncertainty i.e., the value of SO was trivial. This was validated, as ECIU in Table 5.4 was less than 1%. Although all ML models had a similar ECIU, LSTM had a higher EVPI, which implies that it could not handle uncertainties as well as

the LR and the ANN models.

Regardless of the low ECIU, SO was favored for the 15-minute energy dispatch of this comparative study thanks to the fast execution time of the scenario generation and solution of the SO problem, which was approximately 15 seconds in total . However, it should be noted that the SO problem could become computationally heavy if a higher number of scenarios, a higher resolution, or a more complex optimization model e.g., due to more MG resources, are considered.

5.4 Summary

In this chapter, the deterministic MODEFlex model was used to solve the optimal energy management problem for the HSB LL and Brf Viva buildings i.e., the considered BMGs under study. Emphasis was given on the BES dispatch and degradation models presented in Section 4.2.6, as the simulations of this chapter compared the two BES dispatch models i.e., the conventional and the measurement-based BES model, and the two degradation models, which were used to model the dependency of cycle aging on either throughput or DoD. A comprehensive evaluation of the total BMG operation cost and induced BES capacity loss was conducted by simulating the performance of the HSB LL building over a year. Simulation results did not show a clear advantage of the measurement-based model against the simpler and easier to implement conventional model, when no degradation model was incorporated in the MODEFlex model.

The BMG test systems were also used as physical demonstration sites to validate the measurement-based BES model which was used in the simulations of the deterministic MODEFlex model. The Brf Viva demonstration results showed negligible mismatches between requested and delivered BES power irrespective of the BES scheduling model employed to obtain the optimal energy scheduling solution. On the contrary, these mismatches could not be perfectly cancelled for the HSB LL BMG. However, they were substantially reduced when the measurement-based model was employed, thus proving its merits against the conventional model.

In addition, the effect of the load forecasting errors to the BMG's operation cost was analyzed by testing the performance of the MODEFlex model under different load forecasting profiles, optimization methods, and solution approaches. Simulations results showed that using a simpler forecasting model e.g., LR, and methodology to obtain the optimal energy dispatch solution did not compromise the economic benefits for the BMG's customers.

Chapter 6

Scenario-Based Stochastic Energy and Flexibility Dispatch

This chapter is based on Paper II and presents results of the stochastic MODEFlex model applied to the operation of a BMG and used to optimally dispatch the BMG's energy and flexibility. The chapter describes the employed process of the stochastic flexibility assessment and analyzes in detail multiple factors that affect the amount and value of flexibility.

6.1 Aim of study

As identified in Section 2.6, there was a lack of quantification of the economically available flexibility even among the studies that embedded FS models in energy management models used for economic optimization. The aim of this chapter's study was to validate the performance of the most comprehensive formulation of the MODEFlex model which utilized a scenario-based SO approach and integrated an FS model into the optimal energy scheduling model. The stochastic MODEFlex model was used to introduce a methodology for stochastic flexibility assessment and to dispatch flexibility amounts that were both technically available and economically feasible. The study employed SO to account for the uncertainties related to the input values of the BMG i.e., the load demand and PV power output. At the same time, it was important to show that the formulated stochastic model could be compatible for close to real-time flexibility assessment and dispatch of the BMG's power exchange, as SO increases the size of the formulated optimization problem and, by extent, the time required to solve it.

6.2 Study approach

The study's approach is presented in Figure 6.1 for both OL and CL dispatch to illustrate the differences of the two approaches. Most studies apply SO in OL. Even though the RH dispatch reduces the effect of the forecast errors by dynamically

updating the set-points, it requires more frequent simulations, which can be an issue as SO has higher computation time than deterministic optimization. Similar to [165], both the SO and the RH dispatch are used in this study to benefit from the feedback, which is particularly important for close to real-time control. Furthermore, the study considered FS-C as the offered FS and evaluated the BMG's flexibility under different test cases and parameters.

The stochastic MODEFlex model was used to simulate the operation of HSB LL BMG (see Section 3.6.1) implementing RH optimization to dispatch the BMG's energy and flexibility for a day. In order to reduce the size of the SO problem and avoid scalability issues, deterministic control variables were used in the model as explained in Section 4.1.1 i.e., the scheduled BES power is independent of the scenario. Since the RH dispatch is used, it is only the next time-step control decisions that are implemented after each simulation and the deterministic control trajectory can be updated considering the latest forecasts available with every new simulation. The rest of the control trajectory of each simulation is advisory. Despite the advantages of the RH dispatch, the OL dispatch can be useful for practical applications in case of failure to receive feedback. Then, the advisory BES power set-points obtained from the last solution of the SO problem will be applied, thus implementing OL control until the CL control can be restored.

6.2.1 Process of flexibility assessment and dispatch

The proposed process of flexibility assessment and dispatch, which corresponds to an intra-day framework of procuring flexibility, is shown in Figure 6.2 with indicative milestones marking the process. The solution approach is RH optimization and the depicted time discretization step is $\Delta t = 15$ minutes, therefore 96 simulations (solutions of the Stochastic MODEFlex problem) are performed in Day 1. As shown in Figure 6.2, one simulation is performed at each time step τ to solve the following SO problem for a building BMG m:

$$\min f_m = \begin{cases} f'_m \quad (6.2)\,\text{s.t. (4.2b)–(4.4b), (4.6b), (4.23)–(4.39), and (4.41)–(4.42)} & \tau < t_0 \\ f_m^{flex}\,(6.3)\,\text{s.t. (4.2b)–(4.4b), (4.6b), (4.23)–(4.39), (4.41)–(4.42), (4.61b)–(4.62b), (4.64), and (4.65b)–(4.66b)} & \tau = t_0 \\ f''_m \quad (6.4)\,\text{s.t. (4.2b)–(4.4b), (4.6b), (4.23)–(4.39), (4.41)–(4.42), (6.5), and (6.6)} & t_0 < \tau \leq t_2 \\ f'_m \quad (6.2)\,\text{s.t. (4.2b)–(4.4b), (4.6b), (4.23)–(4.39), and (4.41)–(4.42)} & t_2 > \tau \end{cases}, \tag{6.1}$$

$$f'_m = c_m^{im} - r_m^{ex} + c_m^{p} + c_m^{B}, \tag{6.2}$$

$$f_m^{flex} = c_m^{im} - r_m^{ex} + c_m^{p} + c_m^{B} - r_m^{flex}, \tag{6.3}$$

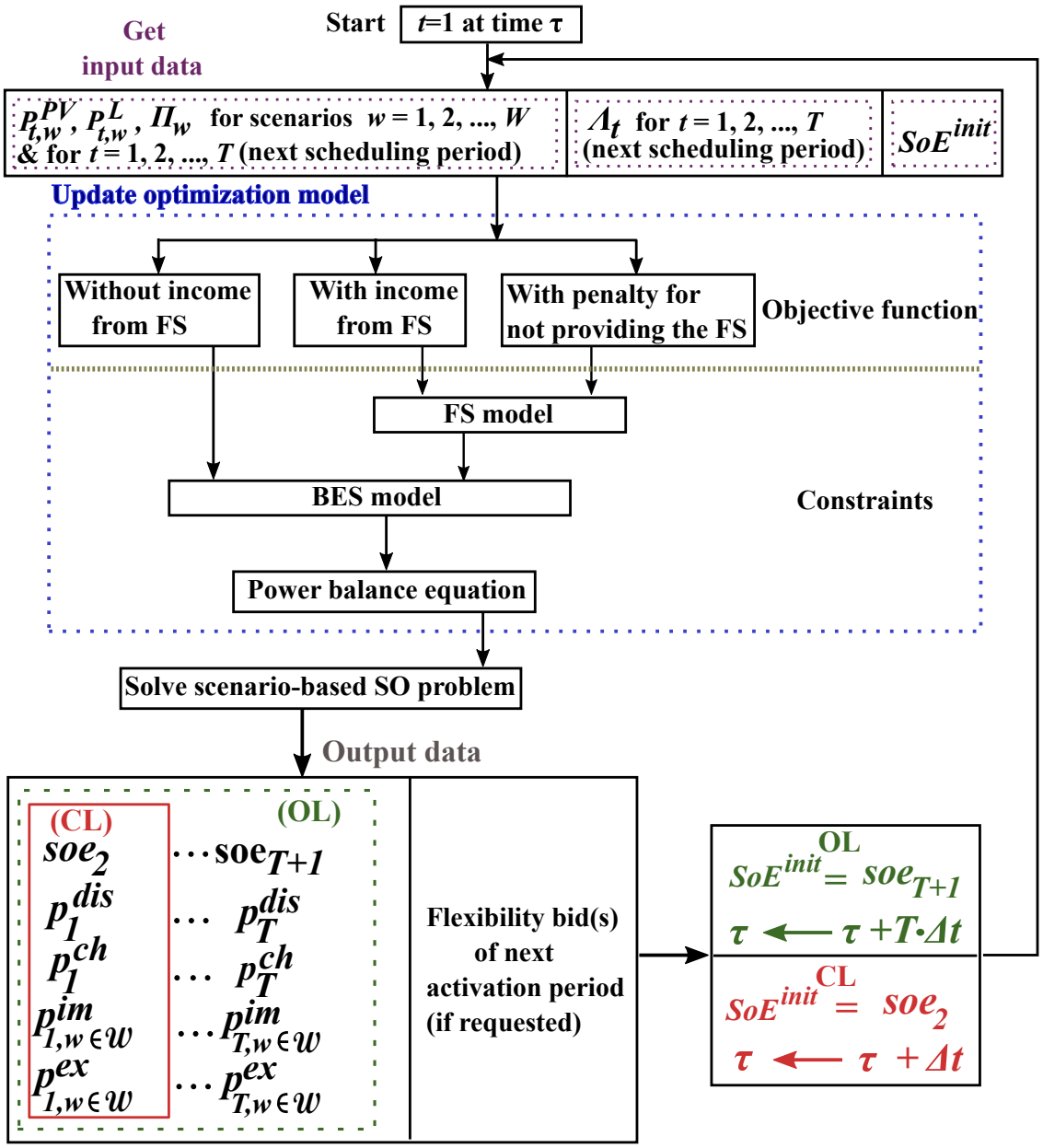

Figure 6.1: Flowchart representing the simulation set-up for the solution of the stochastic MODEFlex problem.

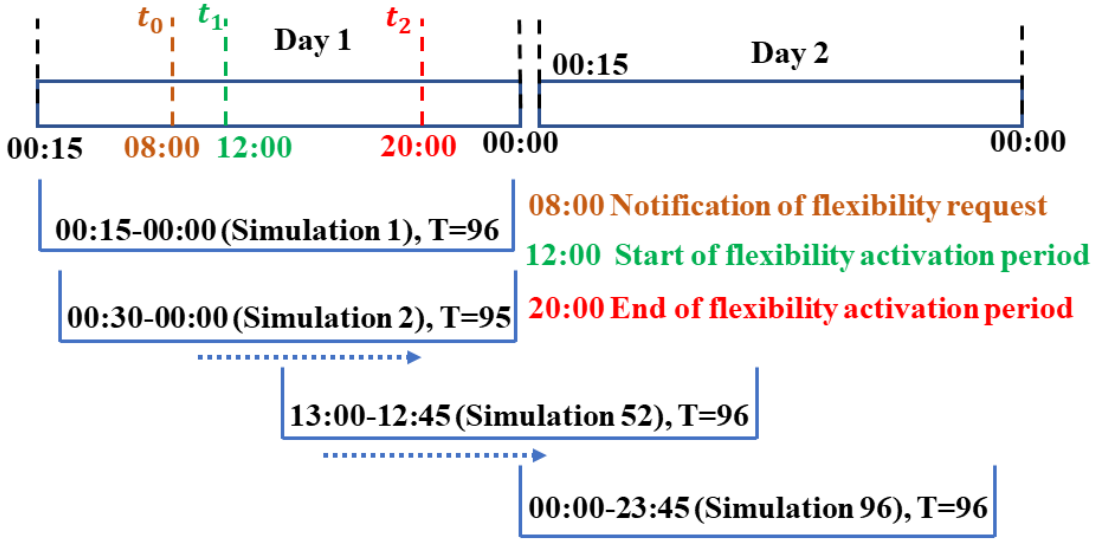

Figure 6.2: Process of flexibility dispatch using the RH approach.

$$f''_m = c^{im}_m - r^{ex}_m + c^{p}_m + c^{B}_m - \sum_{t \in \mathcal{H}_{f'}} \sum_{w \in \mathcal{W}} \Pi_{wm} \beta_{wtm} C^{pen}_m, \tag{6.4}$$

$$\beta_{wtm} \leq P^{fl,p}_m - (p^{im}_{wtm} - p^{ex}_{wtm}), \qquad \forall w \in \mathcal{W},\ \forall t \in \mathcal{H}_{f'}, \tag{6.5}$$

$$\beta_{wtm} \leq 0, \qquad \forall w \in \mathcal{W},\ \forall t \in \mathcal{H}_{f'}, \tag{6.6}$$

where t_0 and t_2 respectively denote the notification time of flexibility request and the end of the flexibility activation period (see Figure 6.2). The flexibility price $\pi^{fl,Cap}_m$ is entered as a parameter in (6.1). The BMG operator implements the optimal energy schedule obtained from solving the SO problem given by (6.1) for $\tau < t_0$ at each time step τ. If the DSO needs to buy flexibility, a request is sent at $\tau = t_0$ to the BMG-EMS, which responds with the amount p^{flex} and a stochastic assessment of the flexibility that can be offered by solving (6.1) for $\tau = t_0$. The response is sent directly after the request e.g., in Figure 6.2, the flexibility request along with information about the activation period is sent at 08:00 (Simulation 32) and the response is sent to the DSO before the next simulation (at 08:15). The BMG-EMS is also notified about the acceptance or decline of p^{flex}_m before the next simulation. If it is accepted, the BMG-EMS solves (6.1) for $t_0 < \tau \leq t_2$ i.e., until the simulation horizon is shifted outside of the activation period (note that $\mathcal{H}_{f'}$ in (6.4)–(6.6) refers to the part of the scheduling period that belongs to the flexibility period, which shrinks as the time horizon shifts). In Figure 6.2, this problem, which minimizes the mismatch between flexibility bid and dispatch, is solved at each simulation between 08:15-20:00 i.e., Simulations 33-80. Thus, the BMG-EMS adjusts its control to provide the flexibility bid both before and during the flexibility activation period which starts at t_1. The mismatch is minimized by penalizing the deviation between

the net power and the expected net power peak $p_m^{fl,p}$, which is now entered as a parameter ($P_m^{fl,p}$).

The non-negative term β_{wtm} in (6.4)–(6.6) represents the deviation between the expected peak and dispatched net power that should be penalized at each time step. If the net power is below its expected peak $P_m^{fl,p}$, which was calculated at t_0 to define the flexibility bid, this deviation should not be penalized. Since the right-side term in (6.5) becomes positive in this case, (6.6) becomes the binding constraint and β_{wtm} becomes equal to zero because a negative term would increase the value of the cost function f_m'' given by (6.4). If the net power exceeds the bid, then (6.5) is binding and β_{wtm} is negative taking the value of $P_m^{fl,p} - (p_{wtm}^{im} - p_{wtm}^{ex})$. This quantity is multiplied by the penalty C_m^{pen} adding a cost in f_m''.

After the look-ahead horizon is shifted past the end of the flexibility activation period, the BMG-EMS continues solving the energy scheduling problem given by (6.1) for $\tau < t_0$. The same problem is also solved after the BMG-EMS receives a decline of the offered flexibility until there is a new flexibility request. It should be noted that the proposed process of flexibility dispatch is independent of the notification time or the duration of the activation period and can even be used for close to real-time flexibility dispatch, when a small Δt is used. Moreover, the BMG's response and the notification of acceptance/decline from the DSO can occur later than t_0. In that case, the BMG-EMS will repeatedly solve (6.1) for $\tau = t_0$ to optimize the flexibility offer at each time step until it sends the response to the DSO.

The following steps can describe each simulation of the RH process performed at τ:

- **Step 1:** The look-ahead horizon extends to include all hours where the electricity price is known, up to a maximum of 24 hours. E.g., in Figure 6.2, the initially 24-hour time horizon is continuously reduced by one time step for Simulations 2-51 and then extends again to 24 hours until Simulation 96, since the day-ahead spot market prices are updated at about 12:45 on the previous day [154].
- **Step 2:** Obtain the day-ahead most recently updated forecasts of load and PV power output which have the same time resolution as the considered scheduling time horizon. Reduce the length if necessary, update the base scenario, and generate new scenarios.
- **Step 3:** Solve the SO problem according to (6.1) using the generated scenarios, the price data, and SoE^{init}, which was obtained from the previous simulation. These are the input data illustrated in Figure 6.1.
- **Step 4:** Obtain and update the set-points p_{tm}^{dis}/p_{tm}^{ch} for $t = 1$. Shift the time horizon by Δt and go to Step 1 (at $\tau \leftarrow \tau + \Delta t$).

6.2.2 Simulation set-up

The BMG characteristics were listed in Table 3.2 and all the parameters related to BES data were taken from the HSB LL [115]. The inputs in the simulation of the DA energy scheduling in RH included electricity load and PV generation data of the HSB LL building as well as electricity prices taken from the Nord Pool market [154] for bidding area 3 of Sweden. All the input data referred to values recorded in 2018. The grid tariffs and the reimbursement fee have been taken from the website of the local DSO [155] and can be found in Appendix C.1.

The DA forecast errors of PV generation and power consumption were assumed to follow the Gaussian distributions given as $\mathcal{E}_t^{PV} \sim N(0, 0.1^2)$ and $\mathcal{E}_t^{L} \sim N(0, 0.05^2)$, respectively, where the standard deviations $\sigma_t^{PV} = 0.1$, $\sigma_t^{L} = 0.05$ were adopted from the day-ahead forecast error distributions of [48, 134]. The accuracy of the forecast values progressively deteriorates for the time steps further ahead in time, which is why B. V. Solanki et al. [166] used non-uniform time resolution. In this study, the horizon is uniform; however, the standard deviations of the distributions gradually increase to account for the reduction of the intra-day accuracy. Thus, for the time steps until the next hour ahead as well as for the time steps after the first hour and until six hours ahead, they are equal to $10\%\sigma_t^{PV}$/$10\%\sigma_t^{L}$ and $50\%\sigma_t^{PV}$/$50\%\sigma_t^{L}$, respectively. The resulting probability distributions and the MC method were used to generate 2000 scenarios of PV generation and load for each simulation, which were subsequently reduced to 120 scenarios.

Simulations were performed according to the test cases described in Table 6.1. To analyze the effect of BES capacity, the simulations were performed from three BES sizes i.e., 7.2 kWh (the capacity of the actual BES installed at the HSB LL system), 14.4 kWh and 18 kWh. The capacity at the connection point was $P^{Cap} = 43.65$ kW, the time discretization step was $\Delta t = 15$ minutes, and the penalty was $C^{pen} =$ 180\$/MW, similar to the one used in [167]. The values of the BES model parameters in (4.25)–(4.26) and (4.41)–(4.42) were: $B_1 = 0.0013$, $B_2 = 0.3534$, $I_c = 0.3$, $H =$ 80%, $SoE^{min} = 10\%$, $SoE^{max} = 90\%$, and the initial SoE was 50%. The flexibility activation periods were between 07:00-20:00, as was requested from small to medium-sized companies offering flexibility in [168]. A base $\pi^{fl,Cap}$ was calculated according to the following assumption: it was assumed that the revenue from offering 1 kW of p^{flex} would be equal to selling 1 kWh of energy at average spot market price at each hour of the activation period. The simulations were conducted considering different flexibility prices within the range of 50%-150% of this base $\pi^{fl,Cap}$, which was different for each test case, depending on the length of $\mathcal{H}_f$ and the method of flexibility dispatch.

6.3 Results and discussions

The stochastic assessment of flexibility was performed at time step $\tau = t_0$ i.e., right after the notification of the flexibility request. The results are obtained by solving the respective SO problem according to (6.1) at $\tau = t_0$.

Table 6.1: Test cases of the study on stochastic MODEFlex

	Time of Notification	Flexibility Activation Period	Flexibility Assessment and Dispatch
Case A	08:00	12:00-20:00	Flexibility amount over entire activation period
Case B	18:00	19:00-20:00	Flexibility amount over entire activation period
Case C	08:00	12:00-20:00	Flexibility amount per time step of activation period

6.3.1 Flexibility dispatch over entire activation period

The simulations showed that p^{flex} generally increased as the BES size increased, which can be observed in Figure 6.3 that presents the stochastic assessment of flexibility for Cases A-B at their base $\pi^{fl,Cap}$ for a 7.2, 14.4, and 18 kWh BES. The actual amount of flexibility that the BMG provided to the grid in each of the 120 scenarios is depicted as a histogram plot. The x-axis represents the amount of dispatched flexibility $P^{Cap} - max(p_{wt}^{MG,im},\ \forall w \in \mathcal{W})$, where $max(p_{wt}^{MG,im})$ refers to the activation period $\mathcal{H}_f$. The y-axis reports the probability of achieving a specific amount of flexibility (in one or more of the 120 scenarios). Thus, the percentage reported in the y-axis is the weighted sum of the scenarios where a given flexibility amount occurs, divided by the weighted sum of all 120 scenarios (which has a 100% probability of occurrence). The weights are the probabilities of occurrence of each scenario assigned by the scenario reduction technique (see Section 4.1). The vertical dashed line in each plot of Figure 6.3 marks the value of p^{flex} implying that the optimal solution involves scenarios where more flexibility is provided, or where the BMG might fall short of meeting its bid.

Under circumstances, the BMG with the 7.2 kWh BES could offer slightly more flexibility than the BMG with the 14.4 kWh BES (compare Figure 6.3 (d) and (e)). In this study, this happened due to the late notification time in Case B. The results are illustrated in Figure 6.4 (a) and (b) which present the corresponding schedules of Figure 6.3 (d) and (e). In Figure 6.4, the power profiles are plotted as bar graphs on the left y-axis (positive values correspond to net power consumption and/or BES charging) and the SoE is given as a line plot on the right y-axis. As can be seen, both BESs stayed idle at their initial SoE until $\tau = t_0$ in preparation for the highest consumption period predicted at $\tau > t_2$ and both were almost at SoE_{min} at the end of the day. Hence, it is evident that the 7.2 kWh BES could not decrease energy and peak power cost as much as the 14.4 kWh BES so the revenue from the FS was more important in reducing the total cost under the considered $\pi^{fl,Cap}$. The 14.4 kWh BES could benefit more from ESs i.e., energy and peak power cost reduction; therefore, more capacity was used for that purpose at the expense of offering flexibility. In Figure 6.4 (b) its injected power resulted in up to 2-3 kW lower BMG imported power at time steps 83-90 in comparison to Figure 6.4 (a), while offering at the same time flexibility only 400 W less than the amount offered

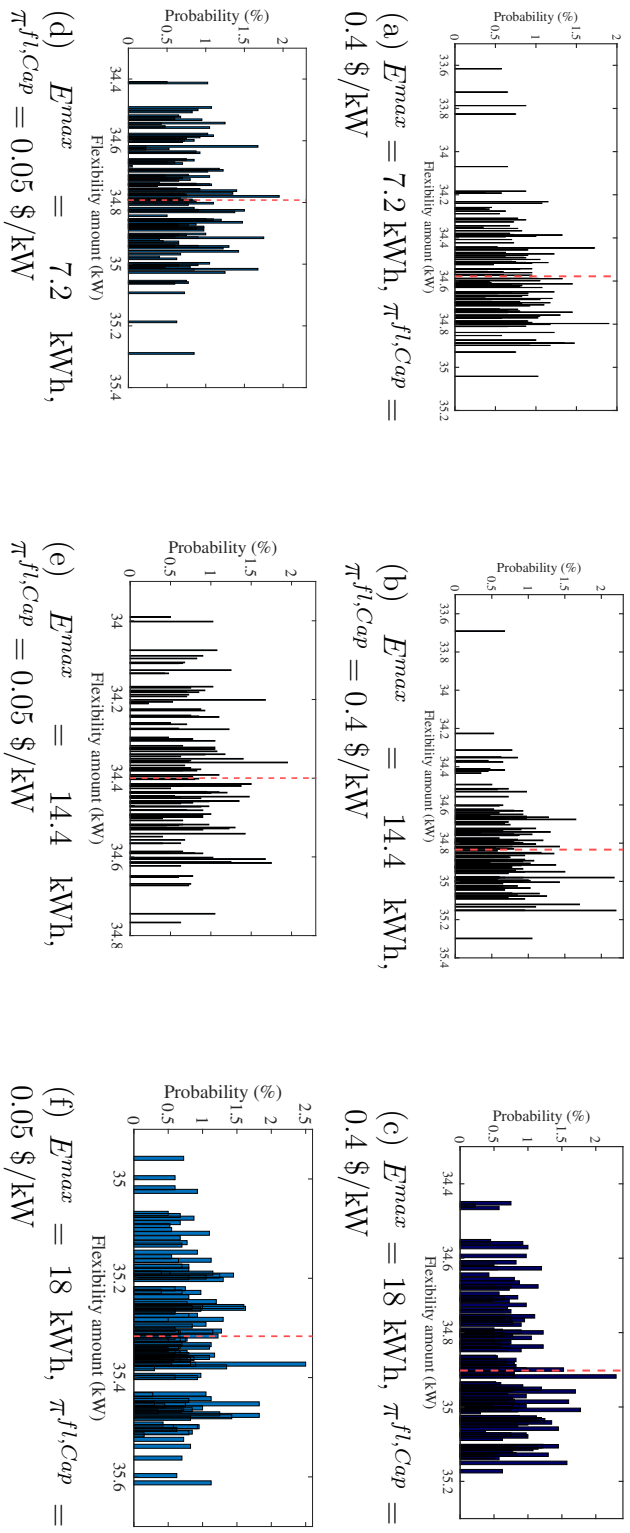

(a) $E^{max} = 7.2$ kWh, $\pi^{fl,Cap} = 0.4$ \$/kW

(b) $E^{max} = 14.4$ kWh, $\pi^{fl,Cap} = 0.4$ \$/kW

(c) $E^{max} = 18$ kWh, $\pi^{fl,Cap} = 0.4$ \$/kW

(d) $E^{max} = 7.2$ kWh, $\pi^{fl,Cap} = 0.05$ \$/kW

(e) $E^{max} = 14.4$ kWh, $\pi^{fl,Cap} = 0.05$ \$/kW

(f) $E^{max} = 18$ kWh, $\pi^{fl,Cap} = 0.05$ \$/kW

Figure 6.3: The probability distribution of dispatched flexibility and the flexibility bid (dashed line) of the BMG operator, considering the base $\pi^{fl,Cap}$ for each case. Figure (a)-(c) correspond to Case A and Figure (d)-(f) correspond to Case B.

by the 7.2 kWh BES. The 18 kWh BES allocated slightly more capacity than the 14.4 kWh BES for the ESs and the rest was used for the FS resulting in a larger p^{flex}.

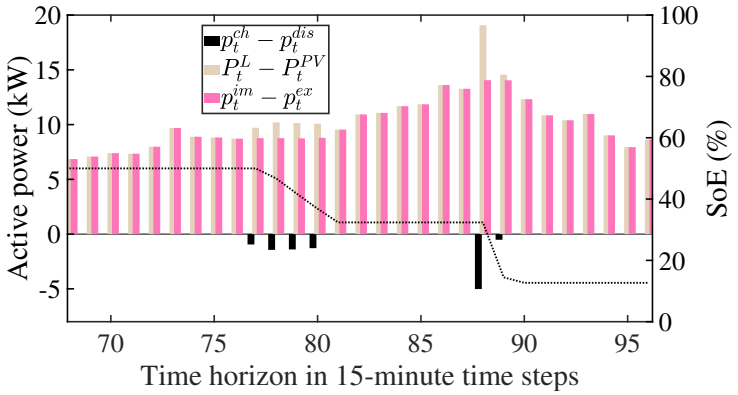

(a) $E^{max} = 7.2$ kWh

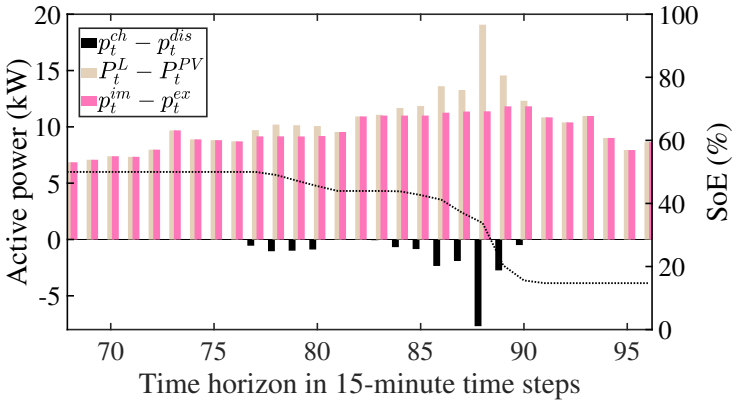

(b) $E^{max} = 14.4$ kWh

Figure 6.4: BMG power flows for Case B with $\pi^{fl,Cap} = 0.05\$/kW$.

Comparing Figure 6.3 (d) with (a) and Figure 6.3 (f) with (c) it can be seen that p^{flex} could be larger in Case B, even though the notification of flexibility request was much closer to the activation period. An explanation for this is that the uncertainty regarding the flexibility dispatch is lower in Case B, since the activation period is shorter and much closer to $\tau = t_0$; therefore, the input data for $t_1 \leq \tau \leq t_2$ are less affected by forecast errors. Despite that, the probability of dispatching the flexibility according to the bid was actually higher in Case A.

6.3.2 Flexibility dispatch per time step of activation period

In Case C, where the flexibility is dispatched per time step, (4.64), (4.65b)–(4.66b) are replaced by (4.60) and (4.63b) in (6.1), while $P_{tm}^{fl,p}$ is indexed by t and refers to the expected net power at each time step. The simulations showed that with the increase in $\pi^{fl,Cap}$ the probabilities of dispatching certain flexibility amounts at the same time steps would also increase. However, this was not always straightforward, as increasing the probability at one step could come at the expense of

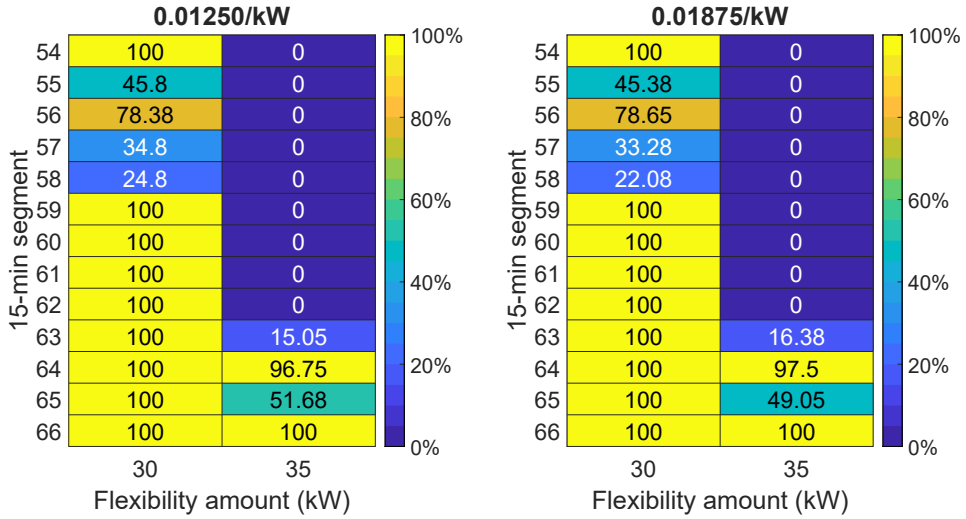

Figure 6.5: The probability distribution of dispatched flexibility per time step (Case C, E^{max} =7.2 kW) for two different prices.

the probability at another step. This can be seen in Figure 6.5 which presents the probability of flexibility dispatch for E^{max} =7.2 kW at $\pi^{fl,Cap}$ =\$0.01250/kW and $\pi^{fl,Cap}$ =\$0.01875/kW.

The probability of flexibility dispatch in Figure 6.5 is shown in the cell numbers of the heatmaps. These correspond to the probability of dispatching a flexibility amount at least equal to the value shown in the x-axis, at the time step shown in the y-axis. The BMG-EMS guaranteed the dispatch of at least 30 kW during the activation period except for time steps 55-58 and at least 35 kW from time step 66 onward for both prices presented in Figure 6.5. As can be seen in Figure 6.5, the probability of dispatching 30 kW at time step 56 and 35 kW at time steps 63–64 increases with the increase in the price. At the same time, though, the respective probabilities decrease for the amount of 30 kW at time steps 55, 57–58 and the amount of 35 kW at time step 65.

6.3.3 Economic value of flexibility dispatch

The probability of dispatching the flexibility amount(s) calculated at $\tau = t_0$ can substantially increase when the SO problem is solved in RH, depending on the chosen penalty and the technical constraints of the BMG resources.

6.3.3.1 Benefit of combining SO with RH dispatch

For all considered values of $\pi^{fl,Cap}$ and E^{max} in Cases A-C, the flexibility amount (p^{flex}) was successfully dispatched. This demonstrated the value of combining SO with the RH dispatch, which contributed to avoiding the payment of penalties and increased the value of flexibility for the BMG operator. The value of flexibility, which was calculated as the cost difference of the daily BMG schedule with and without the FS assuming that the base scenario was realized, is shown in Figure 6.6 along with

the degradation cost and the flexibility bid w.r.t $\pi^{fl,Cap}$. The value of flexibility was also estimated for the DSO assuming that s/he buys the BMG flexibility to reduce the subscription fee that guarantees a certain power level. To calculate this value the cost of buying flexibility was subtracted from the cost reduction achieved by reducing the BMG's peak imported power using the FS.

6.3.3.2 Factors affecting the value of flexibility

Two important factors associated with the value of flexibility are scrutinized: the BES size and the flexibility dispatch parameters t_0, t_1, t_2 i.e., the time of notification and the duration of the activation period. The results indicated that the FS-C can offer value to both the BMG customers and the DSO when flexibility is dispatched over the entire activation period i.e., in Cases A-B, with the BMG's value of flexibility amounting to at least 56% and 7% of the daily BMG operation cost, respectively. As can be seen in Figure 6.6 (a), (d), and (g), the BMG's value of flexibility increased linearly wrt $\pi^{fl,Cap}$, while the BES size did not significantly affect the BMG's daily value of flexibility. This shows that the BMG-EMS favored participation in ESs (energy arbitrage, peak shaving) instead of the FS within the studied range of $\pi^{fl,Cap}$. The BES size played a more important role in the DSO's value. In fact, in Cases A-B, the larger BESs usually increased the economic benefits for the DSO. Case C offered no benefit to the DSO even though the value of flexibility was considerably higher for the BMG.

Analyzing the results in Figure 6.6 (b), (e), and (h), it can be seen that a higher $\pi^{fl,Cap}$ and a larger BES lead to larger p^{flex} in Case A. In Case B, however, the shorter notice limited p^{flex} from the smaller BES, which did not exceed the amount of 34.7 kW despite the increase in $\pi^{fl,Cap}$. Nevertheless, this BES could offer more flexibility than the 14.4 kWh BES (and even the 18 kWh BES at very low $\pi^{fl,Cap}$) for reasons explained in Section 6.3.1 i.e., higher need to increase value through the FS due to lower potential for energy and peak power cost reduction (or profit from energy arbitrage). Figure 6.6 (h) shows the average flexibility bids and their range for the 7.2 kWh BES. The results from other BESs are omitted for clarity purposes, however, they exhibit the same trend, such that the BES size and $\pi^{fl,Cap}$ do not affect the average p^{flex} in Case C.

6.3.3.3 Effect of degradation

Although with the tested flexibility prices the value of flexibility dispatch remained practically unaffected by the BES size as can be seen in Figure 6.6 (a), (d), and (g), the faster degradation of smaller BESs suggests that the investment on the size of a BES that will provide FSs should be determined considering the frequency of providing these FSs. Figure 6.6 (c), (f), (i) depict the degradation cost as a percentage of the BES's purchase cost, where both cycle and calendar aging were considered. Calendar aging was assessed after the simulations using the obtained values of soe_t, as was explain in Section 5.2.2, which explains why e.g., in Figure 6.6 (c), there is a significant decrease in the degradation cost of the 7.2 kWh BES when $\pi^{fl,Cap}$ increases. Comparing the different BES sizes it can clearly be seen

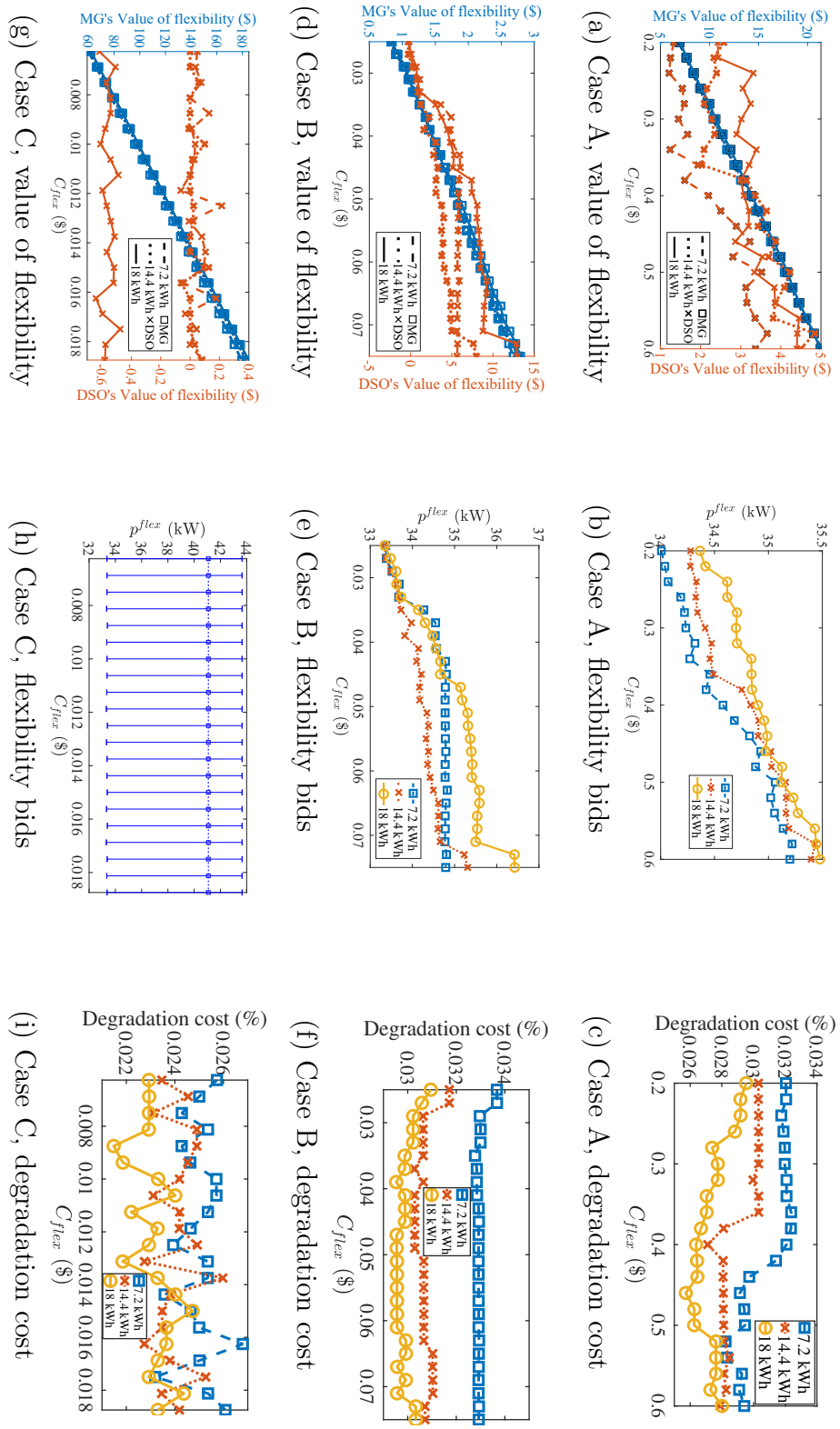

(a) Case A, value of flexibility (b) Case A, flexibility bids (c) Case A, degradation cost

(d) Case B, value of flexibility (e) Case B, flexibility bids (f) Case B, degradation cost

(g) Case C, value of flexibility (h) Case C, flexibility bids (i) Case C, degradation cost

Figure 6.6: The flexibility bid, value of flexibility, and BES degradation cost w.r.t. $\pi^{fl,Cap}$ for Cases A-C.

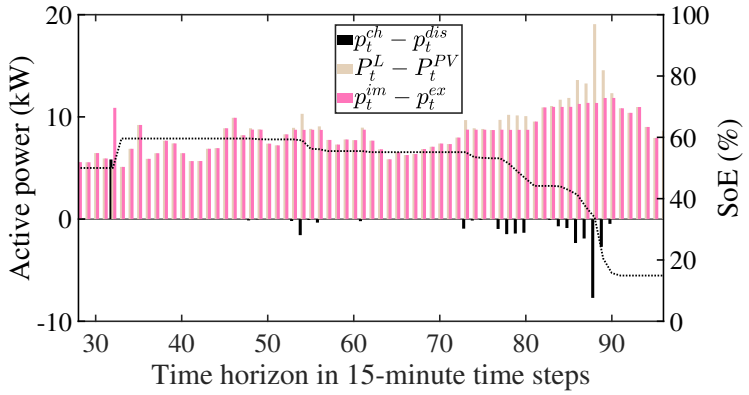

(a) With FS

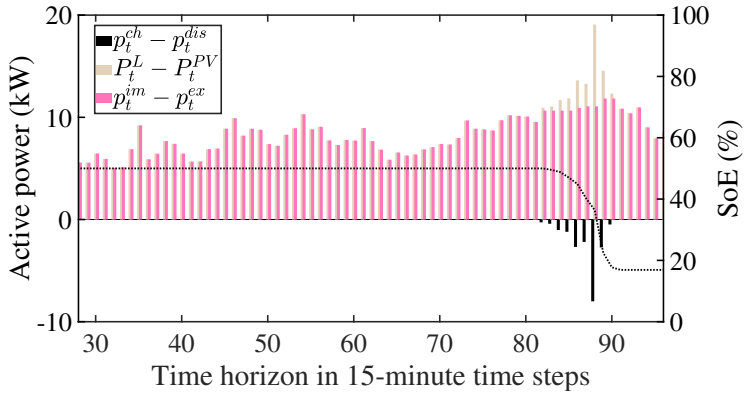

(b) Without FS

Figure 6.7: BMG power flows with and without FS for Case A with $\pi^{fl,Cap} = 0.4\$/kW$ and $E^{max} = 14.4$ kWh.

that the induced aging is worse for the smallest BES. This is more notable in Figure 6.6 (c) and (f) and it can be attributed to the increased utilization (cycling) in an attempt to maximize profit from both ESs and FSs. If the FS is event-based e.g., requested during extreme weather conditions or unexpected failures, the effect of degradation would be trivial. Otherwise, long-term planning studies are required to assess whether the faster degradation of smaller BESs could result in a reduced value of their flexibility.

An example of the different BES utilization is shown in Figure 6.7, which depicts the BMG power flows for Case A, $\pi^{fl,Cap} = 0.4\$/\text{kW}$ and $E^{max} = 14.4$ kWh, comparing the results with and without the FS. Without the FS, the BES was only discharged after the flexibility period, when peak demand was expected (time steps 86-90). When the BMG offered flexibility (Figure 6.7 (a)), the BES's utilization increased, as it started charging at $\tau = t_0$ to be able to inject power both at time steps 86-90 and within the activation period.

6.3.3.4 Number of scenarios and cost of optimal solution

Since all the studied SO problems were linear, the convergence to an optimal solution is guaranteed at each time step. However, the optimality with respect to all possible uncertainty realizations cannot be guaranteed. Scenario-based approaches are based on samples and, therefore, there is a trade-off between the cost of the solution and the execution time. A higher number of scenarios can lead to a lower cost i.e., a solution closer to the optimal solution, however, it also increases the computation time. To investigate the relationship between scenario number, optimality and computation time, a sensitivity analysis was performed for Case A, with E^{max} =7.2 kWh and $\pi^{fl,Cap}$ = 0.4 \$/kW. The results are given in Table 6.2, where the performance of the study whose results have been presented is shown in bold and the negative cost value refers to profit. Since the sampling happens at two stages i.e., first with the MC method and then with the scenario reduction, the analysis accounted for both sample sizes. The execution time refers to the maximum time that was needed for scenario generation, scenario reduction (if applicable), and for the solution of the SO problem.

It can be observed from Table 6.2 that scenario reduction, when considered, accounts for the biggest part in total execution time. For example, a SO problem with 80 scenarios is solved in 9, 34, and 59 sec when obtained from a full set of 2000, 4000, and 5000 scenarios, respectively. Nevertheless, the scenario reduction leads to a significant decrease in execution time, as it reduces the number of variables of the SO problem. The daily cost, which is shown in the last column of Table 6.2, was not directly comparable for the studied sizes of scenario sets, even when no scenario reduction was implemented. This occurs due to the random scenario generation and the RH, since 96 solutions of the SO problem are needed to obtain the daily cost. Despite that, the cost did not vary significantly, and the results yielded a maximum variation of 1.7% from the average cost obtained by these scenario sets.

The results demonstrated that the number of scenarios used in the study was sufficient for the HSB LL BMG, as the cost did not deviate considerably among the scenario sets of the sensitivity analysis. Although there was no proven economic benefit, the larger sets of Table 6.2 could also be used, since their respective solution time was compatible with the chosen time step. Larger sets might not be preferable for real-world applications, however, as communication delays associated with input and output data must also be accounted for.

6.4 Summary

In this chapter, the stochastic MODEFlex model is used to implement energy and flexibility dispatch in RH and conduct a stochastic assessment of the techno-economically feasible MG flexibility. The optimization model is updated at each time step after the time horizon shifts to update its input data by considering the most recent forecasts of the stochastic parameter values i.e., electricity load and PV power output, and adjust the time horizon length depending on the availability of data for the future electricity prices.

Table 6.2: Scenario sensitivity analysis for Case A, E^{max} =7.2 kWh, $\pi^{fl,Cap}$ = 0.4 $/kW.

Full set	Reduction	Reduced set	Execution time (sec)	Cost ($)
5000	no	–	111	-3.58
5000	yes	120	75	-3.66
5000	yes	80	59	-3.69
4000	no	–	81	-3.57
4000	yes	120	45	-3.66
4000	yes	80	34	-3.69
2000	no	–	24	-3.58
2000	**yes**	**120**	**11**	**-3.68**
2000	yes	80	9	-3.69

Three BES sizes i.e., 7.2 kWh, 14.4 kWh and 18 kWh and a capacity limit of P^{Cap} = 43.65 kW have been used to simulate the performance of the stochastic MODEFlex model in three test cases based on the HSB LL BMG, which were described by different notification time, flexibility activation period, and method of flexibility assessment and dispatch i.e., dispatch per time step or over the entire activation period. Simulations were performed for each test case to analyze the impact of multiple factors on the flexibility potential, assessing both the amount and the economic value of flexibility. The main observations regarding the impact of the proposed model on the flexibility potential can be summarized as follows:

1. Combining SO and dispatch in RH ensured the dispatch of the offered flexibility. Therefore, the BMG operator avoided paying penalties which increased the economic benefits from providing the FS.

2. Increasing the BES's size did not significantly affect the BMG's value of flexibility, whereas the larger BES offered higher value to the DSO for Cases A-B.

3. In Case B, where the flexibility activation period was short and close to the notification time for the flexibility request, a larger amount of flexibility was offered in comparison to the other cases, as the dispatch of this amount was less affected by the uncertainties of the input data to the model.

4. The economic value of flexibility for the smallest BES that was tested i.e., the 7.2 kWh BES, could be more severely affected by the induced degradation which was proven to be higher for this BES than for the other two larger BESs. This is especially important to consider when the FSs are offered on a frequent basis instead of being event-based.

Simulation results also showed the impact of the offered FS-C on the BES dispatch by comparing the BES power and SoE profiles with the respective profiles obtained by the same model without considering provision of flexibility. It was revealed that a bigger BES size did not necessarily provide a higher flexibility amount, when the

notification time was close to the flexibility activation period.

Chapter 7

Evaluation of Optimal Energy Scheduling Strategies

This chapter is based on Paper V and evaluates optimal energy scheduling strategies of grid-connected MGs. The impact of the implemented strategy is assessed on the cost and operation of both the MG and the main distribution grid. First, the chapter presents the strategies and the formulation of the optimization problems that are solved in each strategy. Information regarding the considered parameters, assumptions, and simulation set-up related to the study of optimal energy scheduling strategies are also given in this chapter. At the end of the chapter, the results are analyzed and discussed.

7.1 Aim of study

The aim of this chapter's study was to evaluate the cost and performance of the MG operation under different operational objectives. The study also aimed to assess the effect of MG integration to the cost and operation of the main distribution grid assuming the unbundled framework of DSO's operation, which is typically not considered, as discussed in Chapter 1. For this purpose, different MG energy scheduling strategies were tested including MG energy cost minimization, minimization of MG energy exchange with the main grid, minimization of MG imported energy from the main grid, and minimization of the DSO's cost due to grid connection charges. Since the focus was on energy scheduling, the MGs did not participate in any FS.

7.2 Study approach

The study was based on the electric distribution system of Chalmers, which was described in Section 3.6. The MG resource mix could include BESs, DRRs, PV systems, which are non-dispatchable generation sources, and a micro-CHP plant, which is a dispatchable generation source.

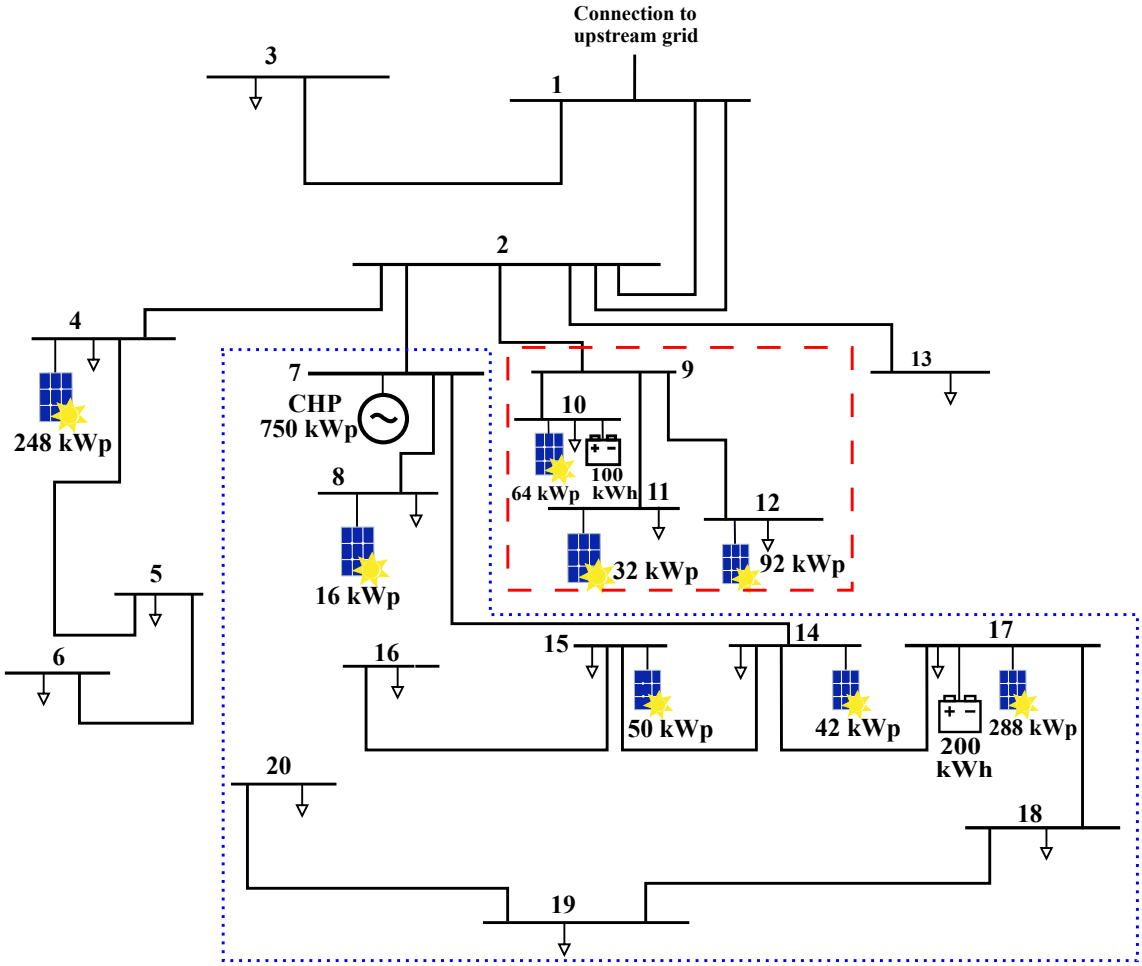

Figure 7.1: The proposed configuration of the distribution network of Chalmers with the interconnection layout of the two MGs (shown with the sections in dashed and dotted lines).

7.2.1 Formulation of the optimization problems

Two network areas of the Chalmers distribution system have been considered as grid-connected MGs, as can be seen in Figure 7.1. Microgrid A (MG-A), shown with dotted lines in Figure 7.1, is a CHP-PV-BES-DRR MG and can produce excess energy, when the CHP is in operation. MG-A has a PV penetration level of 23% (calculated as a percentage of the MG's peak load). Microgrid B (MG-B), shown with the dashed lines in Figure 7.1, is a PV-BES-DRR MG. Since MG-B only hosts a small PV capacity (the penetration level is 5%) and has no other local generation sources, it must continuously import power from the main grid. The MGs are the only network areas, where flexible load is available.

The energy scheduling strategies for these two MGs are summarized in Table 7.1. Strategy 0 is the business as usual (BAU) scenario, where the BES dispatch follows the rule-based algorithm described in Section 5.2, which triggers charging and discharging based on peak and low load thresholds. No DR is considered in BAU. Strategies 1-3 (S1-S3) apply uncoordinated energy scheduling schemes, and thus

Table 7.1: Energy scheduling strategies.

	MG-A	**MG-B**	**DSO**
Strategy 0 (BAU)	no optimization	no optimization	–
Strategy 1 (S1)	max. profit	min. cost	–
Strategy 2 (S2)	min. energy exchange	min. cost	–
Strategy 3 (S3)	min. import	min. import	–
Strategy 4 (S4)	–	–	min. cost

each MG-EMS solves a local optimization problem i.e., an optimization problem that only considers local DERs, constraints and objectives that refer to the specific MG network area, in order to determine the optimal schedule of the available DERs according to the operational targets defined by the MG operator. As can be seen in Table 7.1, the MGs can have different objectives. A centrally coordinated energy scheduling scheme is considered in Strategy 4 (S4) and thus the DMS directly dispatches the MG resources to satisfy a DSO's operational target. In this strategy the DMS solves a global optimization problem i.e., an optimization problem with an objective function and constraints that refer to the operation of the entire distribution grid, including the MG network areas and all available MG DERs.

Depending on the entity (MG operator or DSO) that dispatches the MG resources and its operational objectives, a different DA energy scheduling problem is formulated and solved. All energy scheduling problems that were solved in the study were deterministic implementing DA dispatch of the MG resources for the schedules obtained by local or global optimization i.e., Strategies 1-4 (S1-S4). Note that local and global optimization in this chapter refer to the considered network areas, where the global system is the Chalmers distribution network depicted in Figure 7.1, and not to the value of the obtained optimal point. For example, a global optimum can be retrieved by solving an optimal MG energy scheduling problem, which is defined here as a local optimization problem.

The formulation of the optimal energy scheduling problem for the profit maximization of MG-A is given by (4.1) s.t. (4.2a)–(4.4a), (4.6a)–(4.7a), (4.8)–(4.13), and (4.15)–(4.21), where the term c^{DER} in (4.1) is $c^{DER} = C^{CHP}$, while the term r^{flex} is omitted from it. For the profit maximization of MG-B, the formulation is given by (4.1) s.t. (4.2a)–(4.4a), (4.6a)–(4.7a), (4.10)–(4.13), and (4.15)–(4.21), where the terms c^{DER} and r^{flex} are omitted from (4.1). The optimal scheduling problem for the minimization of the energy exchange with the main grid is given by (4.5) s.t. (4.6a)–(4.7a), (4.8)–(4.13), and (4.15)–(4.21) for MG-A, while for MG-B it is given by (4.5) s.t. (4.6a)–(4.7a), (4.10)–(4.13), and (4.15)–(4.21). The above-mentioned energy scheduling problems are used in Strategies 1-3 and, since no interaction is considered with the DSO, they are solved in an uncoordinated way. The coordinated MG energy scheduling is formulated as an AC optimal power flow (OPF) problem in Strategy 4, since the purpose is to find the energy scheduling of the MG resources that minimizes the cost for the DSO. This problem is given by (4.67) s.t. (4.69), (4.87)–(4.95), (4.10)–(4.13) for m ={MG-A, MG-B}, (4.15)–(4.21) for m ={MG-

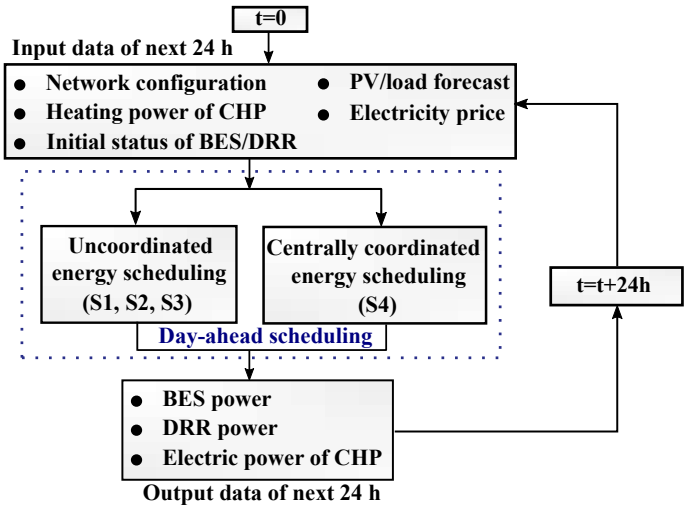

Figure 7.2: The flow diagram depicting the simulation set-up used to evaluate energy scheduling strategies in uncoordinated and centrally coordinated schemes.

A, MG-B}, and (4.8) for m = MG-A. Due to the constraints (4.20)–(4.21) all the formulated optimization problems were MILP problems.

7.2.2 Simulation set-up

The simulation set-up that was used to evaluate the energy scheduling strategies can be seen in Figure 7.2. The results of DA scheduling provide the hourly set-points of operation of the resources for the next day. The status of the resources (e.g., SoE level of BES) at the end of the day is given as input (initial operating status) for the next DA simulation. The rest of the input data, which can be seen in Figure 7.2, are the same across all studied strategies. Therefore, it is the different operation set-points that provide a different solution for each strategy.

Most of the parameters and input data to the MG energy scheduling problems were taken from data obtained from Chalmers campus. The parameters included network configuration, resource topology and resource capacity. Historical data of electricity and heating demand, temperature, and irradiation in 2016 were used as input data. These were treated as "perfect forecasts" by the MG energy scheduling problem. The electricity load data, which were acquired from smart meters at campus' buildings, were aggregated to the corresponding network buses in order to be used as input to the network's power flow. The PV generation was calculated according to [169]. The electricity prices were taken from the Nord Pool market [154] for bidding area 3 of Sweden in 2016. The load consumption and PV generation profiles of the MGs and the electricity prices that were used in the simulations can be found in Appendix C.2. The grid tariffs and the reimbursement fee have been taken from the website of the local DSO [155] and can be found in Appendix C.1.

The parameters that were especially considered for this case study can be seen in Table 7.2. It was assumed that the micro-CHP plant has a fixed electrical power output efficiency ($r^{CHP} = 0.25$) and operates under a constant leading power factor

Table 7.2: Parameters of the case study.

Scheduling horizon	24 hours
Δt	1 hour
η_m^{ch}/η_m^{dis}	95%/95%
SoE_m^{min}/SoE_m^{max}	20%/90%
R_m^{CHP}	0.25
K_m^{BES}	0.5
K_m^{DR}	0.5

of 0.96, while the load (both flexible and inflexible) has a constant lagging power factor of 0.98. Moreover, $\kappa = 0.5$ and $\kappa^{DR} = 0.5$, while it is assumed that 20% of the load consumption at each MG bus is available for DR at each time step i.e., $P_{tm}^{L,r} = 0.2P_{tm}^{L}$ in (4.12). The SoE ranges between 20% to 90% and $\eta_m^{ch} = \eta_m^{dis} = 0.95$, which are typical values used for the BES efficiencies in similar studies [17]. The scheduling horizon was 24 hours with an hourly time discretization step and the MG energy scheduling problem was solved DA repeatedly for each day with a complete input data set (in total it was 358 days).

7.3 Results and discussions

The metrics associated with the operation and cost of the MGs and the main grid are presented in Table 7.3. The generation cost of the micro-CHP plant was entered as a parameter to the optimal energy scheduling problem and, therefore, it is not included in the results of MG-A because it was entered as a parameter to the optimal energy scheduling problem.

Table 7.3: Annual cost and performance metrics.

	BAU	S1	S2	S3	S4
MG-A					
Annual cost (k$)	104	99	110	105	104
Imported energy (GWh)	2.99	2.95	2.95	2.95	2.99
Exported energy (MWh)	337	296	0	295	329
Zero energy exchange hours	0	601	3 211	725	0
MG-B					
Annual cost (k$)	243	239	239	246	243
Imported energy (GWh)	6.95	6.95	6.95	6.95	6.95
DSO					
Annual cost (k$)	312	306	311	314	304
Imported energy (GWh)	28.72	28.72	29.02	28.72	28.72
Peak power (MW)	5.66	5.47	5.61	5.70	5.44

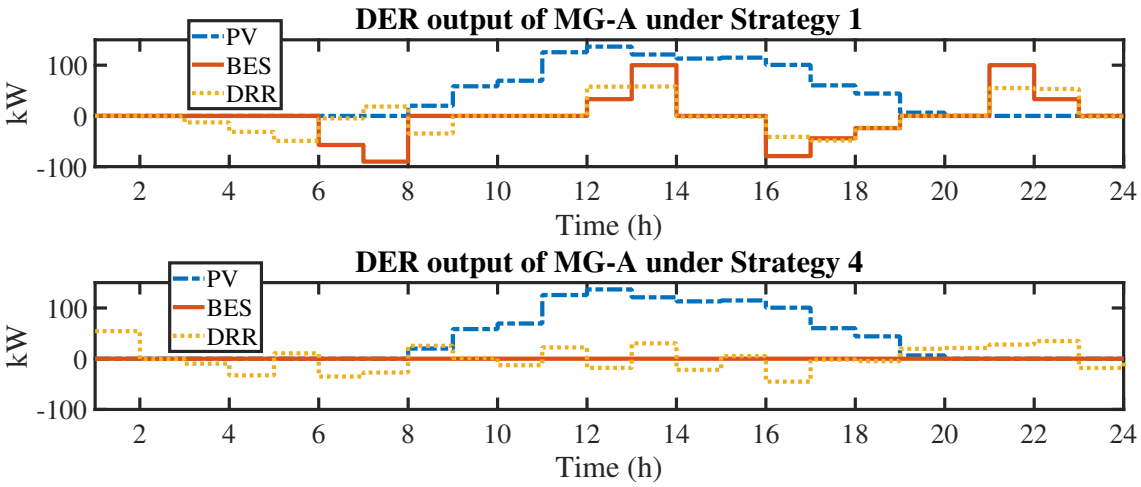

Figure 7.3: The DER output of MG-A for the DA simulation of September 17, 2016 (comparison between S1 and S4).

7.3.1 Comparison of the costs under different strategies

As can be seen in Table 7.3, S1 reduced the cost of all three entities (MG-A, MG-B, DSO) compared to BAU, which means that all interconnected systems benefited from the deployment of two MG-EMSs, each seeking to optimize their respective MG cost. The cost reduction was 2% for MG-B and DSO and 4% for MG-A. When S2 was applied, the cost of MG-A was increased by 7% compared to BAU; however, the self-supply level of MG-A was significantly improved. Specifically, MG-A could operate as a virtual island and supply its customers with its own resources for 3211 hours (about 4.5 months) throughout the year.

The centrally coordinated energy scheduling (S4), yielded the most economic operation for the DSO resulting in a 2.5% reduction compared to the BAU case. However, this solution was not optimal for the MGs, as their costs were similar to the cost of their BAU solution. This shows that there can be a conflict between the objectives of local and global optimization and, as a result, their solutions can yield a different dispatch of the MG resources. As an example, Figure 7.3 shows the variation in the scheduling pattern of the BES and DRRs of MG-A (positive values indicate discharging and load curtailment), when S1 and S4 were applied during an autumn day (the CHP was out of operation). In S4, the BES is only scheduled to contribute to the system's peak reduction (in Figure 7.3 the BES was not used for this day). Unlike S4, the scheduling in S1 is affected by the spot price and follows its fluctuation. Therefore, in this example, the BES was discharged and load was curtailed from 13:00-14:00 at high PV production because the spot price had a high value at that hour.

The peak load consumption of the whole distribution system was kept at its lowest points with S1 and S4 as shown in Table 7.3, whereas S2 and S3 resulted in an increase of 3-5% compared to S4 because with these strategies MG-A interacted less with the upstream network. Therefore, MG-A did not contribute to reduce the peak consumption of neighboring areas in the grid. Considering the low peak as well as

the reduced cost for the DSO it is clear that S1, which was optimal for both MGs, is the best option out of all the simulated strategies. However, with additional MGs and increased local generation or with different load profiles, such as those with rapid variations due to EV charging, it is possible that the need for coordinated MG operation will increase.

7.3.2 Distribution system operation

After the DA simulations, power flow calculations were performed to validate that the uncoordinated energy scheduling solutions satisfied the network constraints (voltage limits, feeder constraints). All the simulations resulted in operation within technical limits. It should be noted, though, that the modeled network has sufficient feeder capacity and relatively low PV penetration level (14%). A minimum interaction between the MGs and the DSO could be applied (e.g., the DSO could approve or reject an MG schedule) to ensure that the MGs' operation does not undermine the operation of a distribution system.

7.3.3 Expected BES lifetime

The link between the BES scheduling of each strategy and the expected BES lifetime was investigated using manufacturers' data of the lifecycle loss function in relation to the DoD, which can be found in [30], in order to evaluate the impact of cycle aging. The rainflow algorithm [75] was used to calculate the number of half cycles and full cycles of the BESs along with the cycle range and an average SoE. From this information, the number of full cycles was calculated and an average DoD was estimated.

The results showed that the proposed strategies were unsuitable for BESs with low lifecycle (e.g., lead acid BESs), since the BES performance could not be guaranteed for more than 5 years. They also showed that energy arbitrage and cost minimization, whether performed locally (S1) or for the entire system (S4), increased the number of cycles resulting in faster cycle-based BES degradation. Therefore, these strategies should only be considered for BESs with high lifecycle (e.g., Li-ion or NaS BESs). Table 7.4 summarizes the results and presents the estimated expected lifetime for Li-ion BESs.

7.4 Summary

The deterministic MODEFlex model was used in this chapter to evaluate energy scheduling strategies. In these strategies, the model could be employed by each MG-EMS to schedule the MG resources in an uncoordinated way (only considering local constraints/targets) or in coordination with the DSO. When the uncoordinated scheme was used, the aim was to obtain the solution that best satisfied the operational objectives of each MG operator. With the centralized coordination scheme, the DMS directly dispatched the MG resources to satisfy an operational target that was applicable to the whole grid, including the MGs. The 12-kV distribution net-

Table 7.4: BES utilization and expected lifetime for Li-ion BESs

	BAU	S1	S2	S3	S4
MG-A					
BES cycles	67	403	153	144	317
Average DoD (%)	78.5	80	80	80	80
Lifetime in years	>15	11	>15	>15	14
MG-B					
BES cycles	200	400	400	0	317
Average DoD (%)	79	80	80	–	80
Lifetime in years	>15	11	11	–	14

work of Chalmers University of Technology was used as a test system, where two areas of the network were considered as grid-connected MGs. It was assumed that the MG-EMSs interacted with the DMS before implementing the energy scheduling solution to ensure technical feasibility.

The impact on the energy transmission and peak power cost of the DSO was evaluated both for the uncoordinated and coordinated energy scheduling. The simulation results of the study showed that, even without assuming any coordination with the DSO, implementing local optimization to minimize the energy and peak power cost of each MG benefited both the MGs' and the DSO's cost in comparison to the base case (BAU). Further optimizing the performance of the DSO's grid to reduce the DSO's operation cost would mean that the MGs' economic benefits against the BAU case would be removed. Therefore, simulating the MGs' and DSO's operation under different strategies is of high value in order to investigate the trade-off between the global and local optimization applied for the energy scheduling of the MG resources.

Chapter 8

Optimal MG Flexibility Dispatch with DSO Coordination

This chapter is based on Paper III and presents simulation results from the bilevel optimization problem used to determine the optimal allocation and dispatch of MG flexibility. Using the proposed framework of bilevel optimization the MGs could coordinate with the DSO, which is the entity that solves the optimization problem, and dispatch their resources based on the flexibility prices obtained from the solution. At the end of this chapter, the value of flexibility for the DSO and the MGs is discussed for two models of FSs considered in the bilevel optimization problem.

8.1 Aim of study

In Chapter 6, the value of flexibility was examined for different flexibility prices. No insight was provided, however, regarding the choice of the suitable flexibility price which determines the optimal dispatch of flexibility. This chapter further analyzes the values of flexibility considering the impact of the distribution operation and configuration, which affects the allocation and value of dispatched flexibility provided by grid-connected MGs. The bilevel optimization framework is proposed to calculate the optimal allocation and dispatch of the MG flexibility via coordination between the DSO's grid operation and the operation of the MGs under the deterministic MODEFlex model.

The aim of this chapter's study is to investigate the changes in the dispatch of the MG resources when the MODEFlex problem is solved assuming coordination between the DMS and the MG-EMSs. The study also aimed to assess the value of flexibility for both the procurer i.e., the DSO, and the FSPs i.e., the MGs.

8.2 Study approach

The performance of the proposed bilevel optimization model, which was formulated in Section 4.4.3, is validated on the standard 33-bus radial distribution network

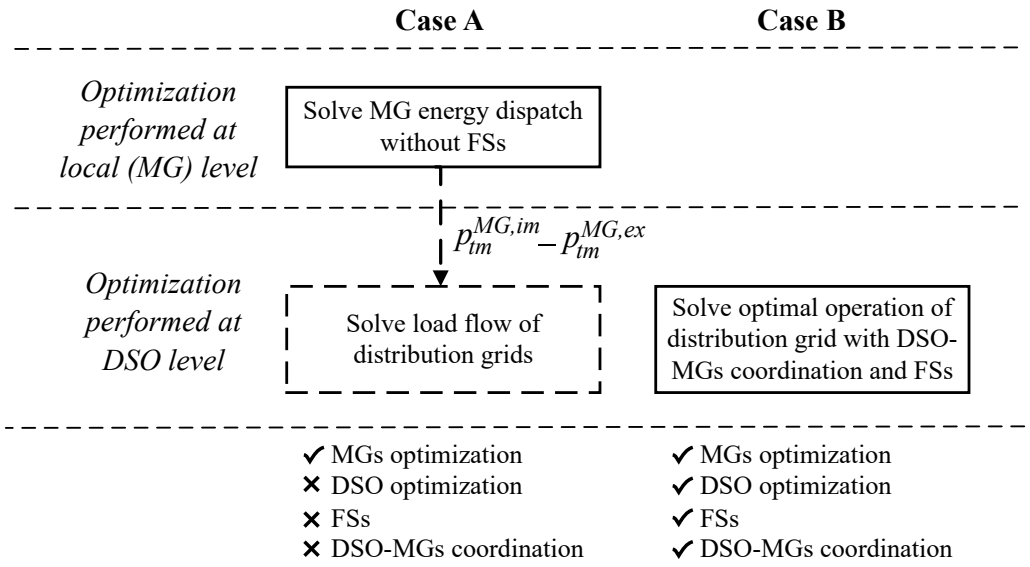

Figure 8.1: The two test cases considered to investigate the value of local flexibility and its impact on the operation of the MGs and the main grid.

described in Section 3.6.4 using the test cases presented in Figure 8.1. The provision of local flexibility through FSs is only considered in Case B, which investigates the relationship between the level of the flexibility price and the amount of local flexibility mobilized by solving the bilevel optimization problem.

When the MG-EMSs coordinate their operation with the DMS i.e., in Case B, they exchange their energy and flexibility dispatch problem formulations, input data, and parameters. The DSO uses this information as an input to the DMS which solves one optimization problem for all connected entities. This problem is the equivalent single-level optimization problem derived from the bilevel optimization problem. The DMS only sends flexibility prices signals, which are obtained by the solution of the problem, to each MG. Since the MG resources are not directly dispatched, this coordination is classified as decentralized, even though the optimization is performed in a centralized manner.

8.2.1 Formulation of the optimization problems

A detailed description of the aim and features of Cases A-B (see Figure 8.1) and the mathematical formulation of the associated optimization problems are given below.

8.2.1.1 Without FSs and DSO-MGs coordination

In Case A, each MG optimizes its energy dispatch without considering the provision of FSs. The optimization problem solved by each MG m is given by (4.1) s.t. (4.2a)–(4.4a), (4.6a), (4.23)–(4.40), without considering the CS conditions and ignoring the terms c_m^p, c_m^{DER}, and r_m^{flex}. The solution of each MG's problem yields the profile of the power exchanges with the distribution network ($p_{tm}^{MG,ex} - p_{tm}^{MG,im}$), which are entered as parameters in the AC OPF problem of the DSO given by (4.68) s.t. (4.69) and (4.78)–(4.86) without considering the term c^{flex}, which is solved to compute the

DSO's grid operation metrics and associated cost. No coordination of the grids' operation is considered at the DSO-MGs interfaces.

8.2.1.2 Bilevel optimization with FSs and DSO-MGs coordination

In Case B, the DSO coordinates with the MGs to jointly optimize the provision of local flexibility within the latter in order to reduce the DSO's peak power cost while minimizing the net cost of each MG. The problem formulations of two sub-cases are considered within this case (see Section 4.4.3) depending on which FS is mobilized. When the offered FS is:

- **FS-B**, the flexibility prices $\pi_m^{fl,im}/\pi_m^{fl,ex}$ and the operation metrics of the DSO's grid and MGs are computed by solving the bilevel optimization problem given by (4.68) s.t. (4.69), (4.78)–(4.86), (4.70), (4.2a)–(4.4a), (4.6a), (4.23)–(4.40), (4.52)–(4.59), and (4.96)–(4.112) .
- **FS-C**, the flexibility price $\pi_m^{fl,Cap}$ and the operation metrics of the DSO's grid and MGs are computed by solving the bilevel optimization problem given by (4.68) s.t. (4.69), (4.78)–(4.86), (4.71), (4.2a)–(4.4a), (4.6a), (4.23)–(4.40), (4.61a)–(4.63a), (4.96)–(4.108), and (4.113)–(4.114).

In the above-mentioned problems, the terms c_m^p and c_m^{DER} are ignored, while the CS conditions of the LL inequality constraints are included.

8.2.2 Simulation set-up

The considered time horizon of the study was 24 hours and the time discretization step was $\Delta t = 1$ hour. The flexibility was dispatched in DA for each time step of the considered flexibility activation period, which is 16:00-20:00 i.e., a time period which lies within the activation periods requested from small to medium-sized companies offering flexibility in [168]. The capacity limits P_m^{Cap} used in FS-C were 110 kW, 154 kW, and 307 kW for the MGs at buses 13, 18, and 30, respectively. Therefore, the results presented below comment on the impact of FS-C.

8.3 Results and discussions

The results computed for the test cases presented in Figure 8.1 demonstrate the effectiveness of the proposed DSO-MGs coordination for the provision of local flexibility. The impact of this coordination on the DSO's and MGs' operation costs, as they are defined by their objective function of their respective optimization problem, and the dispatch of the MG resources is also discussed. After the respective optimization problem was solved for each test case, power flow calculations were performed to validate that the obtained solution lied within the boundaries of the feasible region i.e., that the voltage and feeder capacity limits were not violated.

8.3.1 Impact on the dispatch of local flexibility resources

An example of how the dispatch of the MGs' resources can be affected by the offered FSs is given in Figure 8.2. The comparison between Figure 8.2(a) and Figure 8.2(b) shows the difference in the BES dispatch within MG2 in Case B, when the MG provides FS-C, and the dispatch in Case A, where no FS is offered. It can be seen that in Case B, there is an additional discharge half-cycle of the BES, which occurs at a time step within the flexibility activation period because the MG provides flexibility to the upstream connected system. Figure 8.2(c) shows the net power, where positive values refer to imported power of the MG, and illustrates how the imported power of MG2 is modified in Cases A-B. Right after the flexibility period in Case B, there is large increase in the imported power, as the earlier dispatch of flexibility leaves time for one more BES cycle before the end of the day, which allows the MG to benefit from energy arbitrage. It should be emphasized, however, that having more frequent cycling of BESs can have a long term cost related to the decrease of their lifetime due to degradation. Thus, it is important to implement long-term studies to assess which frequency of flexibility provision is acceptable e.g., whether the flexibility dispatch is going to be event-based or determined by a daily cleared market. This was also pointed out in Section 6.3.3.3, where it was shown that smaller BESs can be more severely affected by degradation when they are utilized to offer FSs.

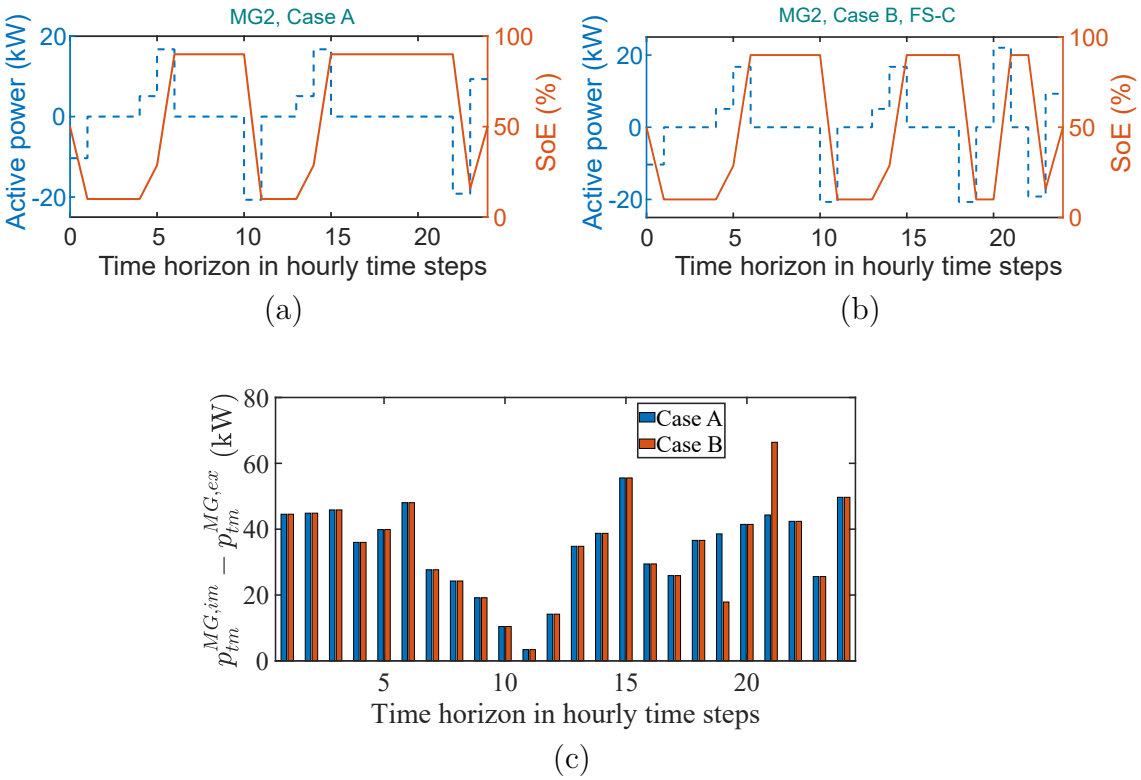

Figure 8.2: Operation of MG2: a) BES dispatch for Case A, b) BES dispatch for Case B with FS-C, and c) net power in Case A and Case B with FS-C.

8.3.2 Impact on the value of local flexibility

Within the study considered here, the local FSPs did not profit from the provision of FS-B. Similarly, this FS offered no benefit to the DSO as, in Case B, no flexibility was bought and the main grid's cost was equal to that of Case A.

The flexibility value of FS-C depends on the choice of P_m^{Cap}, which is affected by the configuration of all connected grids and it should be customized for each specific test system. In the bilevel formulation (Case B), these parameters are eliminated. Therefore, this FS was implemented as the addition of a penalty to the objective function of the FSPs and an income from the payment of this penalty to the objective function of the DSO. This can be understood by setting $P_m^{Cap} = 0$ to (4.71) and (4.60). A sensitivity analysis performed about P_m^{Cap} for Case B showed that when P_m^{Cap} was set to be equal to 25% of the capacity at the MGs' connection points, the DSO and the MGs connected at nodes 13 & 18 had a daily economic value of flexibility of 0.2%, 0.8%, and 1.8%, respectively, of their total daily operation cost. The MG at node 30, however, had an increased cost. Considering that the installed BES capacity at each MG corresponded to a conservative future scenario of BES deployment, it is possible that with the integration of more BESs, FS-C could offer an even higher economic value and potentially benefit all connected systems.

8.3.3 Comparison of the flexibility dispatch studies

In comparison to the study of Chapter 6, the value of flexibility provided by FS-C was significantly lower for the MGs studied in Chapter 8. This showed that the network configuration layout and the coordination of multiple FSPs could substantially reduce the value of flexibility, as the solution of the two-player game in the bilevel optimization framework yielded a flexibility price that would not offer a significant economic benefit to the MGs. It should be noted, however, that the flexibility price is essentially defined by the use of local flexibility. Procuring local flexibility for the purpose of reducing the peak power cost of the DSO's grid offered only small benefits to the cost of the DSO resulting in relatively low incentives for the FSPs in the studies of these two chapters. Under different conditions e.g., daily variation in load demand and local generation, and for different uses of flexibility, higher economic values could be revealed.

8.4 Summary

In this chapter, the proposed bilevel optimization model for the coordinated operation of the MGs and the DSO's grid was tested on the 33-bus radial distribution network to explore the competing needs and synergies among different parties. The linearized AC power flow equations were used in the UL problem to model the operation of the DSO's grid with the DSO acting as the leader and the MODEFlex model was used for the MGs' operation in the LL problem. The quantification of the technically and economically feasible local flexibility was achieved with the integration of the models of two FSs i.e., FS-B and FS-C, in the LL optimal energy

scheduling problem, which is rarely considered in energy scheduling studies. The MG customers could increase their revenues by providing these FSs to the DSO. The DSO procured flexibility from the MGs to minimize the peak power cost of the distribution grid. The MGs implemented economic dispatch of their flexible resources by offering flexibility to the DSO and engaging in energy arbitrage.

The simulation results showed how the proposed bilevel model altered the dispatch of the MGs' resources. The modified dispatch implied that certain limitations might need to be considered with regard to the frequency of the flexibility provision. Additional insights were given regarding the value of flexibility for the DSO and the MGs. FS-B offered no economic value to either the DSO or any of the MGs for the test system and simulation test case of this chapter. Contrary to FS-B, FS-C could reduce the total cost for some parties depending on the choice of the capacity limit. Different uses of flexibility by the DSO might reveal higher economic values offered by the two FSs. The flexibility activation period assumed in the simulations was between the hours 16:00-20:00.

Chapter 9

Conclusions and Future Work

This chapter summarizes the work of the thesis and the key findings from the thesis' studies. The derived conclusions from the simulation and demonstration results provide answers to the formulated research questions and can be used to explain how the MG operators and main grid operators can benefit from practical applications of the proposed MODEFlex model. Lessons learnt from real-life demonstrations and suggestions for future research are also provided in this chapter.

9.1 Conclusions

This thesis has dealt with energy and flexibility dispatch of grid-connected MGs by developing the MODEFlex model. The model can be utilized for optimal dispatch of the MG resources in an uncoordinated way i.e., only considering local constraints and targets, or in coordination with the DSO. A BMG-EMS was designed to integrate the developed model and employ it to demonstrate its performance on two physical test sites i.e., the real residential buildings of HSB LL and Brf Viva, which were treated as BMGs.

Following is a summary of what was studied in the thesis and the main conclusions indicating the relations to the RQs formulated in Section 1.4. With regard to:

- **RQ1**, which was formulated to inquire about *the effect of the MG energy scheduling strategies to the DSO's cost assuming utility restructuring*, the MODEFlex model was tested with different operational strategies and schemes of coordination with the DSO. The impact of these strategies and coordination schemes on the cost and operation of the MGs and the DSO's grid was assessed considering the unbundled framework of operation with a simulation case study based on the Chalmers distribution grid. The results presented in Section 7.3 showed that, **even without coordination, the distribution system can benefit from the implementation of multiple MG-EMSs that locally optimize their DA resource scheduling**. The MG energy scheduling solution that would benefit the DSO the most did not benefit the MGs, as their cost would be the same compared to the base case. Based on

these findings, it can be suggested that the cost difference between the optimal solution for the MGs and the optimal solution for the DSO could be used to define the remuneration that the MG owners should receive for modifying the dispatch of their MGs' resources in order to satisfy the DSO's operational targets.

- **RQ2**, which was formulated to investigate *improvements that can be applied to the BES model to consider real-life performance characteristics and the impact of degradation without increasing the complexity of the MODEFlex model*, two more accurate energy dispatch models were developed i.e., Model-3 and Model-4 given in Section 5.2.1. These models combined the measurement-based BES model with cycle aging models dependent on throughput and DoD, respectively. The incorporated measurement-based BES model can capture realistic performance characteristics, while the cycle aging models can assess the impact of the energy scheduling solution to the capacity of the BES. Model-3 formulated an LP energy scheduling problem and Model-4 formulated an MILP energy scheduling problem i.e., **incorporating the measurement-based model and the cycle aging models did not increase the complexity of the MODEFlex problem**. The calendar aging was also calculated after the final dispatch decisions for a comprehensive evaluation of the degradation.

  The validation of the MODEFlex model with simulations and demonstrations at the HSB LL and Brf Viva BMGs proved the **feasibility and effectiveness of integrating a more detailed mathematical BES model to the linear MODEFlex problem.** In the demonstrations at the HSB LL in particular, there was a considerable improvement in the BES responses when the measurement-based model was used, as compared to the BES responses when the conventional BES model was used. As a result, the daily undelivered BES energy over the total request was reduced from 13.3% to 3.7% at the same time as the BES usage was increased. This result indicated **a more reliable implementation of the BES dispatch according to the measurement-based model**, as the BES could more accurately follow the schedule that reflected the targets of the BMG operator.

- **RQ3**, which was formulated to investigate *the impact of BES degradation on the cost of the optimal MG energy schedule*, the simulation study of the long-term operation of the HSB LL BMG was used to evaluate the BMG's operation cost and BES degradation resulting from the implementatio of the optimal BES dispatch, which was obtained from solving the developed energy management model. The results in Section 5.3.1 showed that the proposed Model-3 and Model-4 **could reduce the annual energy and degradation cost by up to 3.1%** compared to when degradation cost was omitted from the objective function. Moreover, it was shown that it is possible to have **more flexible limits on the SoE levels of the BES and allow more BES capacity to be used**, if these models are employed. On the other hand, if degradation is neglected in the BES dispatch, conservative limits should be applied to prolong the BES lifetime.

- **RQ4**, which was formulated to inquire about *the effect of load forecasting errors on the MG's operation costs*, a comparative analysis was performed where the developed BMG energy management model was employed in multiple test cases investigating all possible combinations of the different optimization methods i.e., DO and SO, and solution approaches i.e., DA and RH dispatch, that were studied in the thesis. Short-term and high-resolution load forecasts provided from ML forecasting models were used as input in each test case. The main conclusion that can be drawn from the results presented in Section 5.3.4.2 is that, **even without high computational requirements or extreme forecasting precision, a near-optimal dispatch can be achieved with a BMG total cost no higher than 1% of the optimal cost**, which would be the cost if the up to 12% daily MAPE of the forecasts could be eliminated. It was also shown that **more accurate forecasts could mostly contribute to reducing the peak power cost, which was 20.2% higher than the optimal**. All ML models resulted in almost equal MG operation costs and using simpler forecast models such as LR and simpler methods or solution approaches such as DO or DA dispatch did not increase the associated costs. This was a promising result, as these simplifications could be used in joint operation and planning studies to simultaneously enable faster and sufficiently accurate solutions.

- **RQ5**, which was formulated to investigate *how the techno-economically feasible MG flexibility could be assessed and which factors affect its economic value*, the detailed models of two FSs i.e., FS-B and FS-C, were separately incorporated in the MODEFlex model. Since the MODEFlex model could combine FS models with the energy scheduling model, it could be employed to calculate the flexibility amount that would be both technically available and economically beneficial. The stochastic formulation of the MODEFlex model was used to introduce a methodology of stochastic flexibility assessment in Chapter 6, determine the offered flexibility amount and estimate the value of flexibility for the FSP. An analysis of the economic value of flexibility for the DSO was performed considering multiple flexibility prices and assuming that the flexibility is procured for peak shaving i.e., to reduce the subscription fee of the DSO.

  The dispatch of flexibility according to the bid was ensured in all simulations for Cases A-C in the study described in Section 6.2 thanks to the RH dispatch which was combined with the SO MODEFlex model. Thus, the payment of penalties was avoided, which increased the economic value of flexibility for the studied BMG. The **value of flexibility was at least 56% and 7% of the daily BMG operation cost under the considered $\pi_m^{fl,Cap}$ in Cases A-B**, respectively. These cases, unlike Case C, also benefited the DSO.

  Regarding the factors that affected the economic value it was shown that **increasing the BES size did not significantly affect the daily value of the BMG's flexibility**, however, long-term studies could give different results, as **the degradation cost was found to be smaller with the**

larger BESs. The simulations also showed that the 7.2 kWh BES could provide more flexibility than the 14.4 kWh BES depending on the notification time and flexibility price $\pi_m^{fl,Cap}$, as the BMG would benefit more from using the additional capacity of the larger BES for ESs instead of the FS.

- **RQ6**, which was formulated to investigate *how the coordinated operation of the DSO's grid with multiple grid-connected MGs could be employed to achieve optimal flexibility allocation and dispatch*, a bilevel multi-follower optimization problem was developed and its application is discussed in Chapter 8. In the bilevel framework, the DSO acted as the leader and the MGs i.e., the FSPs, as the followers. The DSO used the DSO-MGs' interaction to solve the bilevel problem and indirectly dispatch the MG flexible resources through flexibility price signals. The bilevel model was validated on a 33-bus radial distribution network in a study that assessed the value of local flexibility and its impact on the dispatch of the MG resources. The results of the study showed that **FS-C could provide incentives for both the DSO and the MGs** depending on the chosen capacity limit P_m^{Cap}. Not all MGs would necessarily benefit simultaneously, however.

The key findings from the thesis' studies reveal how MG/BMG owners and grid operators can benefit from practical applications of the developed MODEFlex model. As the simulation and demonstration results proved, the model can be used by MG/BMG owners both for close to real-time energy management (i.e., with time scale of 5-15 minutes), in order to reduce the expected MG operation cost in short-term, and for long-term assessment studies such as, for example, the monthly or annual estimation of a building's energy cost, which can help the MG/BMG operator choose the most economic operation strategy. Thus, the model contributes to a more accurate estimation of the economic benefits associated with participation of the MG customers to ESs and FSs. The model can also be used by MG operators to quantify the MG's flexibility potential and assess the value of the MG flexibility.

For the purpose of understanding their financial and technical benefits, system operators can use the proposed coordination schemes to assess the impact of the DSOs' and MGs' coordination and demonstrate the DSOs' and MGs' interoperability in pilot test sites. The bilevel optimization model and the methodology of flexibility assessment can contribute to investigate the appropriate flexibility prices or incentives, for both the DSOs and the MGs, that would lead to the dispatch of the desired flexibility depending on the system's needs. The bilevel model, in particular, could provide valuable info about the benefit of implementing an LFM ran by a DSO. Finally, the computational efficiency of the MODEFlex model, even in its stochastic formulation, confirmed that flexibility could be dispatched promptly (close to real-time) within a day, which can contribute to the reduction of the system's needs for grid capacity reserves, if multiple MGs participate in the provision of FSs.

9.2 Lessons learnt from real-life demonstrations

The demonstrations at the two demo sites validated the BES dispatch models and showed that the measurement-based BES model that was developed for each site was suitable for close to real-time BMG energy management. The BESs could follow the requests that were transmitted from the BMG-EMS, as long as certain operation conditions were satisfied. For example, it was important that the SoE limits of the BMG-EMS would be stricter than the SoC limits of the current limiter function of the BES DC/DC converter. Furthermore, there were additional challenges at each demo site that affected the BES response to the power request commands.

In Brf Viva, the optimal BES dispatch could accurately be implemented for both the conventional and the measurement-based BES model, with only negligible deviations from the obtained solution. Nevertheless, it was not an easy task to employ the BES scheduling models with the designed BMG-EMS, which dispatched the BESs as a system and the power request was equally divided to all BESs. Each BES could end in a different SoC level and this problem was intensified by a maintenance function implemented by each BMS. Therefore, the demonstration at the Brf Viva buildings was only possible after temporarily deactivating this function. Otherwise, the system of BESs would only reliably deliver the rated power within a much stricter SoE range, which was approximately 40%-70%, than the range allowed by the current limiter function, which was 27%-80%.

The results in the HSB LL BMG also showed very good response of the BES. Larger charging requests were not always met, due to the SoH of some battery cells. This is why the value of using the measurement-based model was more evident for this demo site. To improve the performance of the conventional BES model, the BMG operator would need to impose additional charging power limits, which would limit the BES in the whole operational SoE region.

Apart from the accuracy of the BES scheduling models, there are several other factors that may influence the results and the expected costs of the applied BES schedule. One of these factors is the forecast models that are integrated in the BMG-EMS. These models should forecast the load, PV generation, the electricity price (if necessary) with small errors to ensure an accurate cost estimation of the implemented energy scheduling solution. Another factor is the BES degradation model and the considered BES stress factors and degradation parameters. The degradation model and parameters may vary for each specific BES type. Moreover, degradation impacts the performance of the BES, which means that the parameters of the measurement-based BES scheduling model might have to be re-adjusted.

9.3 Future research

In this thesis, the MG energy management was studied with an emphasis on BES flexibility. Although the BES modeling and degradation was studied in greater detail than the majority of the literature on MG energy management, there are still

areas that require further research. Moreover, the accuracy of the estimated aging can vary depending on the BES chemistry. The aging models used in this thesis might not be applicable to all Li-ion BESs and it is therefore advised that tests with different aging models are conducted to further guarantee the benefits in terms of cost reduction for the BMG.

Apart from the accuracy of the mathematical model of the BES, the forecasting errors associated with the input data to the MG-EMS could also influence the results. The thesis studied the effects of short-term and high-resolution forecasting errors of the load profile. The impact of errors of similar types of forecasts should also be investigated for other inputs to the MODEFlex model. Moreover, the forecast error distribution over the time horizon should be modeled in greater detail for a more accurate uncertainty representation in scenario-based SO.

The thesis also studied the interaction between grid-connected MGs and the DSO considering two FS models for flexibility dispatch. Coordination of multiple BES-based MGs or BESs with the control devices of the main grid is a very interesting research area, as existing approaches have so far been using the conventional BES model and neglecting the impact of degradation. It would also be useful to study other types of MGs (e.g., MGs that are based on different resources) and also different configurations of distribution systems with multiple interconnected MGs. If the research gaps that were identified during the work of this thesis are further explored, there will be a deeper understanding of the benefit of BES flexibility both for the MG owner and for the DSO.

Studies with different BES sizes, in particular, should be conducted to explore additional values of flexibility offered with either FS. Furthermore, the bilevel model could easily be modified to be tested with higher time resolution (i.e., intra-hour dispatch of flexibility) and different time horizons to increase understanding of the system's flexibility. However, it should be noted that the high computation time will introduce limitations, which would most likely have to be addressed by reducing the optimality gap i.e., by potentially accepting sub-optimal solutions.

Following are some topics, which are suggested for future research:

- The use of the measurement-based model resulted in a more reliable implementation of the BES scheduling model and simplified the MODEFlex problem. Thus, advanced AC OPF models with fewer relaxations, such as the second-order cone programming (SOCP) BFM, can be used for the distribution network operation, when coordination between the DSO's grid operation and the MG operation is considered. As a result, this coordination can further be developed to consider dispatching the MG energy and flexibility for other purposes such as network loss minimization. Another suggestion is to coordinate the operation of distribution grid components and MGs' resources. For example, it would be particularly interesting to study the benefits of coordinating the operation of on-load tap changers with the dispatch of BESs.
- Future research should expand the MODEFlex model to include the cost of

calendar aging. This can be a challenging task, especially when the MODEFlex model is formulated as an MILP model e.g., Model-4 in Section. 5.2.1, as more integrality constraints will have to be added to the MILP problem in order to incorporate the calendar aging cost. Even when the MODEFlex model incorporates linear models to calculate cycle-based degradation such as e.g., Model-3 Section 5.2.1, it is expected that integrality constraints cannot be avoided altogether, if the optimization problem is to account for the impact of DoD of each BES cycle, which is a requirement for an accurate assessment of calendar aging.

- The MODEFlex model should also be applied for the island operation mode, where the MG's cost minimization should consider seamless transition between the grid-connected and island mode of operation. The trade-off between MG resiliency and cost minimization is a very interesting subject, as these two objectives are expected to result in different utilization of the MGs' resources, especially of the BESs.

- Future studies can explore the effects of short-term and high-resolution PV forecasting errors on the optimal solution of the MODEFlex problem when ML models are used to obtain the forecasts. Note that the development of such models would be quite different in comparison to the ML models that were used for the short-term and high-resolution load forecasting in the thesis. Different ML techniques and training data would have to be employed, as short-term PV forecast is all the more based on sky imagery mechanisms [170]. It would also be interesting to study multiple time-scale scheduling horizons and investigate which horizon length and which time scales would be suitable to minimize the effects of the forecasting errors in close to real-time MG energy and flexibility dispatch. Finally, the effect of the forecast errors may also be studied for MGs with different mix of resources to analyze whether the forecasting accuracy requirements should variate depending on the MG system.

- The MODEFlex model could also be extended to study other revenue streams and quantify the BES degradation induced by each BES service. It would be valuable to compare revenue streams and assess the economic benefits of both portable and stationary BESs as flexible energy resources for a BMG owner. Second-life applications of BESs should also be considered. Participation of residential BESs in frequency regulation would be an interesting topic for future research, although it should be noted that frequency regulation is more practical at the aggregated level, due to minimum capacity requirements [76] and because it depends on signals from the grid operator [171], which would complicate the control of multiple small-scale BESs.

- Future studies could apply the versatile methodology for flexibility assessment and dispatch proposed in the thesis to a wide range of case studies that can employ the MODEFlex model with different selected time horizon lengths and flexibility activation periods, as these factors are a significant part of the flexibility evaluation. For example, the MODEFlex model with minor

modifications can be used to derive the bidding curve of the MG in case the DSO operates an LFM to procure flexibility. In addition, it could be used in a bilevel optimization framework for distribution grid expansion planning, which could reveal additional values of flexibility for the FSPs and the DSO.

- Reinforcement learning could be used to develop a model for optimal allocation and dispatch of flexibility using decentralized coordination, like the bilevel optimization problem, avoiding at the same time the centralized optimization at the DSO level which requires full information regarding MGs' resources and operational targets.

References

[1] Directorate-General for Climate Action, "United nations' science panel issues starkest warning yet to urgently cut global emissions," https://ec.europa.eu/clima/news-your-voice/news/united-nations-science-panel-issues-starkest-warning-yet-urgently-cut-global-emissions-2022-04-04_en, 4 April 2022, Accessed: 23.08.2022.

[2] H.-O. Pörtner, D.C. Roberts, M. Tignor, E.S. Poloczanska, K. Mintenbeck, A. Alegría, M. Craig, S. Langsdorf, S. Löschke, V. Möller, A. Okem, B. Rama (eds.), "Climate change 2022: Impacts, adaptation, and vulnerability." IPCC, Contribution of Working Group II to the Sixth Assessment Report of the Intergovernmental Panel on Climate Change, 2022.

[3] "Sweden's integrated national energy and climate plans," Government Offices of Sweden, Jan. 2020.

[4] IRENA, "Innovative solutions for 100% renewable power in Sweden," *Int. Renewable Energy Agency*, Abu Dhabi, 2020.

[5] ——, "Off-grid renewable energy solutions to expand electricity access: An opportunity not to be missed," *Int. Renewable Energy Agency*, Abu Dhabi, 2019.

[6] I. S. F. Gomes, Y. Perez, and E. Suomalainen, "Coupling small batteries and PV generation: A review," vol. 126, p. 109835, July 2020.

[7] N. Hatziargyriou, "The microgrids concept," in *Microgrids: Architectures and control*. Wiley—IEEE press, 2014, ch. 1, pp. 1–24.

[8] A. Hirsch, Y. Parag, and J. Guerrero, "Microgrids: A review of technologies, key drivers, and outstanding issues," *Renewable and Sust. Energy Rev.*, vol. 90, pp. 402–411, July 2018.

[9] D. Y. Yamashita, I. Vechiu, and J.-P. Gaubert, "A review of hierarchical control for building microgrids," *Renewable and Sust. Energy Rev.*, vol. 118, p. 109523, Feb. 2020.

[10] H. Fontenot and B. Dong, "Modeling and control of building-integrated microgrids for optimal energy management–A review," *Appl. Energy*, vol. 254,

p. 113689, Nov. 2019.

[11] S. Dorahaki, R. Dashti, and H. R. Shaker, "Optimal energy management in the smart microgrid considering the electrical energy storage system and the demand-side energy efficiency program," *J. Energy Storage*, vol. 28, p. 101229, Apr. 2020.

[12] W. Su, J. Wang, and J. Roh, "Stochastic energy scheduling in microgrids with intermittent renewable energy resources," *IEEE Trans. Smart Grid*, vol. 5, no. 4, pp. 1876–1883, July 2014.

[13] M. El-Hendawi, H. Gabbar, G. El-Saady, and E.-N. Ibrahim, "Control and EMS of a grid-connected microgrid with economical analysis," *Energies*, vol. 11, no. 1, p. 129, Jan. 2018.

[14] J. S. Giraldo, J. A. Castrillon, J. C. López, M. J. Rider, and C. A. Castro, "Microgrids energy management using robust convex programming," *IEEE Transactions on Smart Grid*, vol. 10, no. 4, pp. 4520–4530, July 2019.

[15] W. Hu, P. Wang, and H. B. Gooi, "Toward optimal energy management of microgrids via robust two-stage optimization," *IEEE Trans. Smart Grid*, vol. 9, no. 2, pp. 1161–1174, Mar. 2018.

[16] S. Suthar, N. Kumar, and N. M. Pindoriya, "Cost-effective energy management of grid-connected PV and BESS: A case study," in *Proc. IEEE Innovative Smart Grid Technologies-Asia (ISGT Asia)*, Chengdu, China, Oct. 2019, pp. 4122–4127.

[17] B. Zhao, X. Wang, D. Lin, M. M. Calvin, J. C. Morgan, R. Qin, and C. Wang, "Energy management of multiple microgrids based on a system of systems architecture," *IEEE Trans. Power Syst.*, vol. 33, no. 6, pp. 6410–6421, Nov. 2018.

[18] F. Khavari, A. Badri, and A. Zangeneh, "Energy management in multi-microgrids via an aggregator to override point of common coupling congestion," *IET Gener., Transmiss. & Distribution*, vol. 13, no. 5, pp. 634–642, Mar. 2019.

[19] P. Tian, X. Xiao, K. Wang, and R. Ding, "A hierarchical energy management system based on hierarchical optimization for microgrid community economic operation," *IEEE Trans. Smart Grid*, vol. 7, no. 5, pp. 2230–2241, Sep. 2016.

[20] S. Wang, H. Gangammanavar, S. D. Ekşioğlu, and S. J. Mason, "Stochastic optimization for energy management in power systems with multiple microgrids," *IEEE Trans. Smart Grid*, vol. 10, no. 1, pp. 1068–1079, Jan. 2019.

[21] J. H. Yi, R. Cherkaoui, and M. Paolone, "Optimal allocation of ESSs in active distribution networks to achieve their dispatchability," *IEEE Transactions on Power Systems*, vol. 36, no. 3, pp. 2068–2081, May 2021.

[22] IRENA, "Electricity storage and renewables: Costs and markets to 2030," *Int. Renewable Energy Agency*, Abu Dhabi, 2017.

[23] S&C Electricity Company, "Microgrids," https://www.sandc.com/en/solutions/microgrids, Accessed: 23.08.2022.

[24] W. Shi, N. Li, C.-C. Chu, and R. Gadh, "Real-time energy management in microgrids," *IEEE Trans. Smart Grid*, vol. 8, no. 1, pp. 228–238, Jan. 2017.

[25] L. Zhang, N. Gari, and L. V. Hmurcik, "Energy management in a microgrid with distributed energy resources," *Energy Convers. and Manage.*, vol. 78, pp. 297–305, Feb. 2014.

[26] J. A. Pinzon, P. P. Vergara, L. C. Da Silva, and M. J. Rider, "Optimal management of energy consumption and comfort for smart buildings operating in a microgrid," *IEEE Trans. Smart Grid*, vol. 10, no. 3, pp. 3236–3247, May 2019.

[27] C. Ju, P. Wang, L. Goel, and Y. Xu, "A two-layer energy management system for microgrids with hybrid energy storage considering degradation costs," *IEEE Trans. Smart Grid*, vol. 9, no. 6, pp. 6047–6057, May 2017.

[28] C. Liu, X. Wang, X. Wu, and J. Guo, "Economic scheduling model of microgrid considering the lifetime of batteries," *IET Gener., Transmiss. & Distribution*, vol. 11, no. 3, pp. 759–767, Feb. 2017.

[29] Y. Shang, W. Wu, J. Guo, Z. Ma, W. Sheng, Z. Lv, and C. Fu, "Stochastic dispatch of energy storage in microgrids: An augmented reinforcement learning approach," *Appl. Energy*, vol. 261, p. 114423, Mar. 2020.

[30] I. Alsaidan, A. Khodaei, and W. Gao, "A comprehensive battery energy storage optimal sizing model for microgrid applications," *IEEE Trans. Power Syst.*, vol. 33, no. 4, pp. 3968–3980, July 2018.

[31] G. Cardoso, T. Brouhard, N. DeForest, D. Wang, M. Heleno, and L. Kotzur, "Battery aging in multi-energy microgrid design using mixed integer linear programming," *Appl. energy*, vol. 231, pp. 1059–1069, Dec. 2018.

[32] P. Zhuang and H. Liang, "Hierarchical and decentralized stochastic energy management for smart distribution systems with high BESS penetration," *IEEE Trans. Smart Grid*, vol. 10, no. 6, pp. 6516–6527, Nov. 2019.

[33] H. Farzin, M. Fotuhi-Firuzabad, and M. Moeini-Aghtaie, "A stochastic multi-objective framework for optimal scheduling of energy storage systems in microgrids," *IEEE Trans. Smart Grid*, vol. 8, no. 1, pp. 117–127, Jan. 2017.

[34] M. Sedighizadeh, M. Esmaili, A. Jamshidi, and M.-H. Ghaderi, "Stochastic multi-objective economic-environmental energy and reserve scheduling of microgrids considering battery energy storage system," *Int. J. Elect. Power & Energy Syst.*, vol. 106, pp. 1–16, Mar. 2019.

[35] V.-H. Bui, A. Hussain, and H.-M. Kim, "Double deep Q-learning-based distributed operation of battery energy storage system considering uncertainties," *IEEE Trans. Smart Grid*, vol. 11, no. 1, pp. 457–469, Jan. 2020.

[36] Y. Li, Z. Yang, G. Li, D. Zhao, and W. Tian, "Optimal scheduling of an isolated microgrid with battery storage considering load and renewable generation uncertainties," *IEEE Transactions on Industrial Electronics*, vol. 66, no. 2, pp. 1565–1575, Feb. 2019.

[37] C. Deckmyn, T. L. Vandoorn, J. Van de Vyver, J. Desmet, and L. Vandevelde, "A microgrid multilayer control concept for optimal power scheduling and voltage control," *IEEE Transactions on Smart Grid*, vol. 9, no. 5, pp. 4458–4467, Sep. 2018.

[38] F. Garcia-Torres, P. Báez-Gonzalez, J. Tobajas, F. Vazquez, and E. Nieto, "Cooperative optimization of networked microgrids for supporting grid flexibility services using model predictive control," *IEEE Trans. Smart Grid*, vol. 12, no. 3, pp. 1893–1903, 2021.

[39] A. Shakoor, G. Davies, and G. Strbac, "Roadmap for flexibility services to 2030," *A report to the Committee on Climate Change. London: Pöyry*, 2017.

[40] S. Repo, F. Ponci, D. Della Giustina, A. Alvarez, C. C. Garcia, Z. Al-Jassim, H. Amaris, and A. Kulmala, "The ide4l project: defining, designing, and demonstrating the ideal grid for all," *IEEE Power and Energy Mag.*, vol. 15, no. 3, pp. 41–51, May-June 2017.

[41] S. Klyapovskiy, S. You, R. C. Domens, H. W. Bindner, and H. Cai, "Utilizing flexibility services from a large heat pump to postpone grid reinforcement," in *Proc. IEEE Student Conf. Elect. Machines and Syst.*, Huzhou, China, 14-16 Dec. 2018.

[42] G. Tian, Q. Z. Sun, and W. Wang, "Real-time flexibility quantification of a building hvac system for peak demand reduction," *IEEE Trans. Power Syst.*, to be published.

[43] Y. Huo, F. Bouffard, and G. Joós, "Decision tree-based optimization for flexibility management for sustainable energy microgrids," *Applied Energy*, vol. 290, p. 116772, May 2021.

[44] R. Vincent, M. Ait-Ahmed, A. Houari, and M. F. Benkhoris, "Residential microgrid energy management considering flexibility services opportunities and forecast uncertainties," *Int. J. Elect. Power & Energy Syst.*, vol. 120, p. 105981, Sep. 2020.

[45] P. MacDougall, A. M. Kosek, H. Bindner, and G. Deconinck, "Applying machine learning techniques for forecasting flexibility of virtual power plants," in *Proc. IEEE Elect. Power and Energy Conf. (EPEC)*, Ottawa, ON, Canada, 12-14 Oct. 2016.

[46] W. Alharbi and K. Bhattacharya, "Incentive design for flexibility provisions from residential energy hubs in smart grid," *IEEE Trans. Smart Grid*, vol. 12, no. 3, pp. 2113–2124, May 2021.

[47] M. MansourLakouraj, M. J. Sanjari, M. S. Javadi, M. Shahabi, and J. P. Catalão, "Exploitation of microgrid flexibility in distribution system hosting prosumers," *IEEE Transactions on Industrial Applications*, vol. 57, no. 4, pp. 4222–4231, July/Aug. 2021.

[48] M. MansourLakouraj, M. Shahabi, M. Shafie-khah, N. Ghoreishi, and J. P. Catalão, "Optimal power management of dependent microgrid considering distribution market and unused power capacity," *Energy*, p. 117551, June 2020.

[49] "IEC 61970, Energy management system application program interface (EMS-API)—Part 1: Guidelines and general requirements," IEC, 2005.

[50] D. H. Vu *et al.*, "An integrated energy management approach for the economic operation of industrial microgrids under uncertainty of renewable energy," *IEEE Trans. Ind. Appl.*, vol. 56, no. 2, pp. 1062–1073, Jan. 2020.

[51] H. Merdanoğlu, E. Yakıcı, O. T. Doğan, S. Duran, and M. Karatas, "Finding optimal schedules in a home energy management system," *Electric Power Systems Research*, vol. 182, p. 106229, 2020.

[52] R. Godina, E. M. Rodrigues, E. Pouresmaeil, and J. P. Catalão, "Optimal residential model predictive control energy management performance with PV microgeneration," *Computers & Operations Res.*, vol. 96, pp. 143–156, Aug. 2018.

[53] F. Luo, W. Kong, G. Ranzi, and Z. Y. Dong, "Optimal home energy management system with demand charge tariff and appliance operational dependencies," *IEEE Transactions on Smart Grid*, vol. 11, no. 1, pp. 4–14, 2019.

[54] D. Wang, X. Zhang, K. Qu, T. Yu, Z. Pan, and Q. Liu, "Pareto tribe evolution with equilibrium-based decision for multi-objective optimization of multiple home energy management systems," *Energy and Buildings*, vol. 159, pp. 11–23, 2018.

[55] F. Qayyum, M. Naeem, A. S. Khwaja, A. Anpalagan, L. Guan, and B. Venkatesh, "Appliance scheduling optimization in smart home networks," *IEEE Access*, vol. 3, pp. 2176–2190, 2015.

[56] M. F. Zia, E. Elbouchikhi, and M. Benbouzid, "Microgrids energy management systems: A critical review on methods, solutions, and prospects," *Appl. energy*, vol. 222, pp. 1033–1055, July 2018.

[57] R. Luthander, J. Widén, D. Nilsson, and J. Palm, "Photovoltaic self-consumption in buildings: A review," *Applied energy*, vol. 142, pp. 80–94, Mar. 2015.

[58] H. S. Hippert *et al.*, "Neural networks for short-term load forecasting: A review and evaluation," *IEEE Trans. Power Syst.*, vol. 16, no. 1, pp. 44–55, Feb. 2001.

[59] L. Nespoli *et al.*, "Hierarchical demand forecasting benchmark for the distribution grid," *Elect. Power Syst. Res.*, vol. 189, p. 106755, 2020.

[60] J. Zheng, C. Xu, Z. Zhang, and X. Li, "Electric load forecasting in smart grid using long-short-term-memory based recurrent neural network," in *Proc. 51st Ann. Conf. Inform. Sci. and Syst. (CISS)*, Mar. 2017.

[61] Y. Xu *et al.*, "Load forecasting method for building energy systems based on modified two-layer LSTM," in *Proc. 3rd Asia Energy & Elect. Eng. Symp. (AEEES)*, Mar. 2021.

[62] R. Fonteijn, P. H. Nguyen, J. Morren, and J. Slootweg, "Demonstrating a generic four-step approach for applying flexibility for congestion management in daily operation," *Sustainable Energy, Grids & Networks*, vol. 23, p. 100378, Sep. 2020.

[63] Z. Wang, B. Chen, J. Wang, M. M. Begovic, and C. Chen, "Coordinated energy management of networked microgrids in distribution systems," *IEEE Trans. Smart Grid*, vol. 6, no. 1, pp. 45–53, 2015.

[64] Z. Wang, B. Chen, J. Wang, and J. Kim, "Decentralized energy management system for networked microgrids in grid-connected and islanded modes," *IEEE Trans. Smart Grid*, vol. 7, no. 2, pp. 1097–1105, Mar. 2015.

[65] R. Minciardi and M. Robba, "A bilevel approach for the stochastic optimal operation of interconnected microgrids," *IEEE Trans. Autom. Science and Eng.*, vol. 14, no. 2, pp. 482–493, Apr. 2017.

[66] M. Jalali, K. Zare, and H. Seyedi, "Strategic decision-making of distribution network operator with multi-microgrids considering demand response program," *Energy*, vol. 141, pp. 1059–1071, Dec. 2017.

[67] Y. Du and F. Li, "Integrating a multi-microgrid system into real-time balancing market: Problem formulation and solution technique," in *Proc. IEEE Power & Energy Soc. General Meeting (PESGM)*, Portland, OR, USA, Aug. 2018.

[68] M. P. Moghaddam, S. Bahramara, M. Damavandi, and M. Haghifam, "Distribution company and microgrids behaviour in energy and reserve equilibirum," in *Proc. IEEE PES Asia-Pacific Power and Energy Eng. Conf. (APPEEC)*, Brisbane, QLD, Australia, Nov. 2015.

[69] E. Rezaei, H. Dagdougui, and M. Rezaei, "Distributed stochastic model predictive control for peak load limiting in networked microgrids with building thermal dynamics," *IEEE Transactions on Smart Grid*, vol. 13, no. 3, pp. 2038 – 2049, March 2022.

[70] M. Pourakbari-Kasmaei, M. Asensio, M. Lehtonen, and J. Contreras, "Trilateral planning model for integrated community energy systems and pv-based prosumers—a bilevel stochastic programming approach," *IEEE Transactions on Power Systems*, vol. 35, no. 1, pp. 346–361, Jan. 2020.

[71] J. Wang, C. Chen, and X. Lu, "Requirements for DMS integration with DERMS and microgrids," in *Guidelines for implementing advanced distribution management systems.* Argonne National Lab. (ANL), U.S. DOE, Argonne, IL, Aug. 2015.

[72] European Parliament, Directorate-General for Internal Policies of the Union, V. Swinkels, J. Michaelis, R. Villafáfila, M. Voogt, S. Ugarte, M. Wietschel, A. Thielmann, B. Ree, J. Larkin, and N. Friedrichsen, *Energy storage : which market designs and regulatory incentives are needed?* Publications Office, 2015.

[73] M. C. Argyrou, P. Christodoulides, and S. A. Kalogirou, "Energy storage for electricity generation and related processes: Technologies appraisal and grid scale applications," *Renewable and Sust. Energy Rev.*, vol. 94, pp. 804–821, Oct. 2018.

[74] M. N. Akter, M. A. Mahmud, and A. M. T. Oo, "A hierarchical transactive energy management system for energy sharing in residential microgrids," *Energies*, vol. 10, no. 12, p. 2098, Dec. 2017.

[75] Y. Shi, B. Xu, Y. Tan, and B. Zhang, "A convex cycle-based degradation model for battery energy storage planning and operation," in *Proc. Annual American Control Conf. (ACC)*, Wisconsin, US, Aug. 2018, pp. 4590–4596.

[76] J. E. Contreras-Ocana, M. A. Ortega-Vazquez, and B. Zhang, "Participation of an energy storage aggregator in electricity markets," *IEEE Trans. Smart Grid*, vol. 10, no. 2, pp. 1171–1183, Mar. 2019.

[77] M. Koller, T. Borsche, A. Ulbig, and G. Andersson, "Defining a degradation cost function for optimal control of a battery energy storage system," in *Proc. IEEE Grenoble Conf.*, Grenoble, France, Nov. 2013.

[78] C. Bordin, H. O. Anuta, A. Crossland, I. L. Gutierrez, C. J. Dent, and D. Vigo, "A linear programming approach for battery degradation analysis and optimization in offgrid power systems with solar energy integration," *Renewable Energy*, vol. 101, pp. 417–430, Feb. 2017.

[79] A. Perez, R. Moreno, R. Moreira, M. Orchard, and G. Strbac, "Effect of battery degradation on multi-service portfolios of energy storage," *IEEE Trans. Sust. Energy*, vol. 7, no. 4, pp. 1718–1729, Oct. 2016.

[80] Tesla, "Powerwall," https://www.tesla.com/sv_SE/powerwall, Accessed: 23.08.2022.

[81] Samsung, "Samsung SDI," https://www.samsungsdi.com/ess/energy-storage-

system-application.html, Accessed: 23.08.2022.

[82] H. Pandžić and V. Bobanac, "An accurate charging model of battery energy storage," *IEEE Trans. Power Syst.*, vol. 34, no. 2, pp. 1416–1426, Mar. 2019.

[83] A. J. Gonzalez-Castellanos, D. Pozo, and A. Bischi, "Non-ideal linear operation model for li-ion batteries," *IEEE Trans. Power Syst.*, vol. 35, no. 1, pp. 672–682, Jan. 2020.

[84] S. Boulmrharj, R. Ouladsine, Y. NaitMalek, M. Bakhouya, K. Zine-dine, M. Khaidar, and M. Siniti, "Online battery state-of-charge estimation methods in micro-grid systems," *J. Energy Storage*, vol. 30, p. 101518, Aug. 2020.

[85] Y. Naitmalek, M. Najib, M. Bakhouya, and M. Essaaidi, "Forecasting the state-of-charge of batteries in micro-grid systems," in *Proc. 2019 4th World Conf. on Complex Systems (WCCS)*. Ouarzazate, Morocco: IEEE, Apr. 2019.

[86] E. Lannoye, D. Flynn, and M. O'Malley, "Evaluation of power system flexibility," *IEEE Transactions on Power Systems*, vol. 27, no. 2, pp. 922–931, May 2012.

[87] C. Ziras, C. Heinrich, and H. W. Bindner, "Why baselines are not suited for local flexibility markets," *Renewable and Sustainable Energy Reviews*, vol. 135, p. 110357, Jan., 2021.

[88] C. Ziras, J. Kazempour, E. C. Kara, H. W. Bindner, P. Pinson, and S. Kiliccote, "A mid-term DSO market for capacity limits: How to estimate opportunity costs of aggregators?" *IEEE Trans. Smart Grid*, vol. 11, no. 1, pp. 334–345, Jan. 2020.

[89] https://www.hitachienergy.com/offering/solutions/grid-edge-solutions/our-offering/e-mesh/ems, Accessed: 23.08.2022.

[90] https://new.siemens.com/global/en/products/energy/energy-automation-and-smart-grid/microgrid/spectrum-power-mgms.html, Accessed: 23.08.2022.

[91] https://gegridsolutions.com/multilin/catalog/mcs.htm, Accessed: 23.08.2022.

[92] A. Ali, W. Li, R. Hussain, X. He, B. Williams, and A. Memon, "Overview of current microgrid policies, incentives and barriers in the European Union, United States and China," *Sustainability*, vol. 9, no. 7, June 2017.

[93] S. Willette and P. Asmus, "Microgrid Deployment Tracker 2Q19," Navigant Research, https://guidehouseinsights.com/reports/microgrid-deployment-tracker-1q22, 2022, Accessed: 23.08.2022.

[94] L. Cohn. (Jan. 2021) California tribe explores what some see as the future: Networked microgrids. [Online] Available: https://microgridknowledge.com/networked-microgrids-hoopa/, Accessed: 14.04.2022. Source: Microgrid

Knowledge.

[95] EC, "Directive (EU) 2019/944 of the European Parliament and of the Council of 5 June 2019 on common rules for the internal market for electricity and amending Directive 2012/27/eu," Official Journal of the European Union, Brussels, June 2019.

[96] R. Husblad, G. Morén, J. Nordström, C. V. Nylander, L. Tedebrand and S. Wahlberg, "Ren energi inom EU–Ett genomförande av fem rättsakter," Energimarknadsinspektionen, www.ei.se, Feb. 2020.

[97] Schneider Electric Global, "Microgrids," [Online] Available: https://www.se.com/ww/en/work/solutions/microgrids/, Accessed: 23.08.2022.

[98] E. Wood. What Schneider Electric's recent move reveals about the microgrid market. [Online] Available: https://microgridknowledge.com/schneider-microgrid-industry/, Accessed: 23.08.2022. Source: Microgrid Knowledge.

[99] "The rise of clean energy microgrids," Source: Microgrid Knowledge.

[100] P. C. Kotsampopoulos, V. A. Kleftakis, and N. D. Hatziargyriou, "Laboratory education of modern power systems using phil simulation," *IEEE Trans. Power Systems*, vol. 32, no. 5, pp. 3992–4001, Sep. 2017.

[101] G. Agundis-Tinajero, N. L. D. Aldana, A. C. Luna, J. Segundo-Ramirez, N. Visairo-Cruz, J. M. Guerrero, and J. C. Vazquez, "Extended-optimal-power-flow-based hierarchical control for islanded AC microgrids," *IEEE Trans. on Power Electron.*, vol. 34, no. 1, pp. 840–848, Jan. 2019.

[102] A. Charalambous, L. Hadjidemetriou, L. Zacharia, A. D. Bintoudi, A. C. Tsolakis, D. Tzovaras, and E. Kyriakides, "Phase balancing and reactive power support services for microgrids," *Appl. Sciences*, vol. 9, no. 23, p. 5067, Nov. 2019.

[103] B. Aluisio, A. Cagnano, E. De Tuglie, M. Dicorato, G. Forte, and M. Trovato, "PrInCE lab microgrid: early experimental results," in *Proc. Int. Annual Conf. (AEIT)*, Capri, Italy, Oct. 2016.

[104] L. L. Jansen, N. Andreadou, I. Papaioannou, and A. Marinopoulos, "Smart grid lab research in Europe and beyond," *Int. J. Energy Res.*, vol. 44, no. 3, pp. 1307–1336, Dec. 2019.

[105] A. Dimeas, S. Hatzivasiliadis, and N. Hatziargyriou, "Control agents for enabling customer-driven microgrids," in *Proc. IEEE Power & Energy Soc. General Meeting*, Calgary, AB, Canada, July 2009.

[106] J. Østergaard and J. E. Nielsen, "The Bornholm power system An overview," *Kgs. Lyngby, Denmark*, May 2010.

[107] A. Zecchino, A. M. Prostejovsky, C. Ziras, and M. Marinelli, "Large-scale

provision of frequency control via V2G: The Bornholm power system case," *Electric Power Systems Research*, vol. 170, pp. 25–34, May 2019.

[108] B. Washom, J. Dilliot, D. Weil, J. Kleissl, N. Balac, W. Torre, and C. Richter, "Ivory tower of power: Microgrid implementation at the university of California, San Diego," *IEEE Power Energy Mag.*, vol. 11, no. 4, pp. 28–32, July/Aug. 2013.

[109] W. Feng, M. Jin, X. Liu, Y. Bao, C. Marnay, C. Yao, and J. Yu, "A review of microgrid development in the United States–A decade of progress on policies, demonstrations, controls, and software tools," *Appl. Energy*, vol. 228, pp. 1656–1668, Oct. 2018.

[110] N. Akhtar, "Analysis of Simris hybrid energy system design and working and checking the effects of using high capacity factor wind turbine," in Halmstad University Dissertations, 2019.

[111] E.ON. Tekniken i det lokala energisystemett. [Online] Available: https://www.eon.se/om-e-on/innovation/lokala-energisystem/direkt-fran-simris, Accessed: 23.08.2022.

[112] Vattenfall. Mikronät på ö i Stockholms skärgård ökar tillgängligheten i elnätet. [Online] Available: https://energyplaza.vattenfall.se/blogg/mikronat-pa-o-i-stockholms-skargard-okar-tillgangligheten-i-elnatet, Accessed: 23.08.2022.

[113] Ferroamp, EnergyHub System, https://ferroamp.com/en/energyhub-system/, Accessed: 23.08.2022.

[114] K. Antoniadou-Plytaria, A. Srivastava, M. A. F. Ghazvini, D. Steen, L. A. Tuan, and O. Carlson, "Chalmers campus as a testbed for intelligent grids and local energy systems," in *Proc. Int. Conf. Smart Energy Syst. Technol. (SEST)*, Porto, Portugal, Sep. 9–11 2019.

[115] HSB, "HSB living lab," Accessed: 23.08.2022. [Online]. Available: https://www.hsb.se/hsblivinglab/

[116] https://www.riksbyggen.se/ny-bostad/aktuella-projekt/vastra-gotaland/brf-viva/, Accessed: 23.08.2022.

[117] A. Papageorgiou, A. Ashok, T. H. Farzad, and C. Sundberg, "Climate change impact of integrating a solar microgrid system into the Swedish electricity grid," *Appl. Energy*, vol. 268, p. 114981, June 2020.

[118] N. Nazir and M. Almassalkhi, "Grid-aware aggregation and realtime disaggregation of distributed energy resources in radial networks," *IEEE Trans. Power Systems*, vol. 37, no. 3, pp. 1706–1717, May 2022.

[119] b. y. a. Song, Yichen and Wang, Mingqiang and Wang, Mengxia, title=Aggregated Power Flexibility of Active Distribution Network Considering Reliability and Uncertainty.

[120] D. Lee, K. Turitsyn, D. K. Molzahn, and L. A. Roald, "Robust AC Optimal Power Flow With Robust Convex Restriction," *IEEE Trans.Power Systems*, vol. 36, no. 6, pp. 4953–4966, Apr. 2021.

[121] J. Villar, R. Bessa, and M. Matos, "Flexibility products and markets: Literature review," *Electric Power Syst. Research*, vol. 154, pp. 329–340, Jan. 2018.

[122] W. B. Powell and S. Meisel, "Tutorial on stochastic optimization in energy—part i: Modeling and policies," *IEEE Trans. Power Syst.*, vol. 31, no. 2, pp. 1459–1467, Apr. 2015.

[123] M. E. Baran and F. F. Wu, "Network reconfiguration in distribution systems for loss reduction and load balancing," *IEEE Trans. Power Del.*, vol. 4, no. 2, pp. 1401–1407, Apr. 1989.

[124] MQTT, http://mqtt.org/, Accessed: 23.08.2022.

[125] MATLAB 2018b, The MathWorks, Inc., Natick, Massachusetts, United States, Accessed: 23.08.2022. [Online]. Available: https://www.mathworks.com/

[126] GAMS, Accessed: 23.08.2022. [Online]. Available: https://www.gams.com/

[127] A. Fernández-Izquierdo, A. Cimmino, C. Patsonakis, A. C. Tsolakis, R. García-Castro, D. Ioannidis, and D. Tzovaras, "OpenADR ontology: Semantic enrichment of demand response strategies in smart grids," in *Proc. Int. Conf. Smart Energy Syst. & Technol. (SEST)*, Istanbul, Turkey, Sep. 7–9 2020.

[128] UNITED-GRID, "Fiware," [Online] Available: https://www.fiware.org/, Accessed: 23.08.2022.

[129] W. B. Powell, "A unified framework for stochastic optimization," *Eur. J. Oper.Res.*, vol. 275, no. 3, pp. 795–821, June 2019.

[130] A. Ben-Tal and A. Nemirovski, "Robust convex optimization," *Mathematics of Operations Research*, vol. 23, no. 4, pp. 769–805, Nov. 1998.

[131] K. Margellos, P. Goulart, and J. Lygeros, "On the road between robust optimization and the scenario approach for chance constrained optimization problems," *IEEE Trans. Automat. Control*, vol. 59, no. 8, pp. 2258–2263, Aug. 2014.

[132] K. Abdulla, J. De Hoog, V. Muenzel, F. Suits, K. Steer, A. Wirth, and S. Halgamuge, "Optimal operation of energy storage systems considering forecasts and battery degradation," *IEEE Trans. Smart Grid*, vol. 9, no. 3, pp. 2086–2096, May 2018.

[133] E. Mocanu, D. C. Mocanu, P. H. Nguyen, A. Liotta, M. E. Webber, M. Gibescu, and J. G. Slootweg, "On-line building energy optimization us-

ing deep reinforcement learning," *IEEE Trans. Smart Grid*, vol. 10, no. 4, pp. 3698–3708, May 2018.

[134] H. Shuai, J. Fang, X. Ai, J. Wen, and H. He, "Optimal real-time operation strategy for microgrid: An ADP-based stochastic nonlinear optimization approach," *IEEE Trans. Sust. Energy*, vol. 10, no. 2, pp. 931–942, Apr. 2019.

[135] A. Ehsan and Q. Yang, "Scenario-based investment planning of isolated multi-energy microgrids considering electricity, heating and cooling demand," *Applied Energy*, vol. 235, pp. 1277–1288, Feb. 2019.

[136] M. Quashie, F. Bouffard, C. Marnay, R. Jassim, and G. Joós, "On bilevel planning of advanced microgrids," *Int. J. of Elect. Power & Energy Syst*, vol. 96, pp. 422–431, Mar. 2018.

[137] I. E. Grossmann, "Review of nonlinear mixed-integer and disjunctive programming techniques," *Optim. and Eng.*, vol. 3, no. 3, pp. 227–252, Sep. 2002.

[138] C. Liu, H. Zhang, M. Shahidehpour, Q. Zhou, and T. Ding, "A two-layer model for microgrid real-time scheduling using approximate future cost function," *IEEE Trans. Power Syst. (Early Access)*, vol. 37, no. 2, pp. 1264–1273, Mar. 2022.

[139] J. H. Yi, R. Cherkaoui, and M. Paolone, "Optimal allocation of ESSs in active distribution networks to achieve their dispatchability," *IEEE Trans. Power Syst.*, vol. 36, no. 3, pp. 2068–2081, May 2021.

[140] J. Schmalstieg, S. Käbitz, M. Ecker, and D. U. Sauer, "From accelerated aging tests to a lifetime prediction model: Analyzing lithium-ion batteries," in *Proc. IEEE World Electric Vehicle Symp. and Exhib. (EVS27)*, Barcelona, Spain, Nov. 2013.

[141] E. Wikner and T. Thiringer, "Extending battery lifetime by avoiding high SOC," *Appl. Sciences*, vol. 8, no. 10, p. 1825, Oct. 2018.

[142] J. Wang, J. Purewal, P. Liu, J. Hicks-Garner, S. Soukazian, E. Sherman, A. Sorenson, L. Vu, H. Tataria, and M. W. Verbrugge, "Degradation of lithium ion batteries employing graphite negatives and nickel–cobalt–manganese oxide+ spinel manganese oxide positives: Part 1, aging mechanisms and life estimation," *J. Power Sources*, vol. 269, pp. 937–948, Dec. 2014.

[143] D. Wang, J. Coignard, T. Zeng, C. Zhang, and S. Saxena, "Quantifying electric vehicle battery degradation from driving vs. vehicle-to-grid services," *J. Power Sources*, vol. 332, pp. 193–203, Nov. 2016.

[144] M. A. Ortega-Vazquez, "Optimal scheduling of electric vehicle charging and vehicle-to-grid services at household level including battery degradation and price uncertainty," *IET Gener., Transmiss. & Distribution*, vol. 8, no. 6, pp. 1007–1016, June 2014.

[145] M. Farivar and S. H. Low, "Branch flow model: Relaxations and convexification——Part I," *IEEE Trans. Power Syst.*, vol. 28, no. 3, pp. 2554–2564, Apr. 2013.

[146] K. Zhang, S. Hanif, S. Troitzsch, and T. Hamacher, "Day-ahead energy trade scheduling for multiple microgrids with network constraints," in *Proc. IEEE Power & Energy Soc. General Meeting (PESGM)*. Atlanta, GA, USA: IEEE, Aug. 2019.

[147] M. Farivar, X. Zho, and L. Che, "Local voltage control in distribution systems: An incremental control algorithm," in *Proc. IEEE Int. Conf. Smart Grid Commun. (SmartGridComm)*, Miami, FL, USA, Nov. 2015, pp. 732–737.

[148] M. Pourakbari-Kasmaei, M. Asensio, M. Lehtonen, and J. Contreras, "Trilateral planning model for integrated community energy systems and pv-based prosumers—a bilevel stochastic programming approach," *IEEE Trans. Power Syst.*, vol. 35, no. 1, pp. 346–361, Aug. 2019.

[149] A. A. Bashir, A. Lund, M. Pourakbari-Kasmaei, and M. Lehtonen, "Minimizing wind power curtailment and carbon emissions by power to heat sector coupling—AStackelberg game approach," *IEEE Access*, vol. 8, pp. 211 892–211 911, Nov. 2020.

[150] N. Mohammad and Y. Mishra, "Coordination of wind generation and demand response to minimise operation cost in day-ahead electricity markets using bilevel optimisation framework," *IET Gen., Trans. & Dist.*, vol. 12, no. 16, pp. 3793–3802, Sep. 2018.

[151] J. Von Appen and M. Braun, "Strategic decision making of distribution network operators and investors in residential photovoltaic battery storage systems," *Applied energy*, vol. 230, pp. 540–550, Nov. 2018.

[152] X. Cao, J. Wang, and B. Zeng, "A study on the strong duality of second-order conic relaxation of AC optimal power flow in radial networks," *IEEE Trans. Power Syst.*, vol. 37, no. 1, pp. 443–455, Jan. 2022.

[153] L. Eriksson, J. Johansson, R. Johnsson, L. Kötz, J. Lamm, and E. Lundblad, "Comparison of AI models for short-term load forecasting," Bachelor Thesis, Chalmers University of Technology, https://hdl.handle.net/20.500.12380/302491, 2021.

[154] Nord Pool, Accessed: 23.08.2022. [Online]. Available: https://www.nordpoolgroup.com/

[155] Göteborg Energi, Accessed: 23.08.2022. [Online]. Available: https://www.goteborgenergi.se/

[156] X. Li, C. Yuan, and Z. Wang, "Multi-time-scale framework for prognostic health condition of lithium battery using modified Gaussian process regression and nonlinear regression," *J. Power Sources*, vol. 467, p. 228358, Aug. 2020.

[157] C. Heymans, S. B. Walker, S. B. Young, and M. Fowler, "Economic analysis of second use electric vehicle batteries for residential energy storage and load-levelling," *Energy Policy*, vol. 71, pp. 22–30, Aug. 2014.

[158] B. J. Kalkbrenner, "Residential vs. community battery storage systems–Consumer preferences in Germany," *Energy Policy*, vol. 129, pp. 1355–1363, June 2019.

[159] N. Amral, C. Özveren, and D. King, "Short term load forecasting using multiple linear regression," in *42nd Int. Universities Power Eng. Conf.*, Brighton, England, 4-6 Sep. 2007, pp. 1192–1198.

[160] G. Dudek, "Pattern-based local linear regression models for short-term load forecasting," *Elect. Power Syst. Res.*, vol. 130, pp. 139–147, Jan. 2016.

[161] S. Humeau, T. K. Wijaya, M. Vasirani, and K. Aberer, "Electricity load forecasting for residential customers: Exploiting aggregation and correlation between households," in *Proc. Sustainable Internet & ICT for Sustainability (SustainIT)*, 2013.

[162] S.-J. Baek and S.-G. Yoon, "Short-term load forecasting for campus building with small-scale loads by types using artificial neural network," in *Proc. IEEE Power & Energy Soc. Innovative Smart Grid Technologies Conf. (ISGT)*, Washington, DC, USA, Feb. 2019.

[163] W. Kong and Zothers, "Short-term residential load forecasting based on lstm recurrent neural network," *IEEE Trans. Smart Grid*, vol. 10, no. 1, pp. 841–851, Jan. 2019.

[164] S. F. Santos, D. Z. Fitiwi, A. W. Bizuayehu, M. Shafie-khah, M. Asensio, J. Contreras, C. M. P. Cabrita, and J. P. Catalao, "Novel multi-stage stochastic DG investment planning with recourse," *IEEE Trans. Sust. Energy*, vol. 8, no. 1, pp. 164–178, Jan. 2017.

[165] Y. Zhang, F. Meng, R. Wang, W. Zhu, and X.-J. Zeng, "A stochastic MPC based approach to integrated energy management in microgrids," *Sustainable Cities and Soc.*, vol. 41, pp. 349–362, Aug. 2018.

[166] B. V. Solanki, A. Raghurajan, K. Bhattacharya, and C. A. Cañizares, "Including smart loads for optimal demand response in integrated energy management systems for isolated microgrids," *IEEE Trans. Smart Grid*, vol. 8, no. 4, pp. 1739–1748, July 2017.

[167] B. V. Mbuwir, D. Geysen, F. Spiessens, and G. Deconinck, "Reinforcement learning for control of flexibility providers in a residential microgrid," *IET Smart Grid*, vol. 3, no. 1, pp. 98–107, Feb. 2020.

[168] E.ON. E.ON' switch flexibility market. Accessed: 23.08.2022. [Online]. Available: https://www.eon.se/foeretag/elnaet/switch/marknader-produkter

[169] Z. Norwood, E. Nyholm, T. Otanicar, and F. Johnsson, "A geospatial comparison of distributed solar heat and power in Europe and the US," *PLoS ONE*, vol. 9, no. 12, p. e112442, Dec. 2014.

[170] T. Jamal and F. Shahnia, "Data post-processing strategies for the application of short-term PV forecasting in microgrids," in *Proc. Int. Conf. Power & Energy Syst. (ICPES)*, Perth, WA, Australia, Dec. 2019.

[171] B. Cheng and W. B. Powell, "Co-optimizing battery storage for the frequency regulation and energy arbitrage using multi-scale dynamic programming," *IEEE Trans. Smart Grid*, vol. 9, no. 3, pp. 1997–2005, May 2018.

[172] CPLEX Optimizer. [Online] Available: https://www.ibm.com/analytics/cplex-optimizer, Accessed: 23.08.2022.

Appendix A

Abstracts

This appendix presents the abstracts of the publications which were listed in Section 1.7. The numbers below correspond to the numbers given for each paper in the same section.

- Paper I: Effect of short-term and high-resolution load forecasting errors on microgrid operation costs
  The aim of this paper is to evaluate the effect of the load forecasting errors to the operation costs of a grid-connected microgrid. To this end, a microgrid energy scheduling optimization model was tested with deterministic and stochastic formulations under two solution approaches i.e., day-ahead and rolling horizon optimization. In total, twelve simulation test cases were designed receiving as input the forecasts provided by one of the three implemented machine learning models: linear regression, artificial neural network with backpropagation, and long short-term memory. Simulation results of the weekly operation of a real residential building (HSB Living Lab) showed no significant differences among the costs of the test cases for a daily mean absolute percentage forecast error of about 12%. These results suggest that operators of similar microgrid systems could use simplifying approaches, such as day-ahead deterministic optimization, and forecasts of similar, non-negligible accuracy without substantially affecting the microgrid's total cost as compared to the ideal case of perfect forecast. Improving the accuracy would mainly reduce the microgrid's peak power cost as shown by its 20.2% increase in comparison to the ideal case.

- Paper II: Scenario-based stochastic optimization for energy and flexibility dispatch of a microgrid
  Energy storage is one of the most important components of microgrids with non-dispatchable generators and can offer both energy and flexibility services when the microgrid operates in grid-connected mode. This paper proposes a scenario-based stochastic optimization model that can be used to determine the energy and flexibility dispatch of a residential microgrid with solar and stationary battery systems. The objective of the model is to minimize the expected energy and peak power cost as well as the battery aging cost, while maximizing the expected revenue from flexibility. The formulated stochastic

optimization problem is solved in rolling horizon with the uncertainty model being dynamically updated to consider the most recent forecast profiles for solar power and electricity demand. The benefits of the proposed approach were demonstrated by simulating the daily operation of a real building. The results showed that the estimated flexibility was successfully dispatched yielding an economic value of at least 7% of the operation cost of the building microgrid. The model can be used by flexibility providers to assess their flexibility and design a bidding strategy as well as by system operators to design incentives for flexibility providers.

- Paper III: Values and impacts of incorporating local flexibility services in transmission expansion planning
  This paper presents a cost-based TSO-DSO coordination model to quantify the value of local flexibility services and analyze its impact on the transmission grid expansion and the system operation. Flexibility is provided to the DC power flow transmission grid model by microgrids within the integrated AC power flow distribution grid model. The model's objective is to minimize the overall cost of transmission investments and procured flexibility and is achieved using a bilevel optimization approach where the power exchanges on all connected grid interfaces are controlled. Case studies using a combined test system of the IEEE RTS-96 transmission network interfacing multiple 33-bus distribution grids were performed to validate the model and assess the values and impacts of local flexibility on the transmission system expansion. The results showed that the proposed model modified the investment plan and dispatch of flexibility resources reducing the investment and operation cost of the transmission system.

- Paper IV: Market-based energy management model of a building microgrid considering battery degradation
  This paper presents a model for energy management system of a building microgrid coupled with a battery energy storage. The model can be used to dispatch the battery as a flexible energy resource using a market-based setting. The battery is modeled considering battery degradation and real-life operation characteristics derived from measurements at a residential building. The performance of the model was evaluated first with simulations and integrated afterwards to an energy management system, which was demonstrated at a real residential building (HSB Living Lab) equipped with photovoltaic and battery storage systems. The simulation results showed that the building owner, and subsequently the residents, could benefit from the proposed model in reduced annual cost up to 3.1% under the considered pricing scheme. The demonstration results showed that dispatch under the measurement-based model could decrease the undelivered energy over the daily requested amount from the battery from 13.3% to 3.7%. Thus, the proposed model, which couples the measurement-based dispatch with battery degradation, can lead to a more accurate estimation of the building operation cost and an improved overall performance of battery as a flexible resource in building microgrids.

- Paper V: Energy scheduling strategies for grid-connected microgrids: A case study on Chalmers campus
  This paper focuses on the optimal energy management of grid-connected microgrids with battery energy storage systems. The microgrid energy management and the optimal power flow of the distribution network are formulated as mixed-integer linear optimization problems to evaluate microgrid energy scheduling strategies including cost minimization, maximum use of own resources, and minimum energy exchange with the upstream network. The real distribution network of Chalmers University of Technology campus is used as a case study. The study results show that economic optimization yields an annual microgrid cost reduction of 4%. Alternatively, if the microgrid minimizes the energy exchange, virtual islanding operation (zero energy exchange) for 3211 hours can be achieved within a year. The results also present the effects on the operation and cost of the distribution system and highlight a trade-off between microgrid cost minimization and battery lifetime.

- Paper VI: Chalmers campus as a testbed for intelligent grids and local energy systems
  This paper presents an overview of a testbed for intelligent distribution grids, local energy systems, and energy flexible buildings, which is being developed at the campus of Chalmers University of Technology in Gothenburg, Sweden. It describes the test sites, the functionalities, and the planned demonstration activities within the scope of on-going research projects. The proposed demonstrations include a local energy market platform, energy management solutions for microgrids and smart buildings, as well as voltage control in distribution grids. The paper aims to show how the physical energy supply systems of the university are being adapted to integrate the communication and control setups that provide the technical requirements for smart grid interoperability. As an example, the on-site implementation of remote battery control is presented, where initial results show the feasibility and potential benefits of the external control. Finally, challenges and lessons learned during the development of the testbed are highlighted.

Appendix B

Software

Expect for the bilevel optimization model, all other optimization models were developed in GAMS [126], where the interface with the CPLEX optimizer [172] was used to solve the formulated optimization problems on a PC with 4.2 GHz Intel(R) Core(TM) i7-7700K CPU and 64 GB of RA. A GAMS to MATLAB [125] interface was also used to set up the simulations i.e., prepare the input data, run GAMS, and save the results. In scenario-based SO, a mix of fast backward/forward methods in the SCENRED tool of GAMS was used after the scenario generation to create a reduced number of scenarios.

The bilevel optimization model was developed in Pyomo 6.0.1. interfacing the Gurobi 9.1.2 optimizer and Python 3.9.4, which was used to set up the simulations. The bi-level optimization problem was solved on a computer with a 3.40 GHz Intel Core i7-10875H processor and 32 GB of RAM.

Appendix C

Input Data for the Test Cases

This appendix presents the input data that were used in each test case. These include load consumption, PV generation, and electricity prices. The electricity prices are presented in USD, where the average 2018 USD to SEK ratio was used, which is 1:8.6921.

C.1 Network tariffs and fees

The energy and power grid tariffs as well as the reimbursement fee that have been used in the studies of the thesis can be seen in Table C.1. The power grid tariffs are scaled down in each study to apply to the chosen time horizon.

C.2 Electrical distribution system of Chalmers University of Technology

Fig. C.1–C.3 show the load consumption and PV generation profiles of the Chalmers distribution network, MG-A, and MG-B, respectively. The electricity prices that were used in the case study are shown in Fig. C.4.

Table C.1: Network tariffs and fees.

MG company	
Energy transmission cost (¢/kWh)	0.8
Peak power tariff ($/kW/month)	5.0
Reimbursement fee (¢/kWh)	0.3
10 kV distribution grid	
Energy transmission cost (¢/kWh)	0.4
Peak power tariff ($/kW/month)	4.3

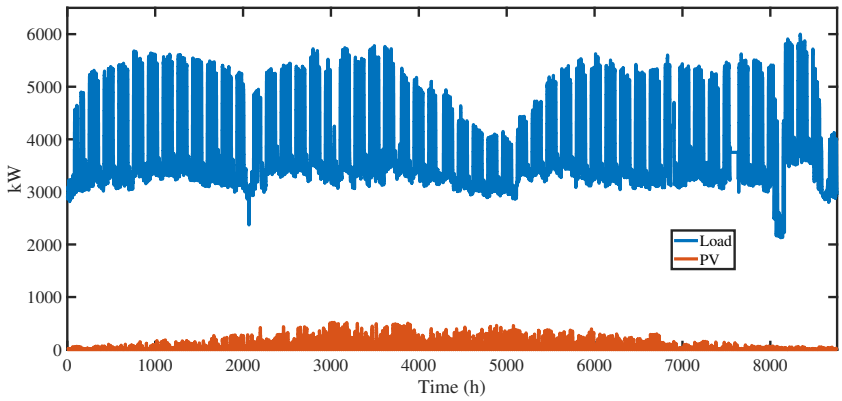

Figure C.1: Load consumption and PV generation in 2016 of the electrical distribution system of Chalmers University of Technology.

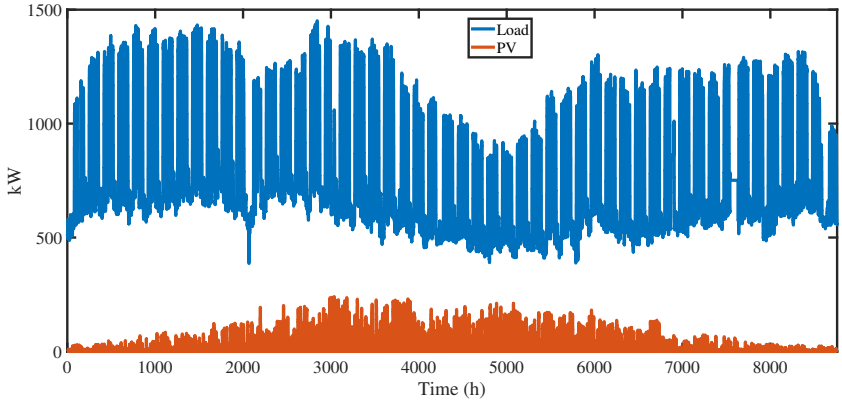

Figure C.2: Load consumption and PV generation of MG-A.

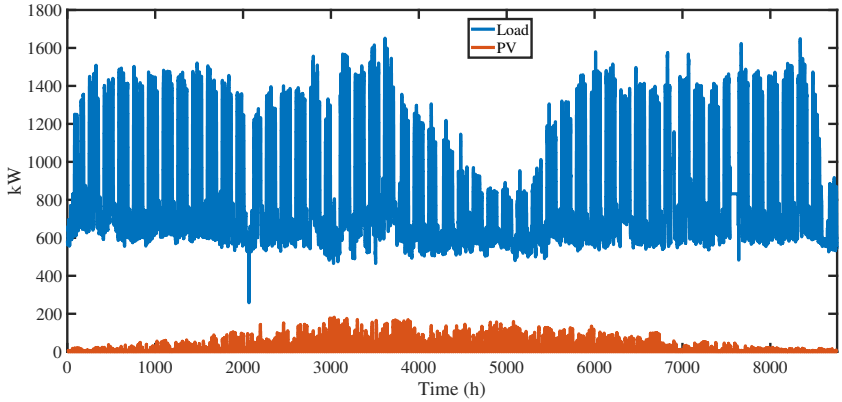

Figure C.3: Load consumption and PV generation of MG-B.

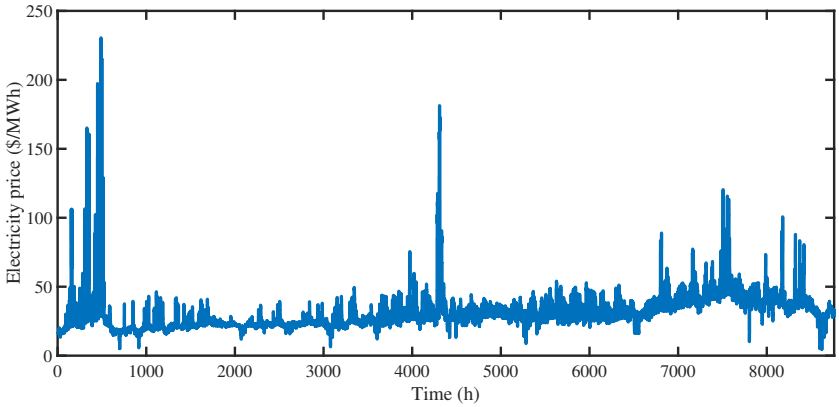

Figure C.4: Electricity prices of the case study on the electrical distribution system of Chalmers University of Technology (Nordpool spot market prices in 2016).

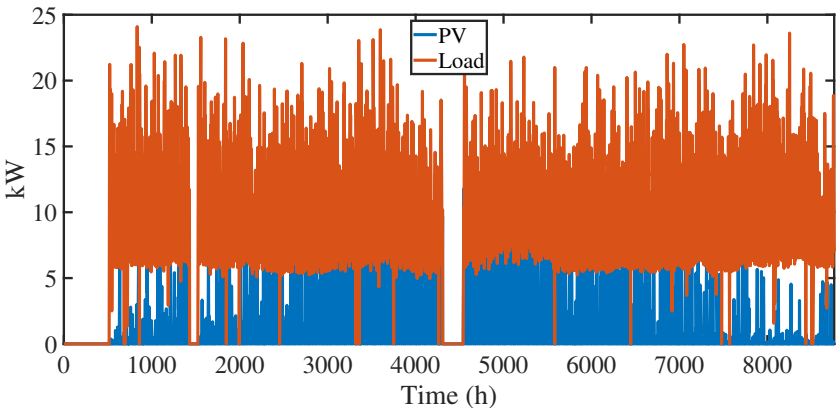

Figure C.5: Building load consumption and PV generation at HSB LL (2018).

C.3 HSB Living Lab

Fig. C.5 shows the HSB LL building load consumption and PV generation in 2018 (where that the profiles are interrupted, it means that data was unavailable), which were used as input to the simulation studies. The input data to the simulation studies also include the 2018 Nordpool spot market prices, which are shown in Fig. C.6.

Fig. C.7 shows the building load consumption and PV generation that was used as input to the BMG-EMS of HSB LL in the demonstrations. The load and PV generation profile corresponds to the first scheduling horizon, when the demonstration started. As the RH approach was used, the input changed every Δt minutes. For the HSB LL demonstration it was $\Delta t = 15$ minutes. The electricity prices that were used in the demonstrations are given in Fig. C.8.

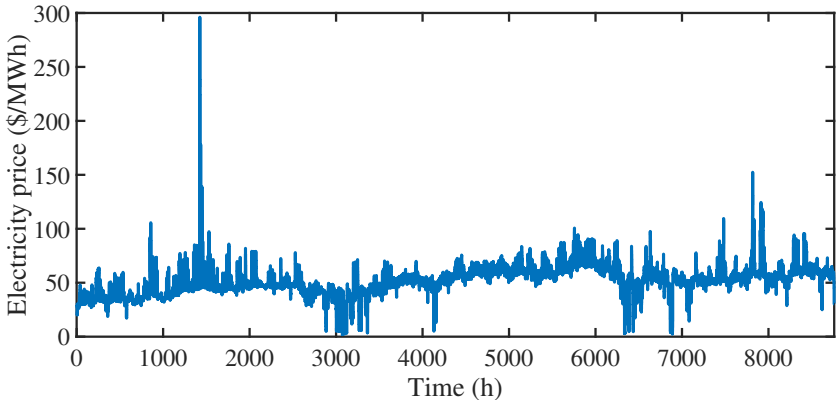

Figure C.6: Electricity prices used as input in the simulation studies of HSB LL (2018).

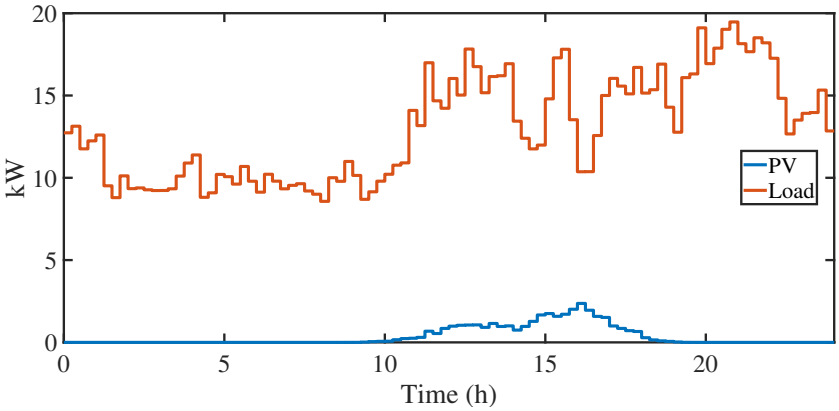

Figure C.7: Daily building load consumption and PV generation at HSB LL (February, 2020).

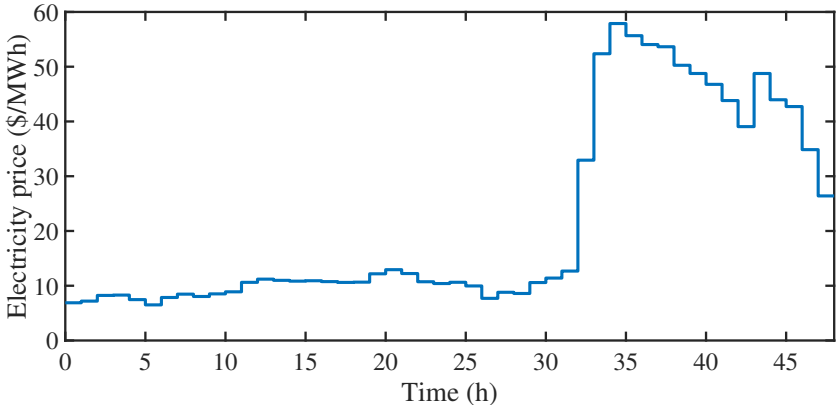

Figure C.8: Electricity prices used as input in the demonstrations at HSB LL (February, 2020).

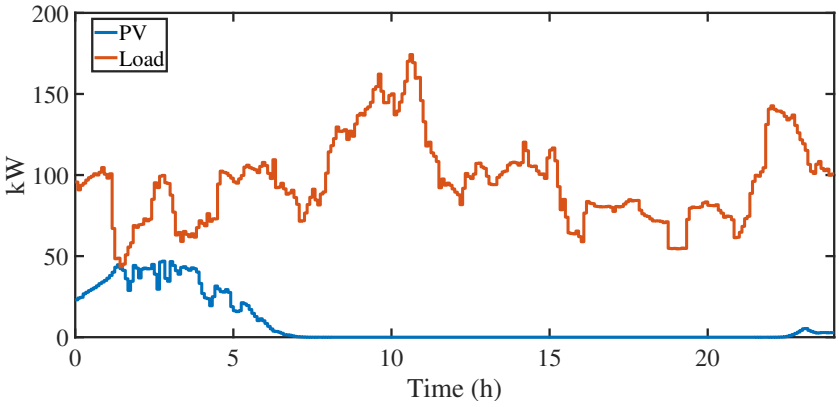

Figure C.9: Building load consumption and PV generation at Brf Viva (February, 2020).

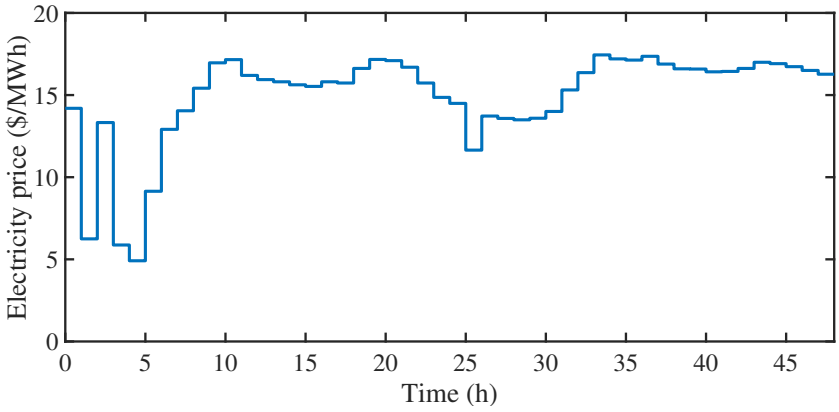

Figure C.10: Electricity prices used as input the simulation studies and demonstrations at Brf Viva (February, 2020)

C.4 Brf Viva

Fig. C.9 shows the building load consumption and PV generation that was used as an input to the Brf Viva test case (both in simulations and demonstrations). An error was introduced in these input data to account for the effect of the forecast error. The load and PV generation profiles correspond to the inputs used for the first 24-hour scheduling horizon, when the demonstration started (at time 09:30). As the RH approach was used, the input changed every Δt minutes. For the Brf Viva simulations and demonstrations it was $\Delta t = 5$ minutes. The electricity prices that were used are given in Fig. C.10.